This dissertation has been
microfilmed exactly as received 67-15,591

BARNES, Charles Edward, 1937-
THERMAL-NEUTRON-INDUCED-DEFECTS IN
CADMIUM TELLURIDE AND CADMIUM SULFIDE.

The University of Michigan, Ph.D., 1967
Engineering, nuclear

University Microfilms, Inc., Ann Arbor, Michigan

THERMAL-NEUTRON-INDUCED-DEFECTS IN CADMIUM TELLURIDE AND CADMIUM SULFIDE

By

Charles Edward Barnes

A dissertation submitted in partial fulfillment
of the requirements for the degree of
Doctor of Philosophy in the
University of Michigan
1967

Doctoral Committee:

Professor Chihiro Kikuchi, Chairman
Professor William Kerr
Professor John S. King
Professor Lawrence H. Van Vlack, Chemical and Metallurgical Engineering Department
Doctor John Lambe, Ford Scientific Laboratory, Dearborn, Michigan
Doctor Robert Oswald, Harry Diamond Laboratories, Washington, D.C.

THERMAL-NEUTRON-INDUCED-DEFECTS IN CADMIUM TELLURIDE AND CADMIUM SULFIDE

By Charles Edward Barnes

In certain materials, such as CdTe, it is possible to produce lattice displacements by a rather unique method, namely, by thermal neutron induced recoil. Briefly, this process involves capture of a thermal neutron by a nucleus which has a significant radiative capture cross-section (Cd^{113}). The resulting excited Cd^{114} nucleus decays to the ground state through the emission of about 9 Mev of "prompt" gamma rays. Conservation of momentum requires that the nucleus recoil during de-excitation. If the recoil energy is large enough, lattice displacements will be produced.

The objective of this investigation is to clarify further the (n,γ) recoil-defect production in CdTe and CdS by measuring changes in Hall effect, electrical conductivity, and luminescence before and after successive thermal neutron irradiations. CdTe and CdS were chosen for study because of the large capture cross-section of cadmium. In addition, radiative capture in cadmium does not lead to transmutation doping since Cd^{114} is a stable nucleus. The Hall effect of n and p-type CdTe and CdS was measured from $4^{\circ}K$ to $300^{\circ}K$ after each irradiation. From this data information on the energy levels and carrier removal rates occurring in these materials is obtained. Luminescence measurements were carried out at $9^{\circ}K$ over the wavelength range 4700 Å to 2.6 microns to ascertain the effect of thermal neutron-induced-defects on the emission bands in CdTe and CdS.

A detailed examination of the thermal neutron induced recoil process reveals that only the first one or two gamma rays emitted contribute significantly to the recoil momentum of the Cd^{114} nucleus. Hence, the majority of recoil events produce only one displacement, the Cd^{114} nucleus itself. Te (or S) displacements are produced only by those occasional recoil events in which an initial high energy gamma ray is emitted. The experimental evidence obtained in this investigation corroborates this picture of the recoil process.

Electrical measurements reveal that the Hall coefficient and resistivity of n and p-type CdTe and CdS increase with irradiation over the entire temperature range. Analysis of these results indicates that, during the irradiation of CdTe, approximately one Cd_v (cadmium vacancy) and one Cd_i (cadmium interstitial) are introduced per absorption event while Te defects are produced at a much slower rate. Annealing of these defects occurs during irradiation but not at room temperature after irradiation. The defects anneal out between 160°C and 200°C.

Electron removal in CdS as a function of the number of absorptions is also explained by the presence of isolated cadmium vacancies. However, it must be assumed that a large excess of Cd defects were present before irradiation. This agrees with the well-known fact that CdS is difficult to produce in exactly stoichiometric proportions.

Luminescence measurements on CdTe show that thermal neutron irradiation causes a decrease in emission intensity over the entire wavelength range. By a comparison with CdS, the changes in edge emission are explained by identifying the Te interstitial as the edge

emission center. In accordance with Hall measurements on p-type CdTe, the identification of a bound exciton emission band leads to an assignment of an energy level at E_v + 0.20 ev for the cadmium vacancy.

ACKNOWLEDGEMENT

This study could not have been carried out without the help of many people. First, I would like to thank Dr. Kikuchi for his many hours of advice and guidance. For their valuable assistance, I wish to express my gratitude to Dr. D. Mason, Dr. R. Oswald, Dr. J. Cleland, Dr. D. O'Kane, and the remainder of my committee. I also want to thank Dr. R. Halsted for supplying crystals and advice for this study, and Dr. Y.S. Park and Mr. D. Reynolds for allowing me to make measurements at the Aerospace Research Laboratory at WPAFB. My sincere thanks goes to Susanne Seifert for patiently typing the manuscript. I am deeply indebted to my wife and children and my parents for all their help and understanding.

TABLE OF CONTENTS

		Page
	LIST OF TABLES	v
	LIST OF FIGURES	vi
I.	INTRODUCTION	1
II.	NEUTRON DAMAGE IN CdTe AND CdS	6
	1. Fast Neutrons	6
	2. Thermal Neutrons	15
III.	EXPERIMENTAL PROCEDURE	27
	3. Electrical Measurements	27
	4. Optical Measurements	32
	A. Emission	32
	B. Transmission	38
	5. Sample Irradiation	38
IV.	EXPERIMENTAL RESULTS	43
	6. Hall Effect, Resistivity and Mobility	43
	A. n-Type Cadmium Telluride	43
	B. p-Type Cadmium Telluride	56
	C. Cadmium Sulfide	66
	7. Luminescence Measurements	70
	A. General Comments	70
	B. p-Type Cadmium Telluride	80
	C. n-Type Cadmium Telluride	88
	D. Cadmium Sulfide	93
V.	DISCUSSION OF RESULTS AND CONCLUSIONS	101
	8. Hall and Resistivity Results	101
	A. n-Type Cadmium Telluride	101

TABLE OF CONTENTS

		Page
	B. p-Type Cadmium Telluride	114
	C. Cadmium Sulfide	120
9.	Luminescence Spectra in Cadmium Telluride	124
10.	Suggestions for Further Experiments	130
VI.	REFERENCES	132

LIST OF TABLES

TABLE		PAGE
1.	Carrier Removal in Various Materials Due to the (n, γ) Recoil Process	25
2.	Emission Bands in CdTe	78
3.	Emission Bands in CdS	79
4.	Bound Exciton Emission Bands in CdTe	86

LIST OF FIGURES

FIGURE		PAGE
1.	Gamma Ray Emission Spectrum for Cd^{114} (20)	18
2.	Uncorrelated (n, γ) Recoil Mechanism in a CdTe Crystal	21
3.	Sample Shape and Mounting Configuration	28
4.	Cryogenic System for Measuring Hall Effect and Resistivity	31
5.	Apparatus for Measuring Emission Spectra (19)	33
6.	Helium Dewar Used in Making Optical Measurements	36
7.	Sample Holder for Optical Measurements	37
8.	Schematic Diagram of Thermal Neutron Irradiation Facility	40
9.	Carrier Concentration of n-type CdTe as a Function of 1/T and Thermal plus Fast Neutron Irradiation	44
10.	Total Number of Electrons/cm^3 Available from Shallow Donors in n-type CdTe versus Cumulative Number of Absorption Events	47
11.	Carrier Concentration versus Reciprocal Temperature as a function of Thermal Plus Fast Neutron Irradiation for Sample GE-232	48
12.	Carrier Concentration versus Reciprocal Temperature as a Function of Thermal Plus Fast Neutron Irradiation for Sample GE-230	49
13.	Resistivity Versus 1/T for n-type CdTe (Sample GE-230) After Long Thermal Neutron Irradiation Times	51
14.	Resistivity Versus 1/T for n-type CdTe (Sample GE-231) After Short Thermal Neutron Irradiation Times	52

LIST OF FIGURES

FIGURE		PAGE
15.	Mobility Versus Temperature for Sample GE-231 After Successive Thermal Neutron Irradiations	53
16.	Change in Carrier Concentration Versus 1/T for n-type CdTe Exposed to Fast Neutrons Only. Sample GE-200	55
17.	Hall Coefficient Versus 1/T as a Function of Thermal Plus Fast Neutron Irradiation for Two Typical p-type CdTe Samples	57
18.	Resistivity Versus 1/T as a Function of Thermal Plus Fast Neutron Irradiation for Two Typical p-type CdTe Samples	58
19.	Mobility Versus Temperature for p-type CdTe as a Function of Thermal Plus Fast Neutron Irradiation	60
20.	Resistivity Versus 1/T for p-type CdTe Before and After Thermal Plus Fast Neutron Irradiation and also Isochronal Annealing. Annealing time: 10 min.	61
21.	Resistivity Versus 1/T for p-type CdTe After Thermal Plus Fast Neutron Irradiation and also Isochronal Annealing. Annealing time: 10 min.	62
22.	Isochronal Annealing Curve for p-type CdTe After Thermal Neutron Irradiation	64
23.	Hall Coefficient Versus 1/T as a Function of Fast Neutron Irradiation of p-type CdTe	65
24.	Hole Concentration in p-type CdTe Versus Cumulative Number of Absorption Events for Short Irradiation Times	67
25.	Hole Concentration in p-type CdTe Versus Cumulative Number of Absorption Events Over the Entire Range of Irradiation	68
26.	Carrier Concentration in Bulk CdS as a Function of 1/T and Thermal Plus Fast Neutron Irradiation	69

LIST OF FIGURES

FIGURE		PAGE
27.	Total Number of Electrons/cm^3 Available from Shallow Donors in CdS Versus Cumulative Number of Absorption Events	71
28.	Resistivity Versus 1/T as a Function of Thermal Plus Fast Neutron Irradiation for CdS	72
29.	A Typical Emission Spectrum for p-type CdTe	74
30.	Emission Spectra of p-type CdTe as a Function of Thermal Plus Fast Neutron Irradiation. (a) No Irradiation, (b) After Second Irradiation	81
31.	Emission Spectra for p-type CdTe as a Function of Thermal Plus Fast Neutron Irradiation (a) After Third Irradiation, (b) After Fourth Irradiation	82
32.	Peak Intensity Versus Cumulative Number of Absorption Events for Emission Bands in p-type CdTe	83
33.	Transmission Versus Wavelength for n-type CdTe as a Function of Thermal Plus Fast Neutron Irradiation. Temperature: $9^{o}K$	85
34.	Emission Spectra of n-type CdTe as a Function of Thermal Plus Fast Neutron Irradiation (a) No Irradiation, (b) After First Irradiation	89
35.	Emission Spectra of n-type CdTe as a Function of Thermal Plus Fast Neutron Irradiation (a) After Second Irradiation, (b) After Third Irradiation	90
36.	Peak Intensity Versus Cumulative Number of Absorption Events for Emission Bands in n-type CdTe	91
37.	Emission Spectrum of n-type CdTe After Long Thermal Neutron Irradiation Time	94
38.	Peak Intensity Versus Cumulative Number of Absorption Events for Emission Bands in CdS	95
39.	The Effect of Thermal Neutron Irradiation on the Edge Emission of CdS	97

LIST OF FIGURES

FIGURE		PAGE
40.	Number of Electrons Removed per cm^3 in CdTe Versus Tanh (γR) where $R = Z_a \bar{\sigma} t$	107
41.	Electron Removal in CdS Based on Constant Cadmium Interstitial Concentration	123
42.	The Effect of Thermal Neutron Irradiation on the Edge Emission in CdTe	126

INTRODUCTION

In certain materials, such as CdTe, it is possible to produce lattice displacements by a rather unique method, namely, by thermal neutron induced recoil. Briefly, this process involves capture of a thermal neutron by a nucleus which has a significant radiative capture cross-section (Cd^{113}). The resulting excited Cd^{114} nucleus decays to the ground state through the emission of about 9 Mev of "prompt" gamma rays. Conservation of momentum requires that the nucleus recoil during de-excitation. If the recoil energy is large enough, lattice displacements will be produced.

The analogy of this process in the field of chemistry, the Szilard-Chalmers (1) reaction used in 1934 to separate iodine from ethyl iodide by thermal neutron irradiation, is well known. Recoil damage in solids was first discussed by Schweinler (2) and later by Walker (3) who demonstrated that exposure to a typical reactor-neutron spectrum results in significant (n, γ) recoil damage for certain elements. Oswald and Kikuchi (4) studied recoil damage in CdS in detail and found that the ratio of the number of displacements produced by thermal neutrons (recoil process) to that produced by fast neutrons is approximately 1.8 $(\phi th/\phi_F)$ where ϕ_{th} is the thermal neutron flux and ϕ_F is the epi-thermal or fast neutron flux. A typical value for the cadmium ratio (ϕ_{th}/ϕ_F) is 10 so that one can expect significant damage from the recoil process according to the ratio found by Oswald and Kikuchi.

The objective of this investigation is to clarify further (n, γ) recoil-defect production in CdTe and CdS by measuring changes in Hall effect, electrical conductivity, and luminescence before and after successive thermal neutron irradiations. CdTe and CdS were chosen for study because of the large capture cross-section of cadmium. In addition, radiative capture in cadmium does not lead to transmutation doping since Cd^{114} is a stable nucleus. The Hall effect of n and p-type CdTe and CdS was measured from $4^{o}K$ to $300^{o}K$ after each irradiation. From this data information on the energy levels and carrier removal rates occurring in these materials is obtained. Luminescence measurements were carried out at $9^{o}K$ over the wavelength range 4700 Å to 2.6 microns to ascertain the effect of thermal neutron-induced-defects on the emission bands in CdTe and CdS.

A theoretical analysis and review of neutron damage in CdTe is presented in Chapter 2. Chapter 3 is devoted to a discussion of the experimental procedures used in making the electrical and optical measurements and the irradiations. The results of these measurements are given in Chapter 4. Analysis and interpretation of the results, which are summarized below, are carried out in Chapter 5.

A detailed examination of the thermal neutron induced recoil process reveals that only the first one or two gamma rays emitted contribute significantly to the recoil momentum of the Cd^{114} nucleus. Hence, the majority of recoil events produce only one displacement, the Cd^{114} nucleus itself. Te (or S) displacements are produced only by those occasional recoil events in which an initial high energy gamma ray is emitted. The experimental

evidence obtained in this investigation corroborates this picture of the recoil process.

The results indicate that, during the irradiation of CdTe, approximately one Cd_v (cadmium vacancy) and one Cd_i (cadmium interstitial) are introduced per absorption event while Te defects are produced at a much slower rate. Consequently, the number of displacements produced per recoil event is about one. Soon after their creation the Cd_v's and Cd_i's trap out electrons and holes, respectively, and move through the crystal and recombine with each other. Electron trapping and defect motion are enhanced by the presence of gamma rays from the decaying Cd^{114} nuclei. Although annealing does not occur at room temperature after irradiation, it does occur between 160°C and 200°C according to electrical measurements on p-type CdTe.

Electron removal in n-type CdTe as a function of the number of recoil events, R, is properly described by the equation,

$$n_e^r = n_e^o \tanh(\gamma R)$$

where n_e^r is the number of electrons removed per cm^3, n_e^o is the number of electrons per cm^3 available from the shallow donors before irradiation and γ is a constant. The derivation of this equation is based on the assumptions that (1) the cadmium vacancy concentration is approximately equal to the cadmium interstitial concentration and (2) the CdTe samples are of near-stoichiometric proportions.

As predicted by the ratio N_{th}/N_F derived in Chapter 2, the effect of the fast neutron flux present during the irradiations is small compared with

the recoil damage.

N-type and p-type CdTe do not change type after long irradiation. This is similar to the behavior of silicon after fast neutron irradiation.

Neither the Cd_v nor the Cd_i possess shallow energy levels near the band edges although the Cd_v may be at $E_v + .15$ ev or $E_v + .20$ ev. However, both defects possess deep energy levels in the band gap which act as non-radiative recombination centers. This follows from the observation that the emission intensity decreases with increasing irradiation time. The assignment of the Te interstitial as the edge emission center agrees with the energy level position of the Te interstitial as $E_v + .06$ ev and also with our hypothesis that Te defects are produced in negligible quantities by the recoil process. The results are also in accordance with the assignment of the Pedrotti model (see page 96) as the edge emission mechanism.

After long irradiation times, a bound exciton band at 1.575 ev dominates the exciton recombination region. This fact leads to an assignment of the $E_v + .20$ ev level to the Cd_v.

Electron removal in CdS is also attributed to the introduction of isolated cadmium vacancies. However, electron removal as a function of $R = \Sigma_\alpha \phi t$ must be analyzed on the basis that a large concentration of excess cadmium was present before irradiation. This agrees with the well-known fact that CdS is difficult to produce in exactly stoichiometric proportions. Consequently, for CdS, the cadmium interstitial concentration is

a constant and the equation for electron removal is

$$n_e^r = 4.5 \times 10^{15} \left(1-e^{-2.2 \times 10^{-17} R}\right)$$

The effect of (n,γ) recoil on the edge emission in CdS is exactly analogous to that in CdTe. The observed behavior can be explained in terms of the Pedrotti model of the edge emission with the S interstitial as the edge emission center.

II. NEUTRON DAMAGE IN CdTe AND CdS

In Section 1 of this Chapter the rate of defect introduction is calculated for fast neutrons. The number of defects produced per absorbed neutron is calculated in Section 2 and compared with the fast neutron defect introduction rate calculated in Section 1. This is followed by a literature review of thermal neutron induced recoil in CdTe and CdS.

The most important result obtained in Sections 1 and 2 is that the number of defects produced in CdTe by thermal neutron induced recoil is about 40 times the number produced by fast neutrons when the ratio of the thermal neutron flux to the fast neutron flux is 10. Based on this result we can proceed to do experiments which will reflect essentially, only the results of thermal neutron induced recoil.

1. Fast Neutrons

The expected number of displacements produced by a fast neutron flux, ϕ_F, in a material with displacement cross-section Σ_d is (5)

$$N_F = \phi_F \Sigma_d \bar{\nu}(K) \quad \text{displacements/cm}^3 \text{ . sec.}$$

where $\bar{\nu}(K)$ is the average number of displaced atoms which will result from the transfer of energy K to a lattice atom at its lattice site. For an elastic collision the maximum energy of the displaced atom or primary knock-on is

$$K_{max} = \frac{4A}{(A+1)^2} E_n$$

where A is the ratio of the nuclide atomic mass to the neutron mass and E_n is the neutron energy. Assuming that the average neutron energy, $\bar{E}_n$, is 1 Mev, and that scattering is isotropic in the center of mass coordinate system

(CMCS), the average energy of the primary knock-on is

$$\overline{K} = \frac{K\,max}{2} \approx \frac{2x10^3}{A}, \text{ Kev}$$

for heavy nuclei. The average number of defects produced per primary knock-on is (5)

$$\overline{\nu}(K) = \begin{cases} 0, & K < E_d \\ 1, & E_d \leq K \leq 2E_d \\ \frac{K}{2E_d}, & 2E_d \leq K \leq E_i \\ \frac{E_i}{2E_d}, & K > E_i \end{cases}$$

where E_d is the minimum or threshold energy of displacement. If the velocity of the primary knock-on is large compared with that of the orbital electrons of the stationary atoms, then the knock-on will dissipate its energy through ionization. Below a certain energy the knock-on will lose its energy primarily through displacement collisions. In reality, this energy is not sharply defined. However, a cut-off energy, E_i, is usually assumed (5). Below E_i, the primary knock-on loses energy only by collisions. E_i has been estimated as (6)

$$E_i = \frac{M}{m_e}\frac{E_g}{8}$$

where M is the mass of the primary knock-on, m_e is the electron mass and E_g is the energy gap (1.45 ev in CdTe). Now for $\overline{E}_n$ = 1 Mev and A_{cd} = 112

$$\overline{K} = 18 \text{ Kev}$$

and

$$E_i = 37.4 \text{ Kev}$$

Therefore, $\overline{K}$ is less than E_i. In CdS, E_d is about 8 ev (7). Using this

value,

$$\bar{\nu} = \frac{\bar{K}}{2 E_d} = 1.13 \times 10^3 \text{ displaced atoms/primary knock-on}$$

Assuming that $\Sigma_d = \Sigma_s$,

$$N_F = \phi_F \Sigma_s 1.13 \times 10^3 \text{ displacements/cm}^3 \text{ sec.}$$

For CdTe, $\Sigma_s = .186 \text{ cm}^{-1}$ (8) and

$$N_F = 210\ \phi_F \text{ displacements/cm}^3 \text{ . sec in CdTe.} \qquad (1)$$

The above calculation is inaccurate because scattering off heavy nuclei is not isotropic in the CMCS for neutrons with energies $\geq$ several hundred Kev (9). In this range, forward scattering predominates. This leads to an overall reduction in the energy transmitted to the lattice through collisions and, consequently, in the number of defects produced. Also, the calculation is more accurate if one uses a neutron energy spectrum characteristic of the reactor instead of an average energy, $\bar{E}_n$.

To begin the calculation, we adopt a scattering frequency function which takes p-wave scattering into account (10):

$$f(\mu')d\mu' = 1/2\ (1 + a\mu')\, d\mu'$$

$f(\mu')d\mu'$ = the probability that a neutron is scattered into $d\mu'$ about μ'

where μ' = cos of the scattering angle in the CMCS and a = constant which determines the strength of p-wave (that is, neutrons with angular momentum, $\ell = 1$) scattering. From conservation of momentum and energy (10),

$$E_1 = \frac{E_n}{(A+1)2}\ (A^2 + 2\mu' A + 1)$$

where E_n = neutron energy before collision, E_1 = neutron energy after collision, and K = energy of struck nucleus after collision. (target nucleus at

rest before collision). Since $K = E_n - E_1$

$$K = E_n \left[1 - \frac{(A^2 + 2\mu'A + 1)}{(A+1)^2}\right] = 2AE_n \frac{(1-\mu')}{(A+1)^2} \qquad (2)$$

For a given E_n, K depends only on μ'. Therefore,

$$f(K)\, dK = f(\mu') \left|\frac{\partial \mu'}{\partial K}\right| dK$$

From equation (2) $\left|\frac{\partial \mu'}{\partial K}\right| = \frac{(A+1)^2}{2AE_n}$

and, substituting for μ' from equation (2),

$$f(K)\, dK = \frac{(A+1)^2}{4AE_n}\left[1 + a\left(1 - \frac{(A+1)^2}{2A}\frac{K}{E_n}\right)\right] dK$$

To find a, one calculates $\bar{\mu}'$, the average of the cos of the scattering angle in the CMCS,

$$\bar{\mu}' = \int_{-1}^{1} \mu' f(\mu')\, d\mu' = 1/2 \int_{-1}^{1} \mu'(1+a\mu')\, d\mu' = \frac{a}{3}$$

Therefore,

$$f(K)\, dK = \frac{(A+1)^2}{4AE_n}\left[1 + 3\bar{\mu}'\left(1 - \frac{(A+1)^2}{2A}\frac{K}{E_n}\right)\right] dK \qquad (3)$$

This is the same as the result stated by Schweinler (11).

To find $\bar{\mu}'$, μ' is averaged over the differential scattering cross-section (12):

$$\bar{\mu}' = \overline{\cos\theta} = \frac{\int \sigma_s(\theta) \cos\theta \sin\theta\, d\theta}{\int \sigma_s(\theta) \sin\theta\, d\theta} \qquad (4)$$

To evaluate the integrals, $\sigma_s(\theta)$ is expanded in terms of Legendre

polynomials (13):

$$\sigma_s(\theta) = \sum_{L=0}^{n} B_L \; P_L \; (\cos\theta)$$

The coefficients B_0, B_1, B_2, B_3 are given for Cd in reference (13) over the neutron energy range, 0.2 to .85 Mev. To use these coefficients, we assume that the curves given for the B_L's are valid at higher energies and that the B_L's given for Cd can also be used for Te. The first assumption is reasonable because B_0 and B_1 both approach constant values at the high energy end. In reference (13), B_L's are also given for other elements with A near 100. The B_L's have about the same values for all four elements studied. Since A for Te (127.6) is also near 100, the second assumption is reasonable. Substituting in equation (4),

$$\bar{\mu}' = \frac{\sum_{L=0}^{3} B_L \int_{-1}^{1} P_L(\mu')\mu' \; d\mu'}{\sum_{L=0}^{3} B_L \int_{-1}^{1} P_L(\mu') \, d\mu'}$$

Since

$$\mu' = P_1(\mu') \quad \text{and} \quad P_0(\mu') = 1$$

and

$$\int_{-1}^{1} P_L(\mu) \, P_{L'}(\mu) \, d\mu = \frac{2\,\delta_{LL'}}{2L+1}$$

one obtains

$$\bar{\mu}' = (2/3)\frac{B_1}{2B_0} = \frac{B_1}{3B_0}$$

From reference (13), B_0 is 0.58 barns/sterad over the entire energy range. B_1 is roughly exponential in form and can be fitted by the following equation:

$$B_1 = 0.666 - 0.935 \exp\left[-6.3\,E_n\right], \; E_n \text{ in Mev}$$

$$= 0 \text{ for } E_n < \text{approximately 54 Kev}$$

Therefore,

$$\bar{\mu}' = 0.383 - 0.537 \exp\left[-6.3\, E_n\right], \quad E_n \text{ in Mev}$$

$$= 0, \quad E_n \leq 54 \text{ Kev}$$

The number of primary knock-ons produced per sec. per cm^3 with energies in dK about K by neutrons with energies in dE_n about E_n is

$$\Sigma_s(E_n)\ \phi(E_n) f(K)\ dK\ dE_n$$

where the previous equation for $\bar{\mu}'$ is used in f (K). To find the number of displacements produced by these particular primary knock-ons, one must multiply by $\bar{\nu}(K)$ (see page 6). Harrison and Seitz (14) give an expression for $\bar{\nu}(K)$ which is more accurate than that used earlier:

$$\bar{\nu}(K) = 0.56 \left(\frac{K + E_d}{E_d}\right)$$

An expression for the total number of displacements produced/sec. per cm^3 can now be written:

$$N_F = \int_{E_n} \int_K \bar{\nu}(K)\ \Sigma_s(E_n)\ \phi(E_n)\, f(K)\, dK\, dE_n \qquad (5)$$

with the following restriction on the limits of integration:

$$0 \leq K \leq 4AE_n/(A+1)^2$$

or $0 \leq K \leq 4E_n/A$ for heavy elements such as Cd. The integral for N_F must be broken down into four parts because the functions contained within the integrand do not have the same form over the entire energy range. The lowest energy region extends from $E_n = AE_d/4$ to $E_n = 54$ Kev. The lower limit is the minimum neutron energy which will result in the transfer of $K = E_d$ ev to the struck nucleus and, therefore, produce a lattice displacement. 54 Kev is taken as the upper limit because $\bar{\mu}'$ is non-zero above this energy.

The microscopic scattering cross-section, σ_s, for Cd and Te equals about 6 barns (8) from 300 ev to 10 Mev neutron energy. Resonance scattering is ignored because most of the resonances for Cd and Te lie below $E_n = AE_d/4 = 224$ ev (for $E_d = 8$ ev) (8).

Within a few centimeters of the core face the flux varies exponentially with E_n (15) for $E_n \geq 1$ Mev:

$$\phi(E_n) = \alpha e^{-aE_n}$$

where $AE_i/4 = 1.05$ Mev $\leq E_n \leq 12$ Mev and $a = 6.62 \times 10^{-4}$ for E_n in Kev. By analogy with the Bulk Shielding Reactor at ORNL, which is very similar to the FNR, a $1/E_n$ spectrum is assumed to exist in the Kev neutron energy range (16) (17):

$$\phi(E_n) = C/E_n$$

Since the two forms of $\phi(E_n)$ must be equal at 1.05 Mev,

$$\frac{C}{1.05 \times 10^3} = \alpha \exp\left[-(6.62 \times 10^{-4})\ (1.05 \times 10^3)\right]$$

and $\alpha = 1.91 \times 10^{-3}\ C$

C is found by relating the flux to the activation of a Cd covered gold foil. If the Cd-cutoff energy is assumed to be 0.4 ev, then

$$A_{cd} = N_w \int_{0.4}^{\infty} \sigma_a^{Au}(E_n)\phi(E_n)\, dE_n$$

where A_{cd} is the saturated activity of a Cd-covered gold foil in units of $sec^{-1}\ gm^{-1}$ and N_w is the number of atoms per gram of foil. The activation can be divided into two parts, that due to the gold resonance at 4.9 ev and the remaining 1/v region:

$$A_{cd} = N_w C \left[\left(\int_{0.4}^{\infty} \frac{\sigma_a^{Au}(E_n)\, dE_n}{E_n} \right)_{res.} + \left(\int_{0.4}^{\infty} \frac{\sigma_a^{Au}(E_n)\, dE_n}{E_n} \right)_{1/v} \right]$$

The values of these two integrals are given by Price (18):

$$A_{cd} = N_w C \left[1,558 \text{ barns} + 48 \text{ barns} \right]$$

Solving for C,

$$C = 0.204\, A_{cd}$$

and

$$\phi(E_n) = 0.204\, A_{cd}/E_n \qquad (6)$$

Since the samples were irradiated in boron nitride containers, $\phi(E_n)$ must be modified in the low energy range($AE_d/4$ to 54 Kev) to take into account the $(\frac{1}{v})$ absorption cross-section of boron:

$$\phi'(E_n) = \frac{C}{E_n} e^{-x \Sigma_a(BN)} \equiv \frac{C}{E_n} e^{-xb/\sqrt{E_n}}$$

where x is the wall thickness of the boron nitride (BN) container.

The equation for the number of displacements produced by neutrons in the energy range, $AE_d/4$ to 54 Kev is

$$N_F^1 = \Sigma_s \int_{AE_d/4}^{54} dE_n \int_{E_d}^{4E_n/A} 0.56 \left(\frac{K + E_d}{E_d} \right) \frac{C}{E_n} e^{-xb/\sqrt{E_n}} \frac{A}{4E_n} dK \qquad (7)$$

In the second neutron energy region, from 54 kev to $AE_i/4 = 1.05 \times 10^3$ Kev, $\bar{\mu}'$ is no longer zero and f (K) dK must be used in its complete form. The upper limit, $AE_i/4$, is the cutoff for the $1/E_n$ spectrum and also for the value of $\bar{\nu}(K)$ used in N_F^1 and N_F^2. Because σ_a for BN is much smaller at these higher energies, the $1/E_n$ spectrum is no longer modified by $e^{-x\Sigma_a(BN)}$ The number of displacements produced in this energy range is,

$$N_F^2 = \Sigma_s \int_{54}^{AE_i/4} dE_n \int_{E_d}^{4E_n/A} \left(\frac{K + E_d}{E_d}\right) \frac{C}{E_n} \frac{A}{4E_n} \left[1 + 3\left(0.383 - 0.537 e^{-6.3\times10^{-3} E_n}\right)\left(1 - \frac{AK}{2E_n}\right)\right] dK \quad (8)$$

The third neutron-energy region, from $AE_i/4 = 1.05 \times 10^3$ Kev to $E_n^{max} = 12$ Mev, must be subdivided into two portions because the primary knock-on dissipates its energy, K, by ionization for $K > E_i$. Therefore, for $K > E_i$

$$\bar{\nu}(K) = 0.56\left(\frac{E_i + E_d}{E_d}\right) \approx 0.56 \frac{E_i}{E_d}$$

However, a neutron in the energy range, $AE_i/4$ to E_n can transfer an amount of energy, K, to a knock-on which is either greater than E_i or less than E_i. Consequently, one must integrate over the range of K from E_d to E_i and over the entire neutron energy range, $AE_i/4$ to E_n^{max}. In addition, one must integrate over the K-range, E_i to $4E_n/A$ and, again, over the entire neutron energy range. In both terms, the flux is given by the exponential form:

$$N_F^3 = \Sigma_s \int_{AE_i/4}^{E_n^{max}} dE_n \int_{E_d}^{E_i} 0.56 \left(\frac{K + E_d}{E_d}\right) \propto e^{-aE_n} \frac{A}{4E_n} \left[1 + 3\left(0.383 - 0.537 e^{-6.3\times10^{-3} E_n}\right)\left(1 - \frac{AK}{2E_n}\right)\right] dK \quad (9)$$

$$N_F^4 = \Sigma_s \int_{AE_i/4}^{E_n^{max}} dE_n \int_{E_i}^{4E_n/A} 0.56 \frac{E_i}{E_d} \propto e^{-aE_n} \frac{A}{4E_n} \left[1 + 3\left(0.383 - 0.537\ (x)\ (x)\, e^{-6.3\times10^{-3} E_n}\right)\left(1 - \frac{AK}{2E_n}\right)\right] dK \quad (10)$$

The result for the total number of displacements is

$$N_F = N_F^1 + N_F^2 + N_F^3 + N_F^4 = (12.7 + 115 + 218 + 179)C = 525C \text{ disp./sec. cm}^3$$

The first term in the preceding equation indicates that a small percentage of the displacements is produced by neutrons with energies less than 54 Kev. Details of the calculation show that the largest contribution comes from neutrons in the range 0.5 to 2 mev. Also, the number of displacements produced by neutrons with energies greater than 6 Mev is negligible because of the low flux above this energy.

The importance of taking p-wave scattering into account ($\bar{\mu}' \neq 0$) can be illustrated by calculating N_F^2 for $\bar{\mu}' = 0$. The result is

$$N_F^2 \ (\bar{\mu}' = 0) = 234C$$

as compared with $N_F^2 \ (\bar{\mu}' \neq 0) = 115$ C. This is the result one would expect since predominant forward scattering ($\bar{\mu}' \neq 0$) will result in lower energy transfer to the struck nuclei. In terms of the saturated activity of a Cd-covered gold foil, N_F is

$$N_F = (525)(0.204) A_{cd} = 107 \ A_{cd} \qquad (11)$$

2. Thermal Neutrons

The production of lattice displacements by thermal neutrons begins with the reaction,

$$Cd^{113} + n_{th} \rightarrow [Cd^{114}]^* \longrightarrow Cd^{114} + \gamma \ (9.04 \text{ Mev})$$

Oswald (4) showed that the product of the abundance and the cross-section for the remaining Cd isotopes and all the S isotopes is negligible compared to Cd^{113}. In CdTe, the cross section of Te ($\sigma_a = 4.7$ barns) is significantly larger than that of sulfur ($\sigma_a = 0.52$ barns). However, the major portion of the absorptions in Te will yield other stable Te isotopes. The added number

of recoil defects produced in this manner is negligible, compared to the expected number of defects from Cd^{113}. Te^{126} is the only Te isotope with a non-vanishing cross-section that will lead to transmutation doping. For this isotope,

$$\sigma_a \times \% \text{ abundance} \approx 0.2 \text{ barns}$$

and

$$Te^{126} + n_{th} \longrightarrow Te^{127} \xrightarrow[9.3\ hr]{\beta^-} I^{127}$$

A rough calculation shows that an $(nvt)_{th}$ of 10^{16} neutrons/cm^2 will result in 3×10^{13} I^{127} nuclei/cm^3. As will be evident from the following discussion, this is much smaller than the expected number of recoil defects. However, it is conceivable that I^{127} doping could have some influence. This will be discussed further in a later section.

Having established that the Cd^{113} reaction is the major process, one can proceed to calculate the recoil energy of the Cd^{114} nucleus. Assuming that only one gamma ray is emitted, the recoil energy E_r, can be calculated from conservation of momentum:

$$P_{cd} = \frac{h\nu_\gamma}{c} = \frac{E_\gamma}{c}$$

and

$$E_r = \frac{P_{cd}^2}{2M_{cd}} = \frac{E_\gamma^2}{2M_{cd}c^2} \qquad (12)$$

$$E_r \text{ (ev)} = 4.71\ E_\gamma^2 \text{ (Mev) for } Cd^{114}$$

For

$$E_\gamma = 9.04 \text{ Mev},$$

$$E_r = 385 \text{ ev}$$

However, the excited Cd^{114} nucleus decays to the ground state through the emission of a complex cascade of gamma rays. Assuming that

1. The gamma rays are all emitted instantaneously. That is, the nucleus leaves its lattice position with a momentum which is the negative of the vector sum of all the gamma ray momenta.
2. There is no angular correlation between the gamma rays; the gamma emission is isotropic.

Schwinler (11) calculated the average recoil energy to be:

$$\bar{E}_r = \frac{1}{2M_{cd}c^2} \sum_i f(E_{\gamma i}) \quad E_{\gamma i}^2$$

where $f(E_{\gamma i})$ is the emission probability of the ith gamma ray. Oswald (19) calculated $\bar{E}_r$ from the above equation as 35.4 ev. Because much of the gamma ray energy emitted is not resolved, the continuous distribution of emitted gamma rays (20), shown in Figure (1), yields a more accurate value of $\bar{E}_r$. In this case, the summation goes over to an integral:

$$\bar{E}_r = \frac{1}{2M_{cd}c^2} \int_0^{E_{max}} f(E_\gamma)\, E_\gamma^2 \, dE_\gamma \quad (13)$$

Oswald (19) obtained $\bar{E}_r$ = 143 ev from this equation which agrees with the value calculated by Coltman (21) ($\bar{E}_r$ = 133 ev) in his study of recoil damage in Cd metal. Since E_d = 8 ev in CdS (4), recoil damage should result in multiple displacements in CdS and CdTe.

The mechanics of the recoil process merit further discussion because of the assumptions made in calculating $\bar{E}_r$. Recall that the gamma emission was assumed to be instantaneous. This is correct if the lifetimes

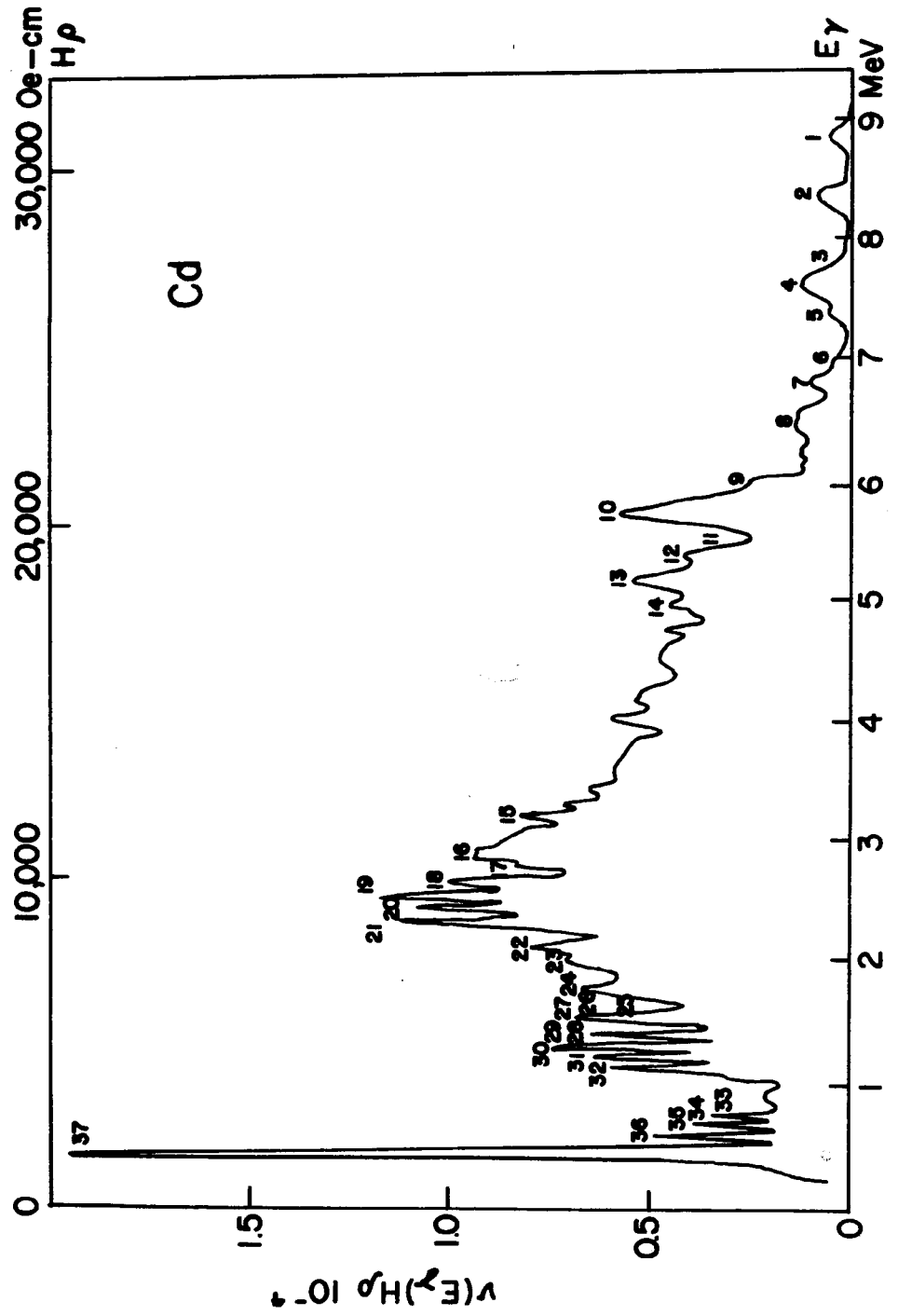


Fig. 1. Gamma Ray Emission Spectrum for Cd^{114} (20)

of all the excited states are short compared to the collision time of the recoiling atom with its neighbors. However, assuming a collision distance of about 1 Å, the collision time, t_c for a recoiling Cd^{114} nucleus with a kinetic energy of 10-20 ev is given by

$$\frac{E_{\text{kinetic (Mev)}}}{0.51} = \frac{M_{cd}\ v_{cd}^2}{2\ m_e c^2}$$

or

$$t_c \approx \frac{10^{-8}}{v_{cd}} = \frac{10^{-8}}{2c\left(\frac{E_k}{A}\frac{me}{mp}\right)^{1/2}} \approx 2 \times 10^{-14}\ \text{sec.}$$

where (m_e/m_p) is the electron to proton mass ratio and v_{cd} is the velocity of the Cd^{114} nucleus. Now, the lifetimes of some of the lower excited states are (22):

Level	Lifetime
0.556 Mev	9.2×10^{-12} sec
1.210	1.7×10^{-12}
1.36	1.3×10^{-12}

The lifetime of the higher excited states is estimated using the level width, Γ_{rad}, of the Cd resonance which is about 0.1 ev:

$$\text{Lifetime} \approx \frac{\hbar}{\Gamma_{rad}} \approx \frac{10^{-15}}{10^{-1}} = 10^{-14}\ \text{sec.}$$

Consequently the collision time is less than the prompt gamma lifetime except for the highest excited states.

The maximum of the energy distribution curve of the gamma rays emitted by the excited Cd^{114} nucleus is at approximately 2 Mev. As indicated in

Figure (2), because of the short lifetime of the highly excited states, it is quite probable that two 2 Mev gamma rays will be emitted before the first collision takes place. Following this, the Cd^{114} nucleus will emit gamma rays intermittently as it travels through the crystal colliding with other nuclei as shown on Figure (2). The momenta of the gamma rays emitted between collisions are treated separately and, hence, are uncorrelated with respect to the recoil momentum of the Cd^{114}. The later gamma rays will also possess lower energies of approximately the same value as the minimum gamma energy required to cause a displacement. Consequently, they will not contribute significantly to $\bar{E}_r$ and the recoil energy will be determined by the two 2 Mev gammas emitted initially. Using a similar approach to calculate the recoil energy, Walker (23) excluded all gamma rays whose energy was less than $1/2\ E^{max}$ and integrated over the continuous distribution given in reference (24) from $1/2\ E^{max}$ to E^{max} to obtain $\bar{E}_r = 48$ ev which is significantly lower than the value of 143 ev calculated by Oswald (19). Consequently, if one considers only the first two 2 Mev gamma rays emitted, the recoil energy, $\bar{E}_r$, is $4.71\,(2^2 + 2^2) = 37$ ev. Assuming that the number of displacements is given by $\bar{E}_r / 2E_d$, and that $E_d \approx 15$ ev for CdTe, we can expect only one displacement, the recoiling Cd nucleus itself.

Concerning the validity of the second assumption, that is, isotropy of the emitted gamma rays, Brazos (25) demonstrated that directional correlation does exist between the 0.722 Mev gamma and the 0.556 Mev gamma in Cd^{114}. In Brazos' experiment, E_r would be less than $\bar{E}_r$ because the coincidence counting rate increased as the angle between the gamma rays approached

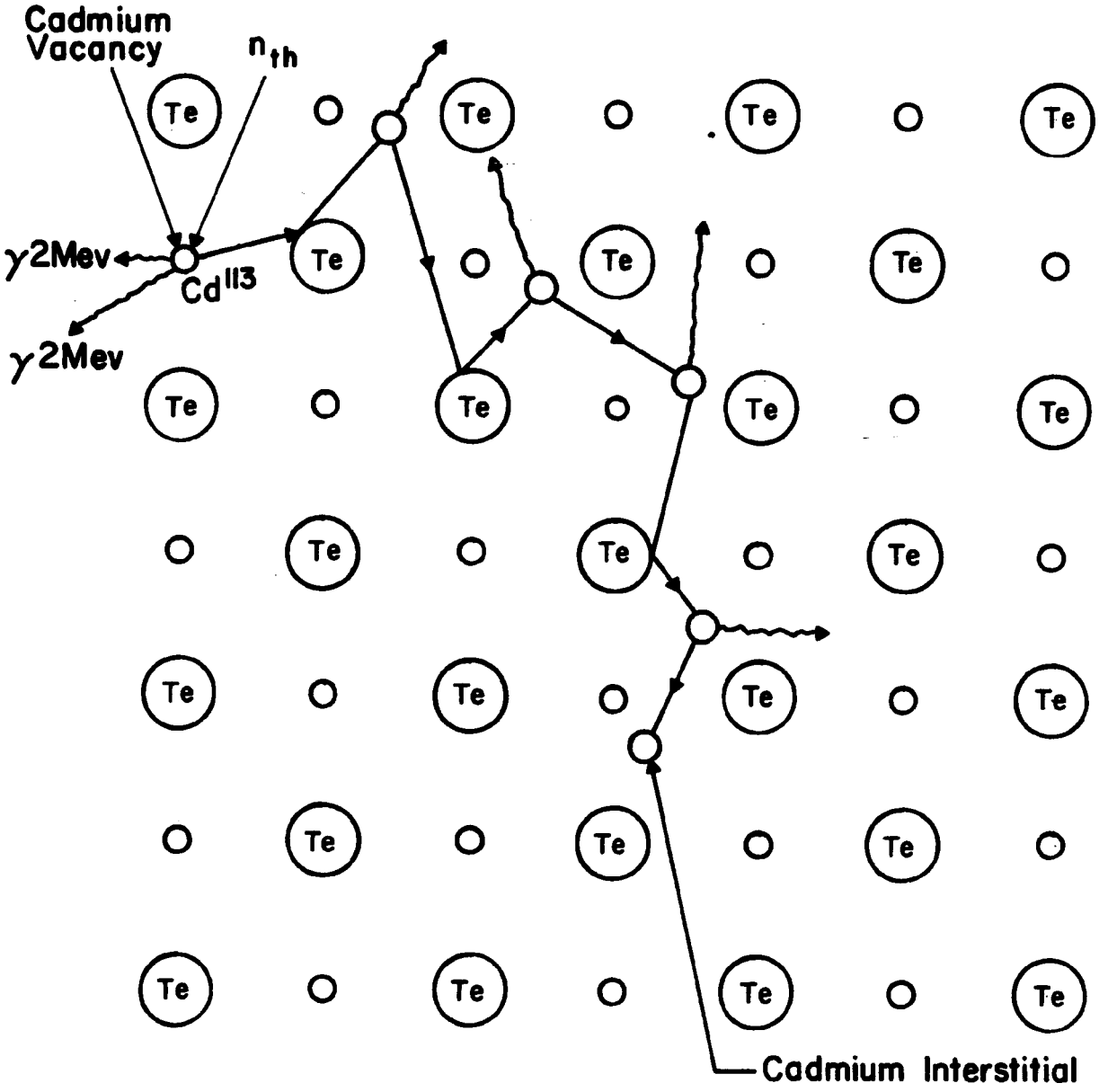


Fig. 2. Uncorrelated (n, γ) Recoil Mechanism in a CdTe Crystal

180^{o}. Although the angular correlation is not known for most of the emitted gamma rays, an analogy with the higher excited states could also exist.

To summarize, the general picture is that only Cd displacements occur for the majority of recoil events as shown in Figure (2). For those less frequent recoil events when an initial high energy (5-9 Mev) gamma ray is emitted a larger number of displacements are produced. Therefore, from a theoretical viewpoint, one expects more Cd than Te defects.

Because of flux depression, the value of the average thermal neutron flux, $\bar{\phi}$, within the sample is needed to calculate the total number of defects. For a thick foil the average absorption rate can be approximated by (26):

$$\Sigma_a \bar{\phi} \approx \frac{\phi_s}{d} \quad cm^{-3}\ sec^{-1} \tag{14}$$

where d is the sample thickness and ϕ_s is the thermal flux at the foil (sample) surface. ϕ_s is determined from the activation of a gold foil placed near the sample:

$$\phi_s = 3.73\,(A_{th} - A_{cd}) \tag{15}$$

where A_{th} is the saturated activity of a bare foil and A_{cd} is the saturated activity of a Cd covered foil. The coefficient, 3.73, is equal to $\bar{v}_{th}/N_w \sigma_{ao} v_o$ where $\bar{v}_{th}$ is the average speed and v_o is the peak speed for a Maxwell-Boltzmann distribution. σ_{ao} is the gold cross-section at the neutron energy corresponding to v_o. Therefore,

$$\Sigma_a \bar{\phi} = \frac{3.73}{d} (A_{th} - A_{cd}) \tag{16}$$

Now, the total number of displacements produced/cm^3/ sec is

$$N_{th} = \bar{\nu}(\bar{E}_r)\, \Sigma_a \bar{\phi} = 0.56 \left(\frac{\bar{E}_r + E_d}{E_d} \right) \Sigma_a \bar{\phi}$$

Using the value of $\bar{E}_r$ calculated by Oswald (143 ev) and E_d = 10 ev,

$$N_{th} = \frac{31.9}{d} (A_{th} - A_{cd}) \quad (17)$$

A typical sample thickness is d = .025" = .0635 cm. For this d,

$$N_{th} = 503 (A_{th} - A_{cd})$$

Recall that the number of displacements produced by fast neutrons is

$$N_F = 107 A_{cd}$$

Therefore, the ratio of N_{th} to N_F is

$$\frac{N_{th}}{N_F} = 4.7 (R_{cd} - 1) \quad (18)$$

where R_{Cd} is the cadmium ratio. For example, if R_{Cd} = 10

$$\frac{N_{th}}{N_F} = 42.3$$

From the point of view of simple damage theory the number of displacements produced by thermal neutron induced recoil is

$$N_{th} = \Sigma_a \phi_{th} \bar{\nu}$$

For CdTe, σ_a(Cd) = 2450 barns (8) and

$$N = 1.55 \times 10^{22} \text{ atoms Cd/cm}^3$$

Therefore,

$$\Sigma_a = N\sigma_a = 38.0 \text{ cm}^{-1}$$

Also

$$\bar{\nu} = \frac{\bar{E}_r}{2E_d} \approx \frac{143}{20} \approx 7 \text{ displacements/absorption}$$

Then

$$N_{th} = (38.0)\ (7)\phi_{th} = 266\ \phi_{th}$$

For simple damage theory,

$$\frac{N_{th}}{N_F} = \frac{266}{210} \times \frac{\phi_{th}}{\phi_F} = 1.27\ \frac{\phi_{th}}{\phi_F} \qquad (19)$$

If $\phi_{th}/\phi_F = 10$, then $N_{th}/N_F = 12.7$ which agrees with the ratio of N_{th} to N_F calculated by Walker (23). The major source of disagreement between this value and the more exact estimate (42.3) is the difference between the fast neutron spectra used in each calculation. In both cases, however, the predicted value of N_{th}/N_F indicates that thermal neutron induced recoil damage is the predominant effect for $R_{cd} = 10$.

Discrepancies between the theoretically predicted N_{th} and the experimentally determined rate have been found for several materials after thermal neutron irradiation. This can be attributed to defect annealing during irradiation. We will show that this explanation can account for the results observed in this study. Irradiation annealing was demonstrated by Coltman (21) (27) who irradiated cadmium metal with thermal neutrons at 4.2°K and found that annealing takes place even at this low temperature. As expected, the experimental damage rate was less than that predicted by Coltman (21). Similar results have been found in silicon and germanium. The possibility or producing thermal neutron induced recoil defects in Si and Ge was first discussed by Schweinler (2). In an experimental study of Si, Chukichev (28) found that the experimental electron removal rate was only 25% of the predicted removal rate after room temperature irradiation. Cleland (29) found that the removal rate was only 1/10 the calculated introduction rate

in Si and Ge. Later, Cleland, et al (30) showed that the removal rate approaches the predicted defect introduction rate as the irradiation temperature is lowered. This is evident in Table (1) which is from this paper.

TABLE (1)

Carrier Removal in Various Materials Due to the (n, γ) Recoil Process

Material	Number of absorptions (N_A)	Kinetic Energy of Recoil (eV)	Calculated Number of Frenkel Defects	Irrad. Temp.	Carrier Concentration Change (dn/dN_A)	Net dn/dN_A After Room Temperature Anneal	Number and Type of Transmutations
n-type Ge	0.108 nvt_{th}	182	6	40 °C	— 1.0		0.12 $N_A = N_{As}$ 0.3 $N_A = N_{Ge}$
				195 °K	— 1.7 to — 2.0	— 1.7 to — 2.0	
				78 °K	— 2.0 to — 2.5	— 1.0 to — 1.3	
n-type Ge^{74}	0.038 nvt_{th}	150	5	40 °C	+ 0.10		0.76 $N_A = N_{As}$
				78 °K	— 1.7 to — 2.5	+ 0.5 to + 1.0	
n-type Si	0.007 nvt_{th}	780	26	40 °C	— 2.0		0.04 $N_A = N_P$
				78 °K	— 3.7	— 1.8	
n-type GaAs	0.14 nvt_{th}	160	5	40 °C	— 3.0		0.33 $N_A = N_{Ge}$ 0.66 $N_A = N_{As}$

Thermal neutron induced recoil defects in CdS have been studied by Cleland (31) and Chester (32) and more extensively, by Oswald (4) (19) (33). Cleland (31), and also Chester (32), found a 10 to 25% reduction in electron concentration after irradiation with an electron removal of only 0.1 per absorption event. About 60% of the damage annealed out after 23 hours at 100°C.

Oswald (4) (19) (33) investigated the effect of thermal neutron induced recoil defects by measuring changes in emission spectra, electrical conductivity and photoconductivity of CdS. Measurement of emission spectra at 77°K showed that both the blue exciton emission and green edge emission decreased in intensity with thermal neutron irradiation. This was accompanied by the appearance of a broad emission band at 7200 Å which increased in intensity with irradiation. Similar effects were

observed for fast neutron irradiation, but at a much slower rate. These changes were observed in both conducting and insulating CdS crystals.

Oswald (4) (19) also measured the changes in conductivity of low resistivity bulk and platelet crystals at 295°K and 78°K as a function of irradiation. The conductivity of the bulk crystals, which was higher at 78°K than at 295°K before irradiation, decreased with irradiation. After $(nvt)_{th} = 3 \times 10^{16}$ cm^{-2}, the temperature behavior of the conductivity was inverted. Measurement of the conductivity at various temperatures after further irradiation (total = 1.2×10^{17} neutrons/cm^2) revealed an energy level at $E_c - 0.5$ ev where E_c is the bottom of the conduction band.

Following exposure to thermal neutrons at 30°C, Chester (32) showed that high purity n-type CdTe invariably changed to p-type. However, Urli (34) found that p-type CdTe converts to n-type with a shallow donor at $E_c - .02$ ev following thermal neutron irradiation.

III. EXPERIMENTAL PROCEDURE

3. Electrical Measurements

Undoped Cadmium telluride from several different sources was used in this study.*

In all cases, the CdTe was received as an ingot. The diameter varied from 5 mm to 10 mm while the length of the ingots varied between one and three inches. The ingots were cut into wafers about 3 mm thick with a Dimet diamond saw. Cutting was done at a very slow rate (approximately 45 minutes for a 10 mm diameter ingot) in order to avoid fracture. In cases where the plane of the cut was nearly parallel to a cleavage plane, fracture occurred quite easily. The wafers were then mechanically polished on both sides to a thickness of .015 to .025 in. After polishing, grain boundaries and twinning planes were plainly visible. For electrical measurements, wafers with large single crystal sections were selected so that the finished sample would be a single crystal. Samples containing twinning planes could be used since Kroger (35) has shown that these planes do not perturb the electrical characteristics of the crystal. The wafers were mounted on a glass plate and samples of the shape indicated in Figure (3) were cut out using an S.S. White sandblasting machine. In this machine, a mixture of fine abrasive and CO_2 was forced through a nozzle which has a slit about 1.5 mm long. After removal from the glass plate, the sample was given a brief, fine polish and washed in ethyl alcohol. The samples were then etched in a room-temperature solution of 70%, by volume, potassium dichromate and 30% concentrated

* We are indebted to R.E. Halsted of G.E. Research Lab. for generously supplying n-type CdTe crystals for this study.

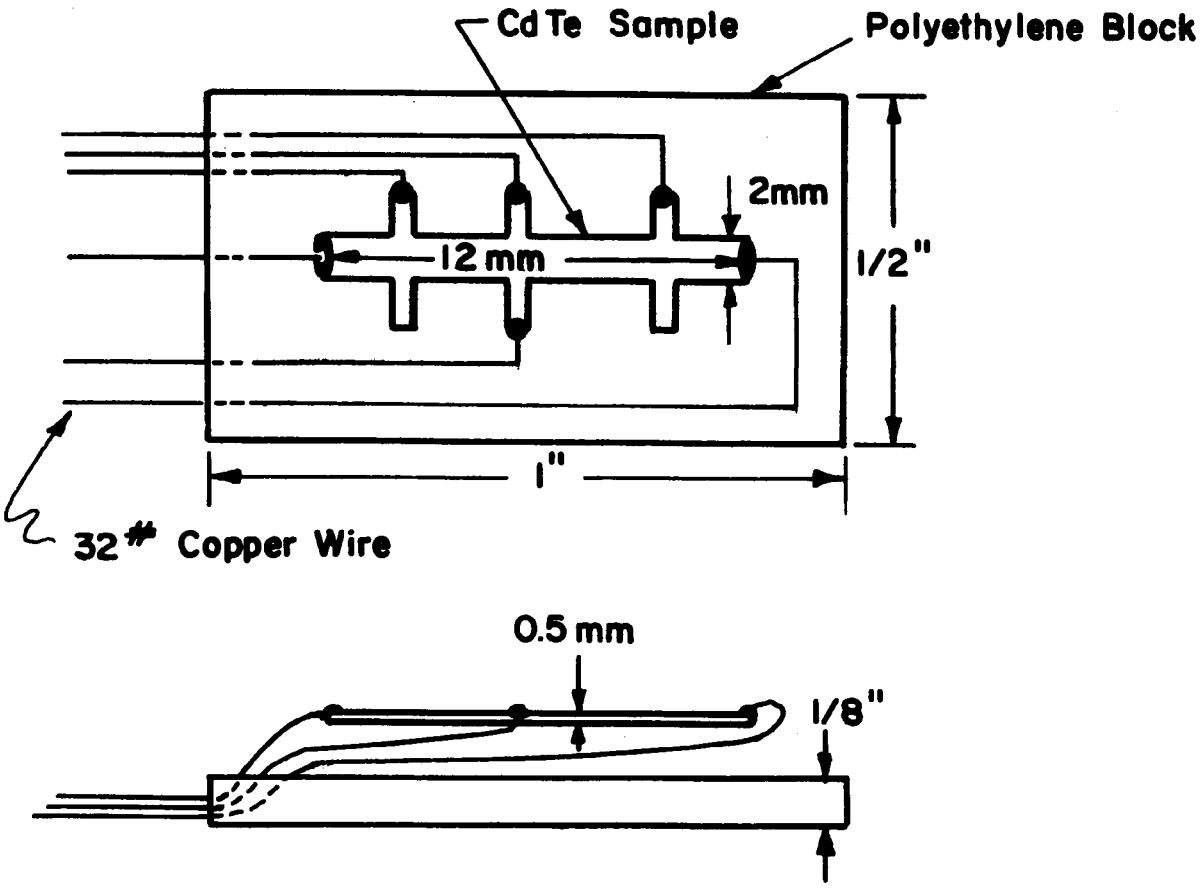


Fig. 3. Sample Shape and Mounting Configuration

sulfuric acid (36).

Electrical contacts were made to n-type CdTe using the procedure given by Segall (37). The arms of the sample were rubbed with a Hg-In amalgam in order to wet the surface and thirty-two gauge copper wires were then soldered on with indium solder. This method provided good Ohmic contacts.

Achieving Ohmic contacts on p-type CdTe was somewhat more difficult. Immediately after etching, the sample arms were dipped in a dilute solution of $AuCl_3$. A saturated solution was not used because the bond between the sample and the gold film was stronger if the gold plated out slowly. Copper wires were soldered to the gold film with a low temperature solder (melting point = 100°C) available from Jensen Tools and Alloys, Phoenix, Arizona. Those samples which had Ohmic contacts at low temperatures were selected for measurement.

In the case of CdS, Hall samples were prepared from bars purchased from Harshaw Chemical Company. Electrical contact was made by soldering copper wires to the sample with In solder.

Because of the possibility of annealing during soldering, it was desirable to leave the contacts on the sample during irradiation. For this reason, the samples were mounted on polyethylene blocks, 1"x 1/2" x 1/8" as shown in Figure (3). Polyethylene was selected because of its good radiation resistance. The sample was held in position by bending the copper leads and melting them into the polyethylene block. This allowed handling

of the sample without endangering the contacts. Also, expansion or contraction of the polyethylene block with temperature did not affect the sample.

Hall effect and electrical conductivity measurements were made using standard D.C. methods. The current passing through the sample was monitored with a Keithley micro-micro-ammeter having a range of 10^{-3} to 10^{-12} amps. Hall and resistivity voltages were measured with a Leeds and Northrup K-3 potentiometer and a Leeds and Northrup null detector. At low temperatures, or after long irradiation times, the resistivity of the samples was often quite large and it was necessary to measure Hall and resistivity voltages with a Keithley electrometer having an input impedance of 10^{14} ohms. The magnetic field for the Hall measurements was provided by a 6 in. Varian magnet. The maximum field was 3.90 kilogauss with a 4 in. air gap.

The general features of the cryogenic system used for Hall measurements are shown in Figure (4). The system consisted of an outer nitrogen jacket, a helium dewar and a third inner dewar. At temperatures between $4^{o}K$ and $77^{o}K$, the annular vacuum space of the third dewar was partially evacuated so that heat transfer between the sample compartment and the liquid helium was minimized. This procedure provided good temperature control and conserved liquid helium in the range, $4^{o}K$ to $77^{o}K$. The sample holder, which was placed in the third dewar, consisted of a stainless steel tube attached to a flange at the top and to a copper plate at the bottom. Twelve electrical leads were connected to a vacuum header mounted in the flange, and then passed down through the tube to lavite connector blocks mounted on the

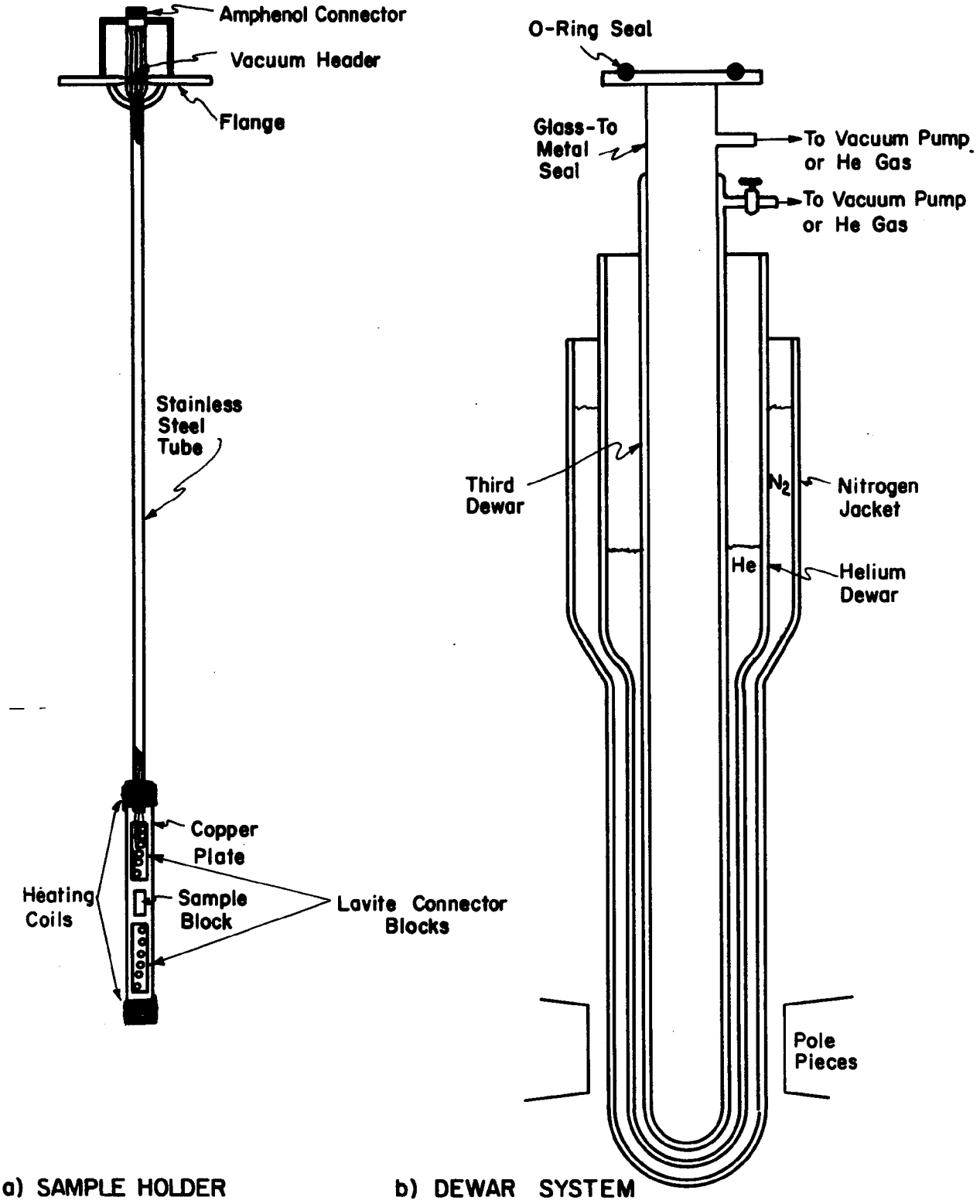


Fig. 4. Cryogenic System for Measuring Hall Effect and Resistivity

copper plate. The polyethylene block, with its sample, was attached to the copper plate between the lavite blocks with vacuum grease. Sample heating was accomplished with wire wound heaters mounted on the top and bottom of the copper plate. The flange at the top was fitted with an 0-ring seal so that the sample compartment could be pumped on or filled with 1-10 mm Hg of helium exchange gas to ensure a uniform sample temperature. From 70°K to 300°K, the temperature was measured with a copper-constantan thermocouple placed near the sample while a calibrated germanium resistance thermometer was used below 70°K.

4. Optical Measurements

A. Emission

Emission samples were prepared by cleaving a portion of the ingot near where the Hall samples were cut. CdTe cleaves rather easily so that relatively large cleaved surfaces could be obtained for emission measurements. The samples were irregular in shape with the cleaved surfaces varying roughly from 8 mm x 8 mm down to about 2 mm x 2 mm.

A few emission spectra were also taken on platelet and bulk crystals of CdS. The emission samples were not from the same source as the Hall samples.

With the exception of the dewar system, the equipment used for the fluorescence measurements, shown in Figure (5), was essentially the same as that used by Oswald (19) in his study of CdS. The crystal was

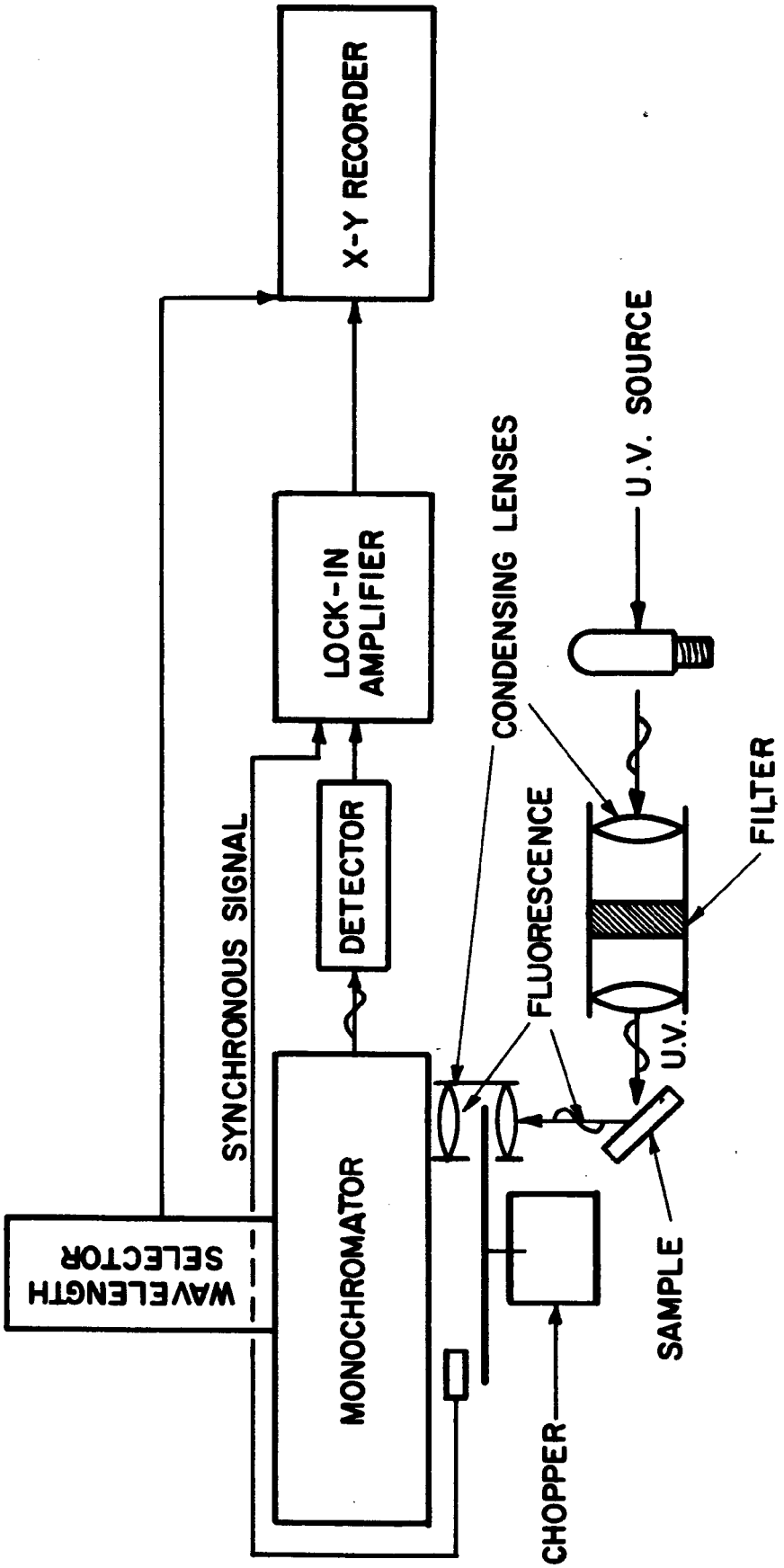


Fig. 5. Apparatus for Measuring Emission Spectra (19)

excited with the 3650 Å line from a super high pressure mercury lamp. This line was isolated with a Corning 7-51 filter and a $CuSO_4$ solution. After being modulated by a 90 cps mechanical chopper, the emitted light was focused on the entrance slit of a Bausch and Lomb monochromator. This instrument could be fitted with either one of two gratings, a grating with 600 lines/mm blazed at 7500 Å or a grating with 300 lines/mm blazed at 2 microns. With the first grating, the monochromator produced a reciprocal linear dispersion of 30 Å/mm; with the second, 60 Å/mm. Emission spectra were taken over the wavelength range, 7600 Å to 2.6 microns. The first grating was used from 7600 Å to 1.4 microns; the second from 1.3 microns to 2.6 microns. Light detection was also divided into two ranges. A cooled RCA 7102 photomultiplier tube having S-1 response was used from 7600 Å to 1.0 micron while a Kodak Ektron PbS detector was used in the remainder of the range. The signal from the detector was fed into a Princeton Applied Research lock-in amplifier. The reference signal for this amplifier was supplied by a PbS detector and a small tungsten lamp with the mechanical chopper interposed between the two. The input signal to the amplifier was amplified 10,000 times and converted to D.C. voltage and then used to drive the y-scale of an x-y recorder. The motor-driven wavelength drum on the monochromator produced a voltage proportional to the wavelength setting which provided the signal for the x-scale of the x-y recorder. Therefore, the emission spectrum was plotted out directly as intensity versus wavelength.

The wavelength range near the absorption edge was calibrated with a

neon lamp each time the grating with 600 lines/mm was removed and then replaced. Also, a standard CdTe sample which was not irradiated, was measured periodically to check the overall response of the system.

Accurate high-resolution spectra of a few unirradiated CdTe samples were measured at the Aerospace Research Laboratory at Wright-Patterson A.F.B. through the courtesy of D.C. Reynolds and Y.S. Park. The instrument used was a 2 meter Bausch and Lomb spectrograph with a reciprocal linear dispersion of 8 $\mathring{A}$/mm. Kodak type 1-N photographic plates were used to record the fluorescence. Neon calibration lines were superimposed on the spectra. The plates were then scanned with a Jarrell-Ash densitometer.

With the exception of the emission measurements done at Wright-Patterson A.F.B., all the emission spectra were taken at approximately $9^{o}K$. The optical glass dewar used, shown in Figure (6) was of the Hersh (38) design and employed a helium finger and a common vacuum which required the dewar to be pumped down for every measurement. Although this was a disadvantage, the simplicity of the dewar and the fact that the sample could be rotated while at $9^{o}K$ made it an attractive cryostat. Four quartz windows, 3/4" in diameter, were used. The distance from the sample to the window was about 2 in. A copper sample holder, illustrated in Figure (7), consisting of a flat vertical plate with a hole in the center for transmission measurements, was mounted at the bottom of the helium cold finger. Three cooling channels passing down through the plate carried liquid helium to a small cylindrical reservoir attached to the bottom of the plate. The samples were mounted on the plate along with the germanium resistance thermometer referred to earlier (see page 32).

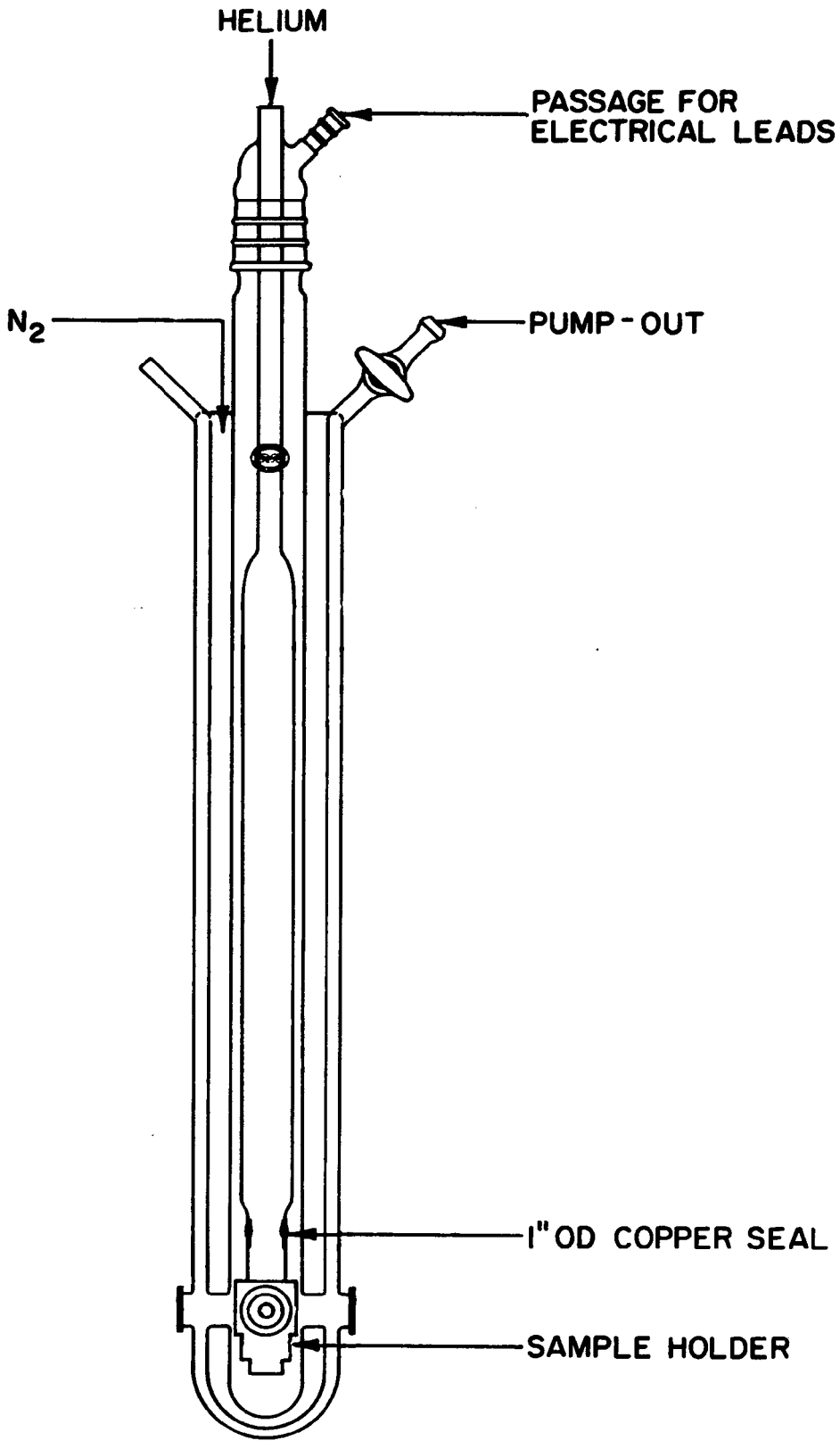


Fig. 6. Helium Dewar Used in Making Optical Measurements

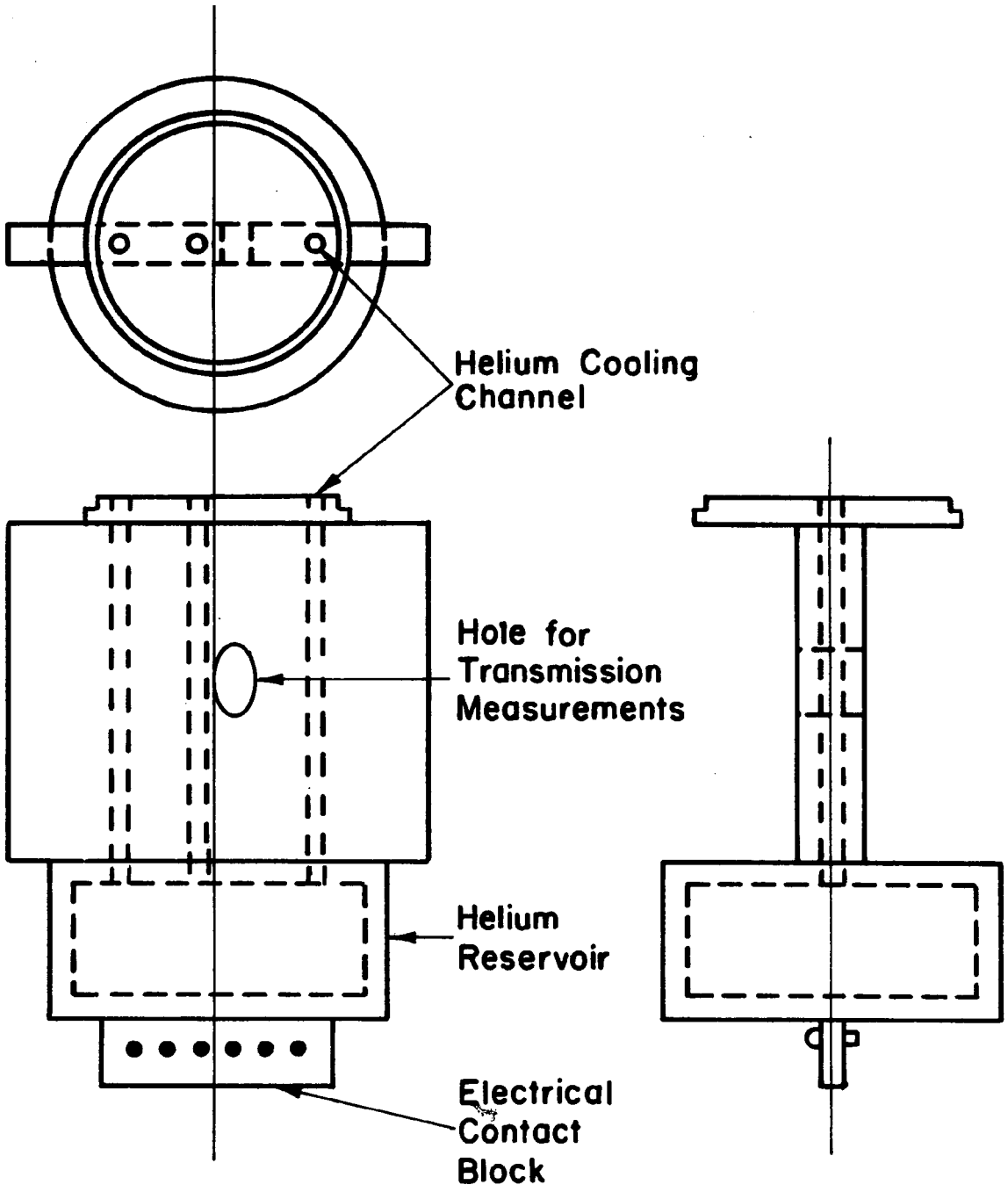


Fig. 7. Sample Holder for Optical Measurements

Since the sample was not immersed in liquid helium, the sample temperature was $9^{o}K$ instead of $4.2^{o}K$. Provision was also made for passing six electrical leads from the sample holder to the outside of the dewar.

For the measurements done at Wright-Patterson A.F.B., the sample was immersed in liquid helium. This provided another objective for these measurements: to determine if the spectra at $4.2^{o}K$ were significantly different in any way from those taken at $9^{o}K$.

B. Transmission

Transmission measurements on CdTe were made with the same dewar and measuring apparatus described in the previous paragraphs. The wavelength range was scanned with and without a sample in position and the two measurements compared. Transmission spectra were taken from 7500 Å to 2.6 microns at $9^{o}K$, using a tungsten projection lamp as a light source.

Transmission samples were prepared by cutting and polishing wafers. Single crystal sections were cut from the wafers and etched in the solution described earlier. Final sample thickness was about 0.5 mm.

5. Sample Irradiation

The University of Michigan Ford Nuclear Reactor, a swimming-pool research reactor which operates at two megawatts, was used for irradiation. The highest thermal neutron flux available in the core, composed of enriched U-235 fuel elements partially surrounded by graphite reflectors, was approximately 2×10^{13} neutrons/cm^2/sec. However, the cadmium ratio (thermal flux/fast flux) at the position of maxium flux was only 6.

To minimize fast neutron effects by using a higher cadmium ratio, the irradiations were done in the water moderator three to twelve inches from the core face at the core centerline. At the closest position the thermal neutron flux was 10^{12} neutrons/cm^2. sec. and the Cd ratio was 12. Other advantages of doing irradiations in the water moderator were that the ambient temperature and the intensity of beta and gamma radiation were lower.

Several types of sample holders were used in the reactor pool over the duration of this study. The most recent, and most widely used, was a horizontal stringer, mounted at the core face, with a series of aluminum cups fastened to it as shown in Figure (8). The cups were four inches apart, centerline to centerline, with the first cup being 3 inches away from the core face. The fluxes in the three closest cups were:

Cup #1 $\phi_{th} = 1.8 \times 10^{12}$ neutrons/cm^2 . sec.

#2 $\phi_{th} = 4.3 \times 10^{11}$ neutrons/cm^2 . sec.

#3 $\phi_{th} = 6.5 \times 10^{10}$ neutrons/cm^2 . sec.

Water temperature at any of these locations did not exceed 100^{o}F.

Preliminary experiments showed that CdTe samples oxidize when placed in a thermal neutron environment. To avoid oxidation, the majority of the Hall and emission samples were placed in glass tubes which were repeatedly evacuated and flushed with argon. The tubes were sealed off with about 2/3 atm. argon and then placed in rubber diaphragms which, in turn, were enclosed in 4 ounce wide mouth polyethylene bottles and lowered into the cups on the stringer.

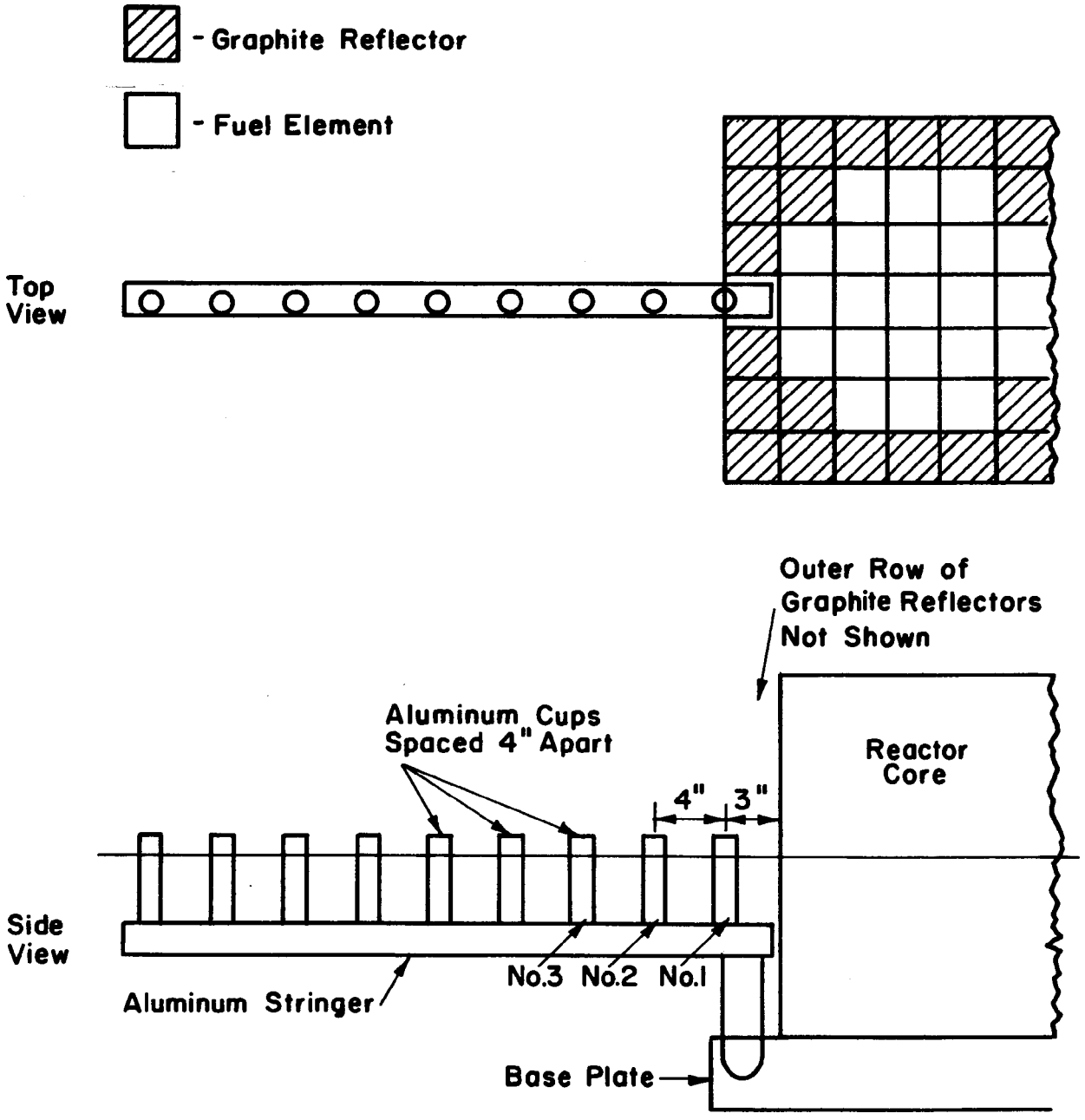


Fig. 8. Schematic Diagram of Thermal Neutron Irradiation Facility

Because of flux depression within the sample the Cd ratio was less than 12, and, hence, a significant amount of fast neutron damage was expected. To separate fast neutron effects from thermal neutron effects a few samples were irradiated in thermal neutron shields. Although Cd shields were used in early experiments, boron nitride containers were employed for most of the samples. There were three advantages to using BN. First, the intense gamma flux from a Cd shield was avoided. Secondly the radioactivity of BN is much less than that of Cd so that the samples could be removed from the pool sooner. Third, BN machines very well, and convenient, easy-to-handle containers could be made. Because the thermal neutron absorption cross-section of BN is less than that of Cd, the wall thickness of the BN containers had to be greater. The minimum wall thickness used was 1/4" which reduced the thermal flux by a factor of 700 at E_n = 0.4 ev.

Following irradiation, the samples were stored in the pool for a period varying from one day to one week depending on the $(nvt)_{th}$ used. After removal from the pool the samples were washed in ethyl alcohol and a dilute solution of HCl.

During each irradiation the flux was monitored with 1 mil gold foils approximately 1/16" x 1/16" which were placed near the sample surface to measure ϕ_s, the surface flux. A Cd covered foil was also enclosed in the sample package at a large enough distance from the sample so that the Cd cover did not perturb the flux at the sample. Gold foils were also enclosed with the samples irradiated in BN containers. After irradiation

the foils were weighed on a Kahn electrobalance and counted in a well counter using a NaI:Tl scintillator. The efficiency of the well counter, 66%, was determined with calibrated gold foils.

An isochronal annealing experiment was done on an irradiated p-type CdTe sample. Annealing time was 10 minutes at temperatures between 100°C and 220°C. Following irradiation, electrical leads were removed from the sample with a minimum of heating. The sample was sealed off in a glass tube containing an argon atmosphere and annealed in a small furnace. After the anneal, electrical leads were replaced and the resistivity was measured as a function of temperature.

IV. EXPERIMENTAL RESULTS

In this Chapter we will present the results of Hall, resistivity and luminescence measurements on CdTe and CdS as a function of thermal neutron irradiation. Thermal neutron irradiation causes a decrease in carrier concentration and conductivity of both p-and n-type CdTe and also CdS. A decrease in the edge emission intensity is also observed with the high energy (X) series (see page 87) predominating after long irradiation times. The defects responsible for these changes anneal out between 160°C and 200°C according to resistivity measurements on p-type CdTe.

The results of electrical measurements on n and p-type CdTe are presented first, followed by Hall data on CdS. This, in turn, is followed by the luminescence results.

6. Hall Effect, Resistivity and Mobility

A. n-Type Cadmium Telluride

Hall and resistivity measurements were made on three samples of n-type CdTe which were exposed to thermal plus fast neutrons. One sample, GE-231, was studied in detail at low dosages. The variation of carrier concentration in this sample as a function of 1/T and thermal plus fast neutron irradiation is shown in Figure (9). The carrier concentration, n, is calculated from the well-known relation

$$|R_h| = \frac{r}{ne} \tag{20}$$

where R_h is the measured Hall coefficient and r is a constant which is

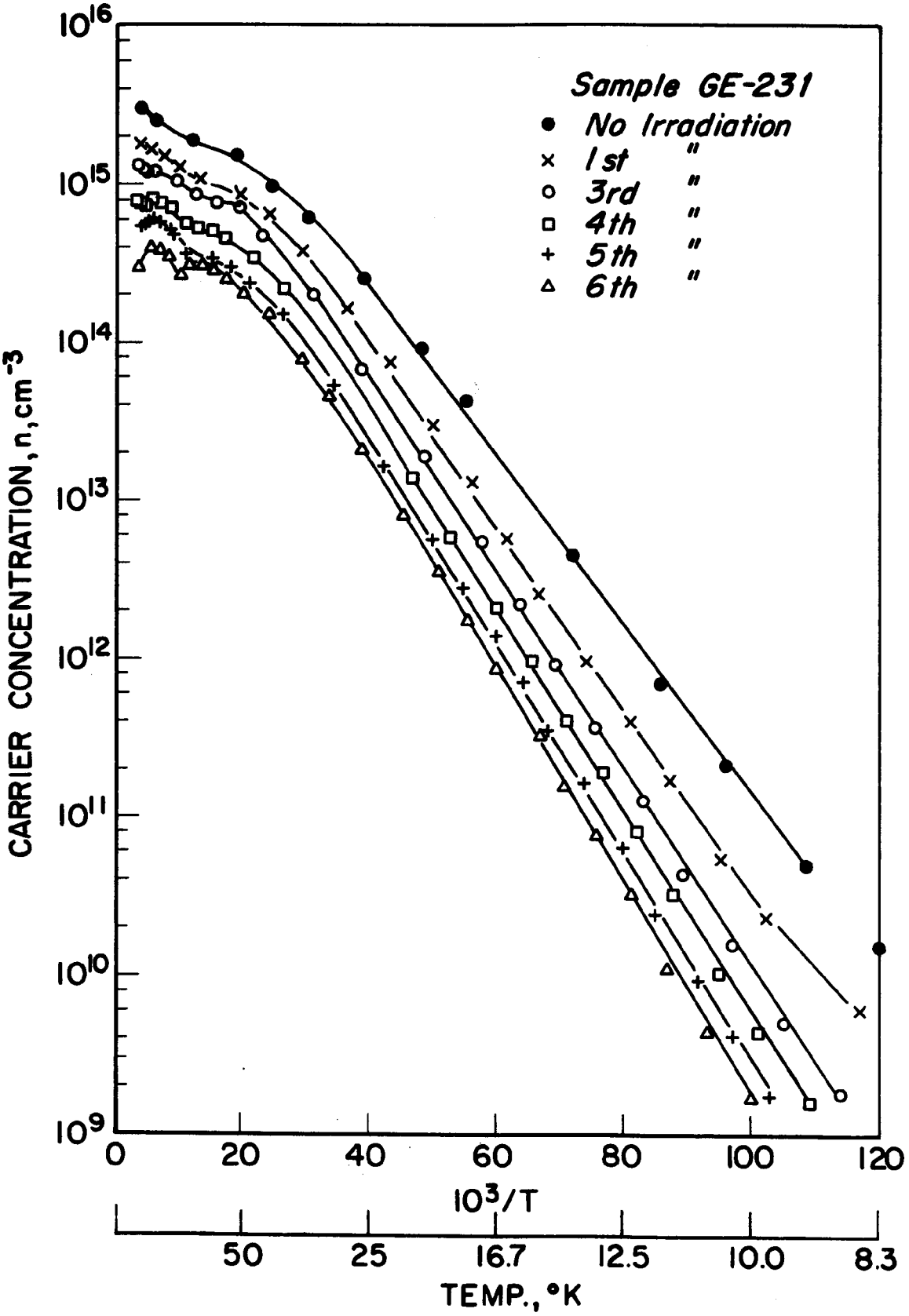


Fig. 9. Carrier Concentration of n-type CdTe as a Function of 1/T and Thermal plus Fast Neutron Irradiation

approximately equal to one. For $10^3/T$ greater than 20 ($T = 50^oK$), these curves are characteristic of freeze-out of electrons into a shallow donor. In this temperature region, the curves can be analyzed using the well-known relationship between n and N_D, the donor concentration, N_A, the acceptor concentration, and E_D, the donor ionization energy:

$$\frac{n(N_A + n)}{N_D - N_A - n} = \frac{N_c}{2} e^{-E_D/kT} \qquad (21)$$

where

$$N_c = \frac{2(2\pi m_e^* kT)^{3/2}}{h^3}$$

for CdTe, $m_e^* = 0.11\, m_e$ (37) and $N_c = 1.778 \times 10^{14}\, T^{3/2}$. At lower temperatures where the curves are straight lines, $n \ll N_D$ and $n \ll N_A$ so that equation (21) simplifies to

$$n = \left(\frac{N_D - N_A}{N_A}\right) \frac{N_c}{2} e^{-E_D/kT} \qquad (22)$$

After correcting for the $T^{3/2}$ term in N_c, the straight-line portions give E_D and $\frac{N_D - N_A}{N_A}$. At higher temperatures where the curves are non-linear ($15 < 10^3/T < 35$) equation (21) is used to fit the curves and obtain N_D and N_A for each irradiation. E_D is .009 ev before irradiation and stabilizes at 0.012 ev after the third irradiation. Segall (37) has shown that this level is due to a chemical impurity.

The number of absorption events occurring during each irradiation,

$\Sigma_a \bar{\phi}\, t$ (where t is the irradiation time) is calculated from equation (17). The data can then be presented in the form shown in Figure (10) where $n_e = (N_D - N_A)$, the total number of electrons available from the shallow donors, and the abscissa is the cumulative number of absorption events. The initial removal rate,

$dn_e/dR\Big|_{R=0}$, where $R = \Sigma_a \bar{\phi}\, t$, is approximately -1.0.

A similar curve for another sample, GE-232, is also shown in Figure (10). The carrier concentration curves from which this curve is derived are shown in Figure (11). This sample, along with a third, was irradiated for longer times in order to verify Chester's statement that n-type CdTe is converted to p-type (32). However, after 3×10^{17} absorptions/cm^3 the material was still n-type.

The behavior of n in the high temperature range for all three CdTe samples is contrary to simple freeze-out of carriers at impurities. That is, the electron concentration increases as the sample is cooled. The same curve is obtained on heating and cooling. Care was also taken in allowing the sample to reach thermal equilibrium in this range. Therefore, the inverse variation of n with 1/T is apparently a real effect and not due to temperature cycling or annealing. After short irradiation times the anomalous behavior of n extends up to room temperature (see Figures (9) and (11)). After longer irradiations the effect is more dramatic as illustrated by the curve for the fourth irradiation of GE-232 in Figure (11). Similar curves are shown in Figure (12) for the third sample, GE-230.

At higher temperature there is some indication of normal freeze-out into a level at .06 ev as shown in Figure (11). However, the existence of

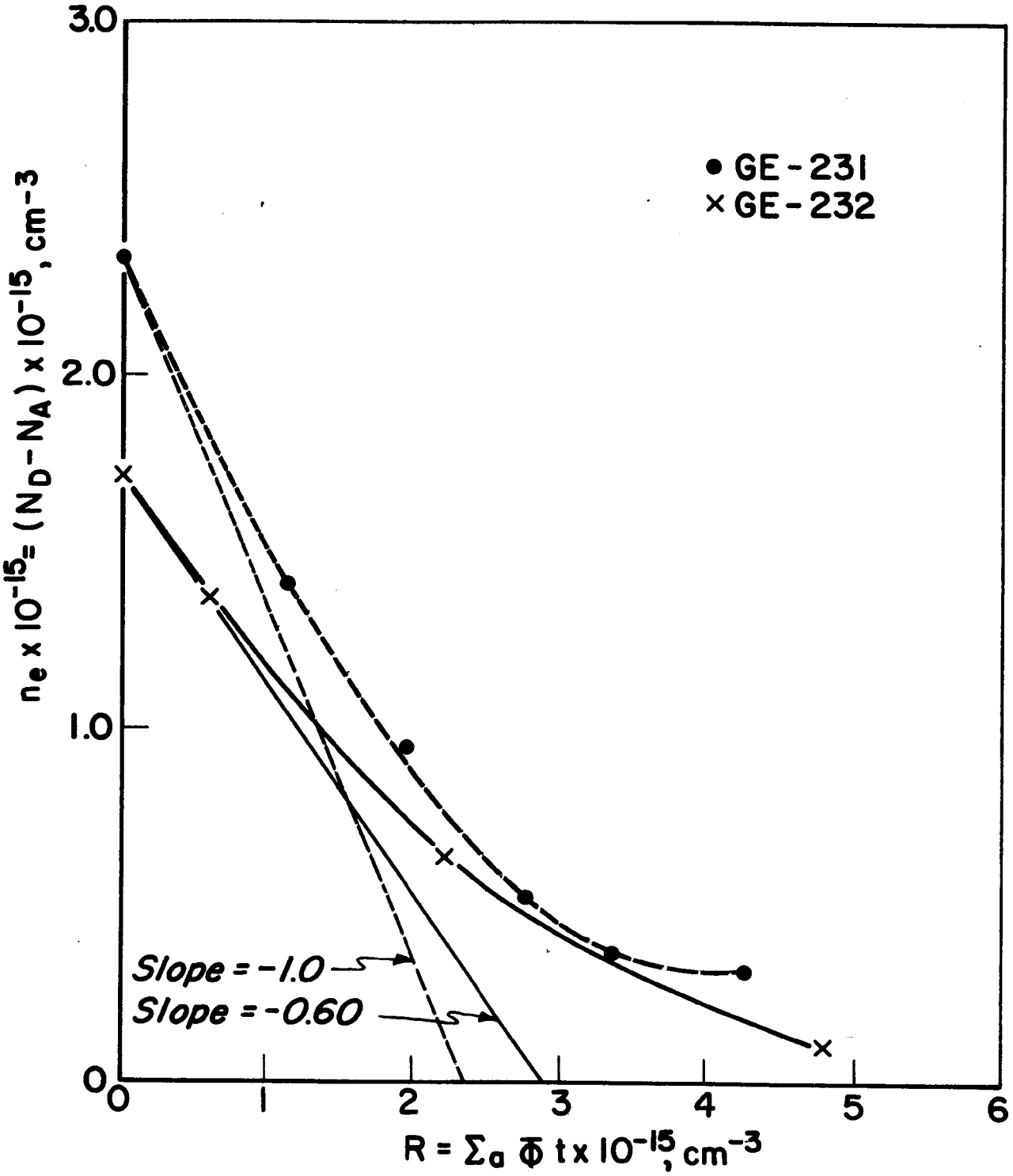


Fig. 10. Total Number of Electrons/cm^3 Available from Shallow Donors in n-type CdTe versus Cumulative Number of Absorption Events

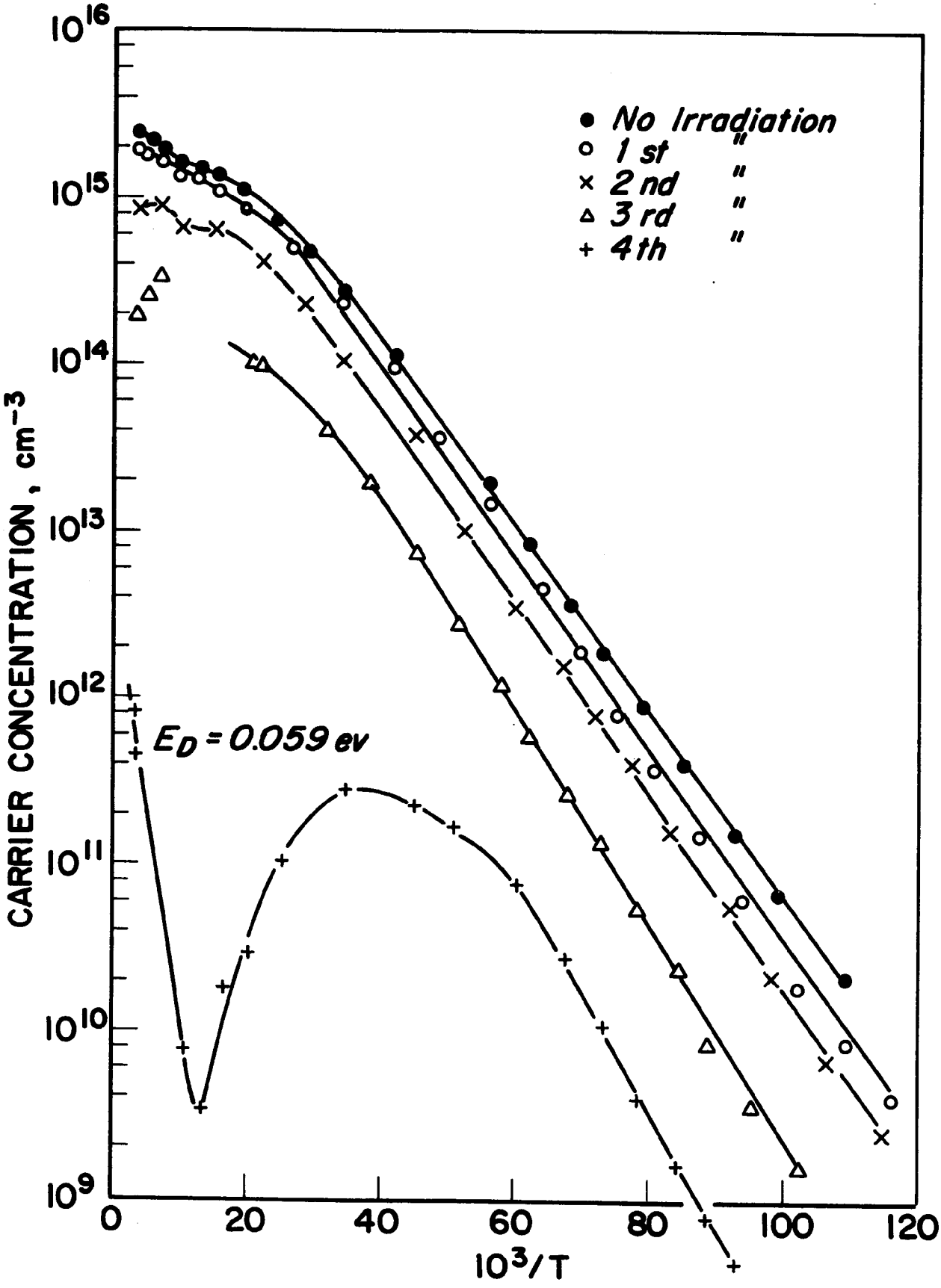


Fig. 11. Carrier Concentration Versus Reciprocal Temperature as a function of Thermal Plus Fast Neutron Irradiation for Sample GE-232

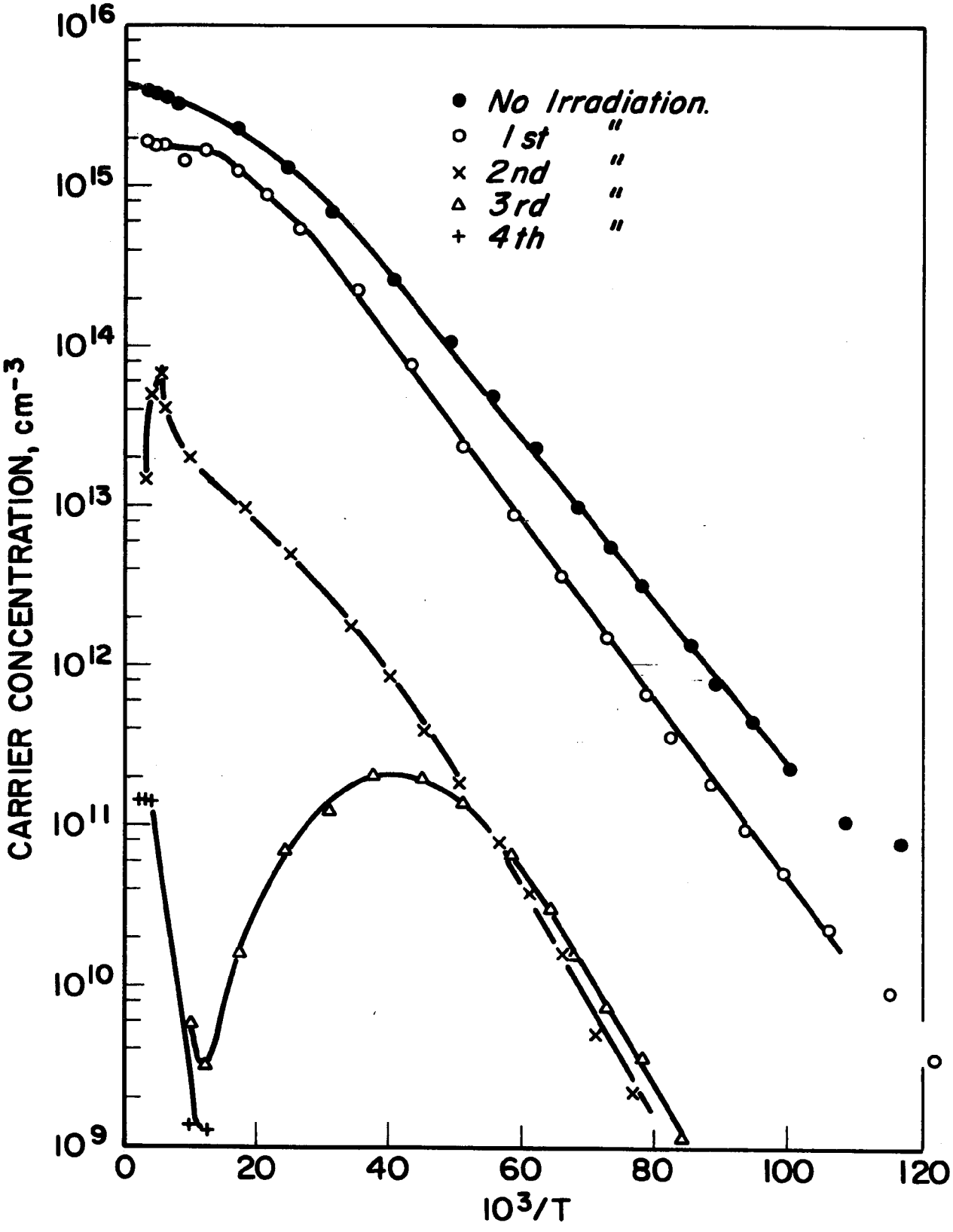


Fig. 12. Carrier Concentration versus Reciprocal Temperature as a Function of Thermal Plus Fast Neutron Irradiation for Sample GE-230

this level as established by carrier concentration (Hall) measurements is tenuous because Hall measurements on CdTe become extremely difficult in the temperature range 77°K to 300°K after long irradiation times. This is illustrated in Figures (9), (11) and (12) by the gaps in the data in this range. In Figure (11), the line establishing the level at .06 ev is determined by only three points. Further evidence for a deeper level at about .06 ev does exist, however. In Figure (12) the few points shown for the fourth irradiation of GE-230 are similar to those in Figure (11) which determine the .06 ev level. The resistivity of GE-230 after long irradiation, shown in Figure (13), also implies a level at .06 ev. The resistivity of CdTe after long irradiation increases with decreasing temperature. However, ρ reverts back to its original behavior (see below) at lower temperatures as indicated by the turn-over in Figure (13). Although there is significant scatter in the data, comparison with the accompanying straight line, corresponding to .06 ev, indicates a deep level at about .06 ev. After long irradiation times one would expect the resistivity curves to have a slope corresponding to the energy level. This is because the mobility at low temperatures is depressed by the introduction of a large number of scattering centers and is relatively constant over the temperature range of interest.

The variation in resistivity and mobility at smaller neutron dosages is shown in Figures (14) and (15) which are for the first sample discussed, GE-231. These curves are fairly representative of all three CdTe samples. As expected, the resistivity increases with irradiation. The curves maintain approximately the same shape until, as indicated above, long irradiation

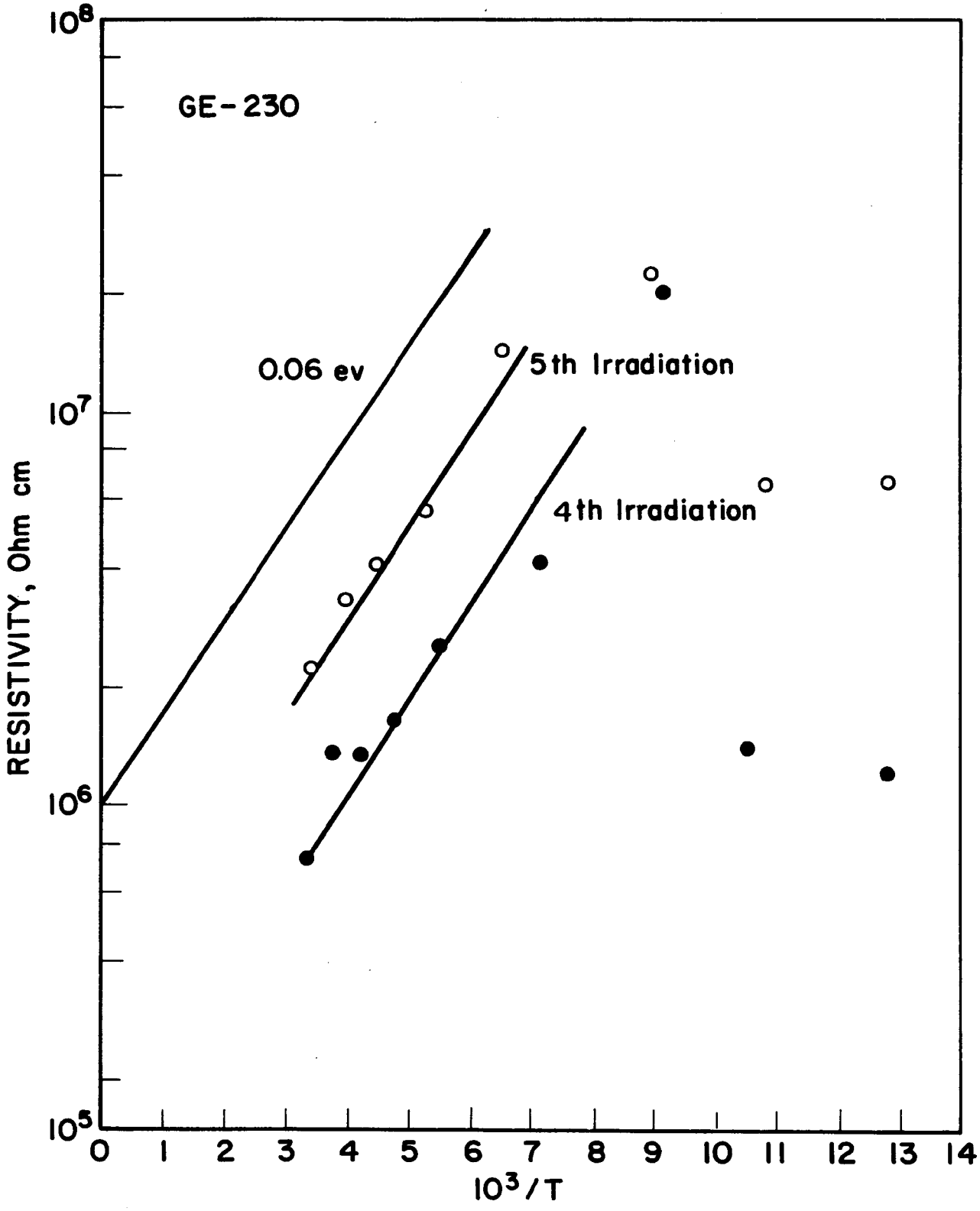


Fig. 13 Resistivity Versus 1/T for n-type CdTe (Sample GE-230) After Long Thermal Neutron Irradiation Times

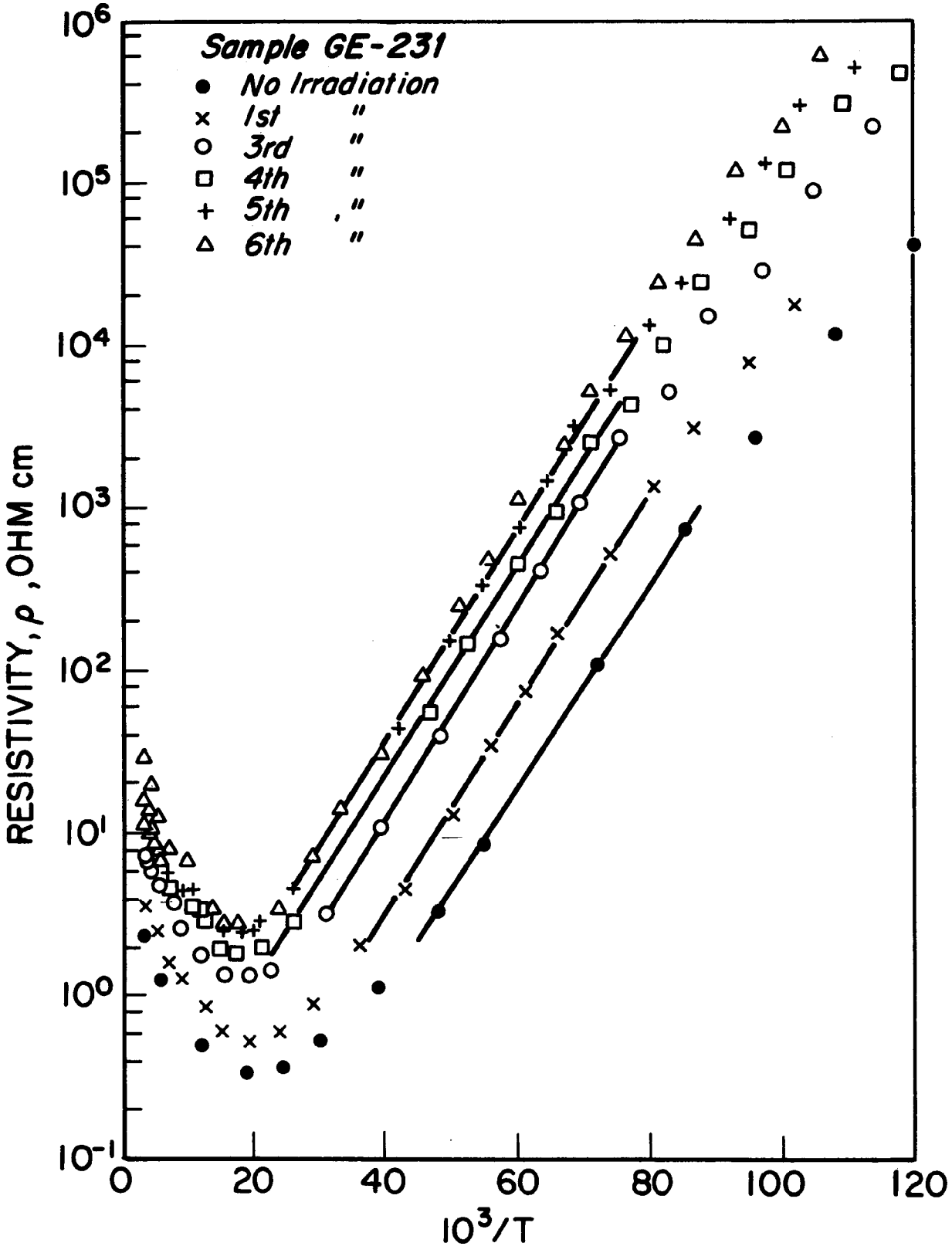


Fig. 14. Resistivity Versus 1/T for n-type CdTe (Sample GE-231) After Short Thermal Neutron Irradiation Times

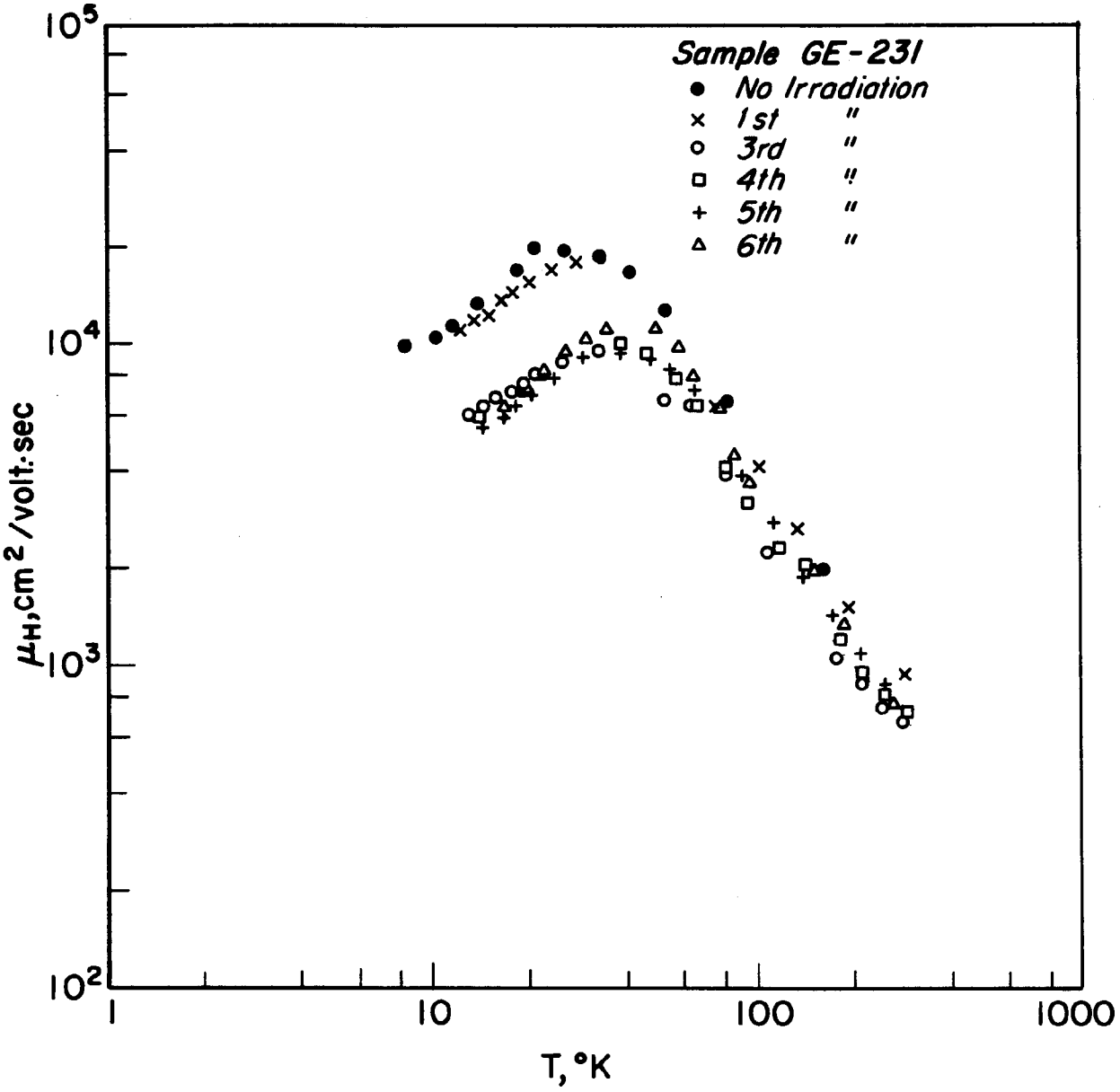


Fig. 15. Mobility Versus Temperature for Sample GE-231 After Successive Thermal Neutron Irradiations

has taken place.

The Hall mobility, which is obtained by dividing the Hall coefficient by the resistivity, is relatively insensitive to irradiation at high temperatures. This follows from the fact that lattice scattering dominates in this temperature range. However, at lower temperatures ionized impurity scattering is most important and the mobility decreases with irradiation indicating the introduction of ionized scattering centers. The decrease in mobility at low temperature cannot be attributed to a movement of the Fermi level, that is, to a change in charge state of defects already present. This follows from the fact that the Fermi level at $20^{o}K$, for example, remains within .003 ev of the shallow donor over the first six irradiations.

In order to investigate the effects of fast neutrons, a fourth n-type CdTe sample, GE-200, was placed in a BN container and irradiated several times at the same position (C-3) that GE-231 was irradiated. As indicated in Figure (16) there is very little change in the electron concentration due to irradiation over the entire temperature range. Total irradiation time for this sample was 4 hours, approximately 4 times that for GE-231. This time is roughly equivalent to the total irradiation time for GE-232 after the fourth irradiation (see Figure (11)). Using the average saturated activity of the Cd-covered gold foils exposed during the irradiations of GE-200, and the average thermal flux in C-3 (6.5×10^{10} cm^{-2} sec^{-1}) for the irradiations of GE-231, one calculates a Cd ratio of 7.1. From a comparison of Figures (16) and (9), one concludes that, for this Cd ratio, thermal neutron induced damage is much more significant than fast neutron damage. Recall that the other

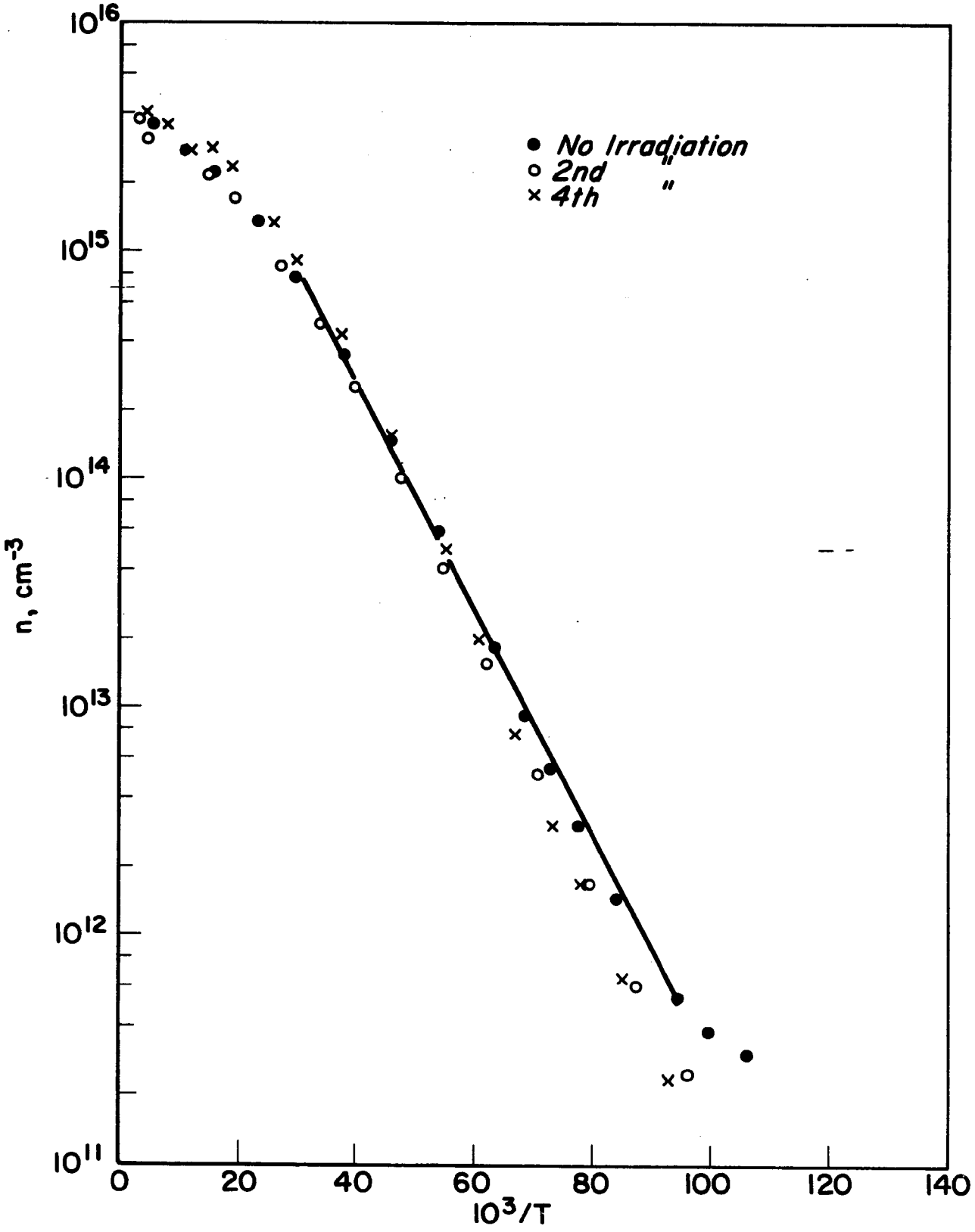


Fig. 16. Change in Carrier Concentration Versus 1/T for n-type CdTe Exposed to Fast Neutrons Only. Sample GE-200

three samples were exposed to thermal plus fast neutrons. Since the changes due to fast neutrons alone are negligible, it is not necessary to modify Figure (10) to account for fast neutron damage.

B. p-Type Cadmium Telluride

Hall measurements on p-type CdTe reveal that thermal neutron irradiation causes a decrease in carrier (hole) concentration in p-type CdTe. This is illustrated in Figure (17) which shows the Hall coefficient vs. reciprocal temperature as a function of thermal plus fast neutron irradiation for two p-type samples. The solid lines are for sample MH-3A while the dashed lines are for the second sample, MH-1. The hole concentration, p, is much less than N_D and N_A over the entire temperature range so that one is restricted to the use of equation (22) (see page45) in analyzing the data and only E_A and $\left(\frac{N_A - N_D}{N_D}\right)$ can be found. Because the levels are deeper, it is not necessary to correct for the $T^{3/2}$ variation in equation (22). Consequently, the slope of the Hall curves gives E_A directly. As in Figure (17), the conduction in all MH samples before irradiation is dominated by a level at about E_v + 0.15 ev. Conduction from this level persists until after the second irradiation. At this point, holes freeze out into a level at E_v + .20 ev. Further irradiation reveals levels at about .3 ev and .44 ev. Several authors (32) (39) showed that many impurities possess energy levels in the range, .28 ev to .5 ev.

Resistivity curves corresponding to the Hall data in Figure (7) are shown in Figure (18). The similarity between the Hall and resistivity curves indicates that the mobility does not change drastically with temperature for

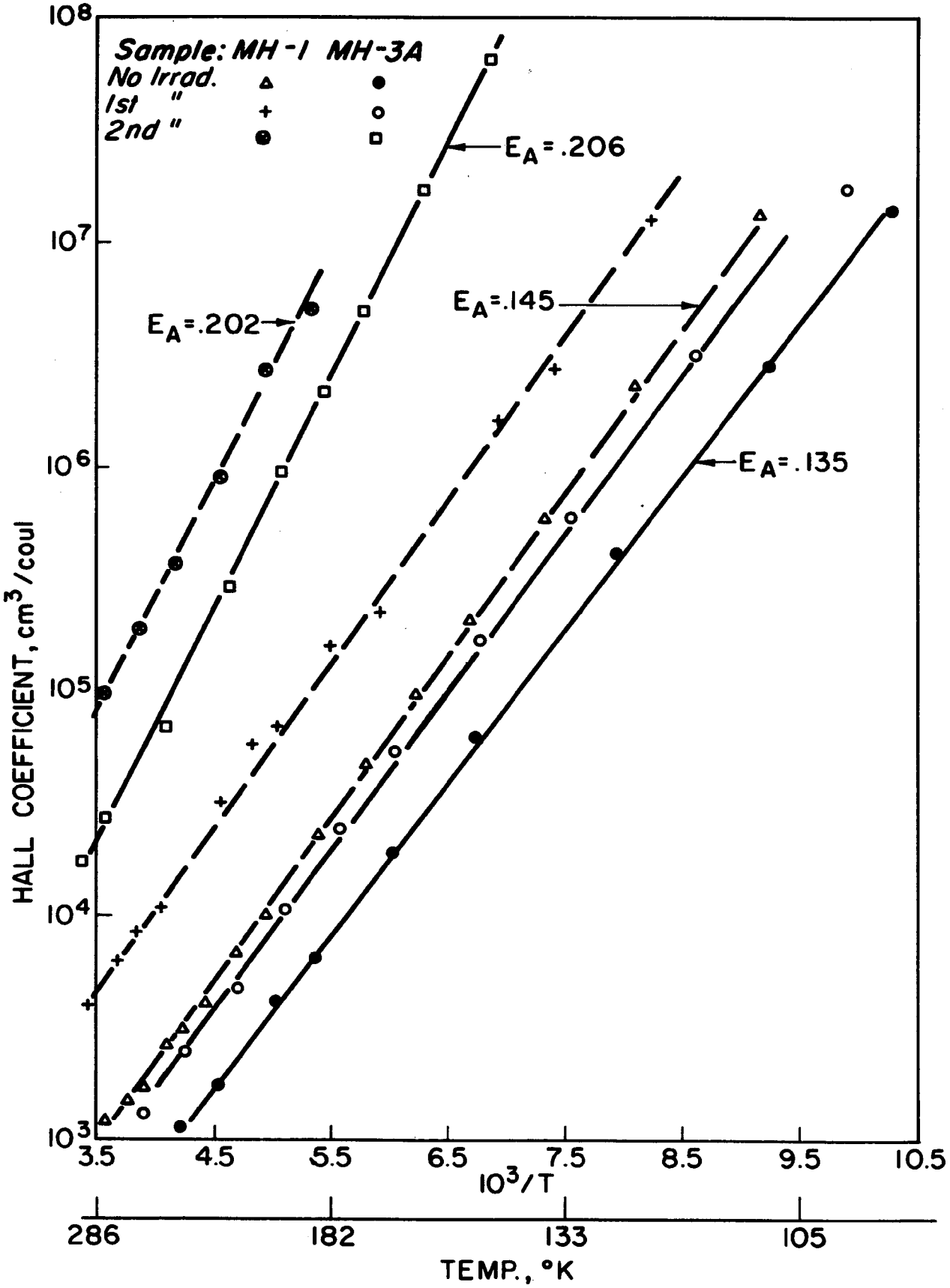


Fig. 17. Hall Coefficient Versus 1/T as a Function of Thermal Plus Fast Neutron Irradiation for Two Typical p-type CdTe Samples

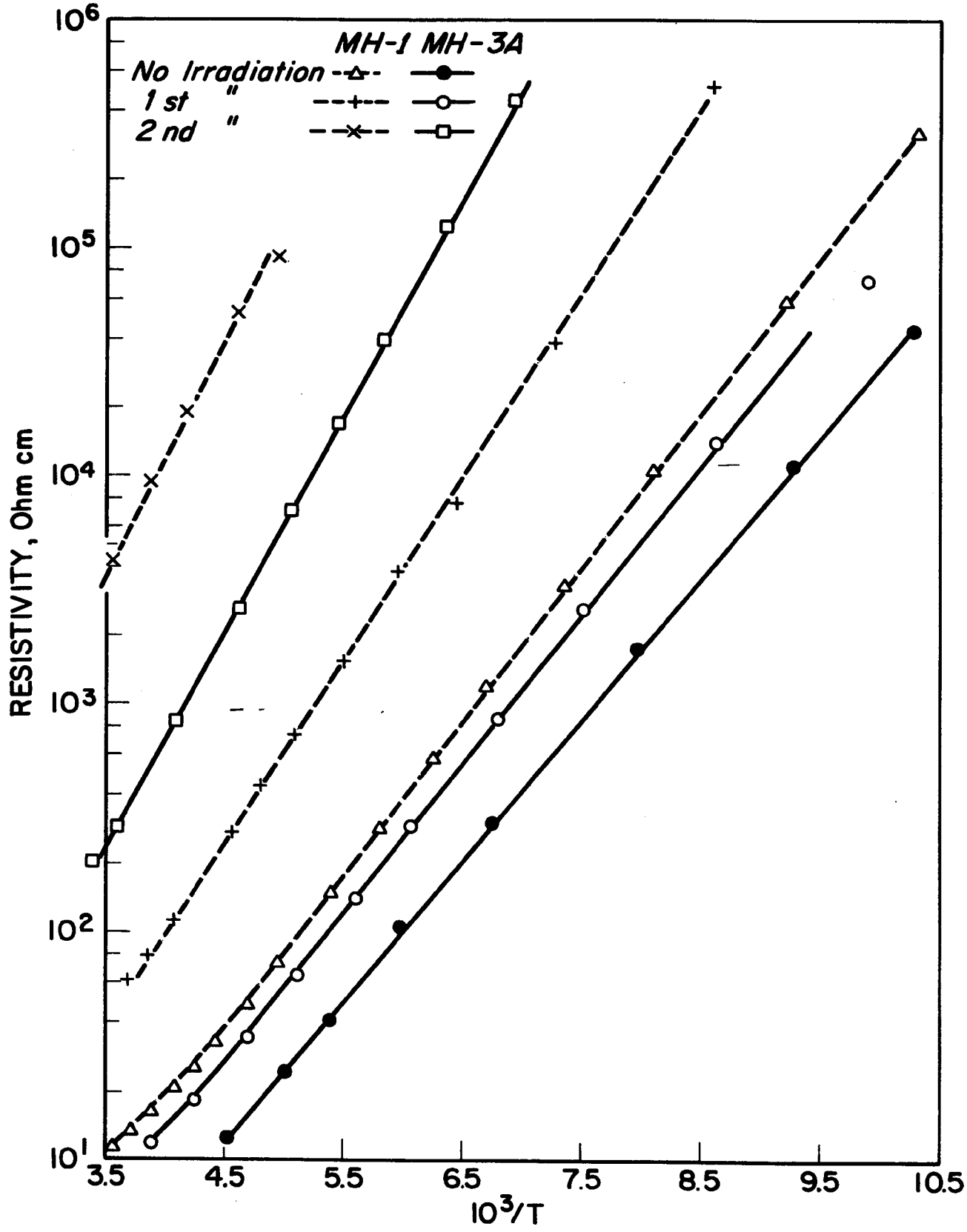


Fig. 18. Resistivity Versus 1/T as a Function of Thermal Plus Fast Neutron Irradiation for Two Typical p-type CdTe Samples

these p-type samples. This is illustrated in Figure (19) which gives the Hall mobility as a function of temperature for one of the samples, except that most of them do not show quite as large a reduction in mobility after the second irradiation. Generally speaking, the room temperature mobility lies between 50 and 100 cm^2/volt. sec over all the irradiations. After irradiation, the mobility is a slowly varying function of temperature. Therefore, the slope of the resistivity curves after irradiation should also give E_A directly since $\rho = \frac{1}{pe\mu}$

To determine whether p-type CdTe will change into n-type, sample MH-3A was subjected to longer irradiation times. After a total $(nvt)_{th}$ of nearly 10^{16} neutrons/cm^2, the room temperature resistivity was 2×10^7 ohm cm and the sample was p-type. An additional $(nvt)_{th}$ of 10^{18} neutrons/cm^2 did not change the resistivity. Because the Hall coefficient could not be measured after this last irradiation, it is conceivable that the sample was n-type. However, it is rather doubtful, especially if conduction was supposedly due to a shallow donor.

Resistivity curves for a third sample exposed to thermal plus fast neutrons are shown in Figures (20) and (21). The energy levels are quite similar to those shown in Figure (17). Following the third irradiation, this sample was annealed for 10 minute periods at five different temperatures. The resistivity curves following each anneal are given by dashed lines. The resistivity curve taken after the fifth anneal coincides with the resistivity curve measured before irradiation. Consequently, one can conclude that the hole removal which follows irradiation is due to the production of lattice displacements

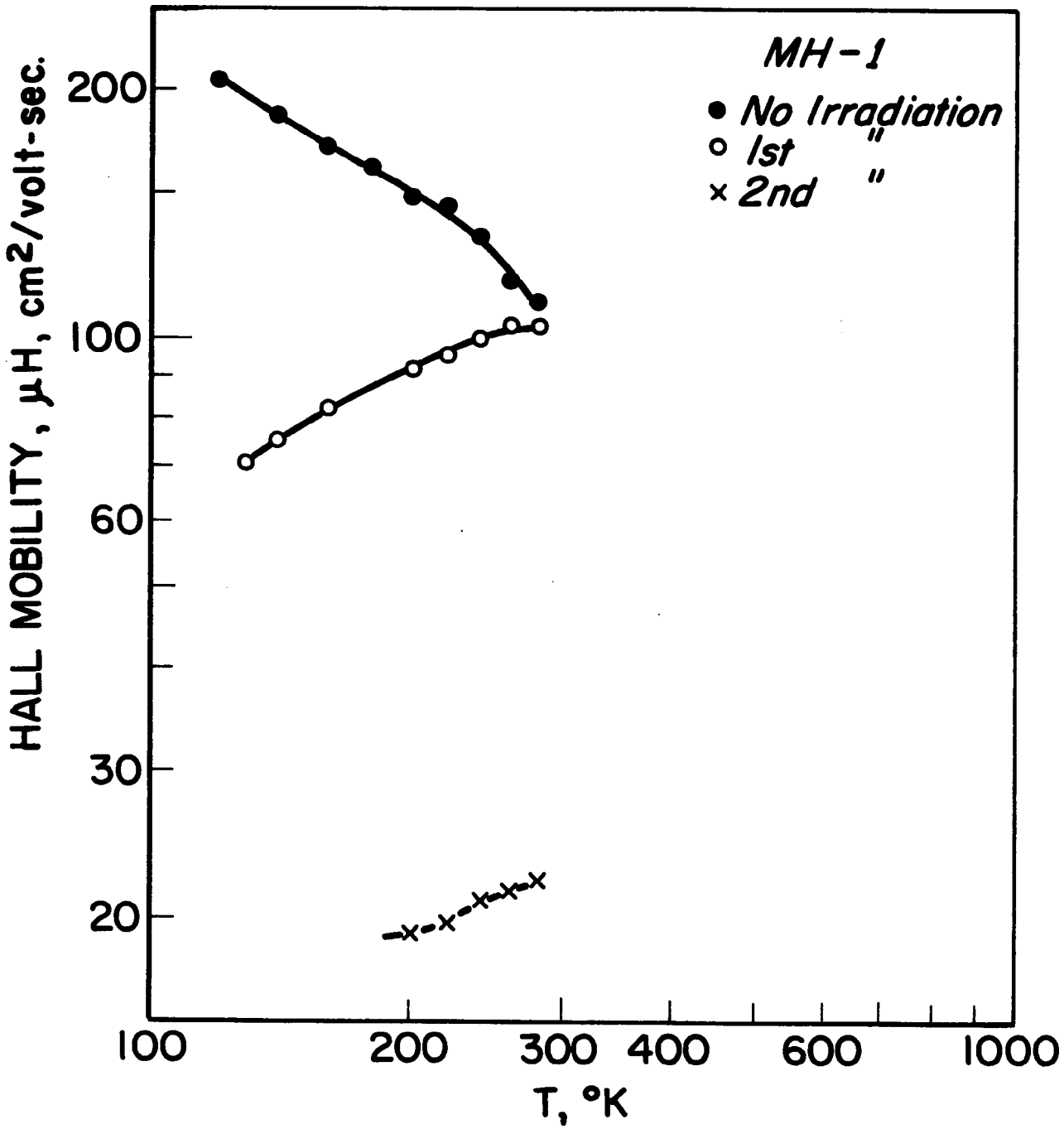


Fig. 19. Mobility Versus Temperature for p-type CdTe as a Function of Thermal Plus Fast Neutron Irradiation

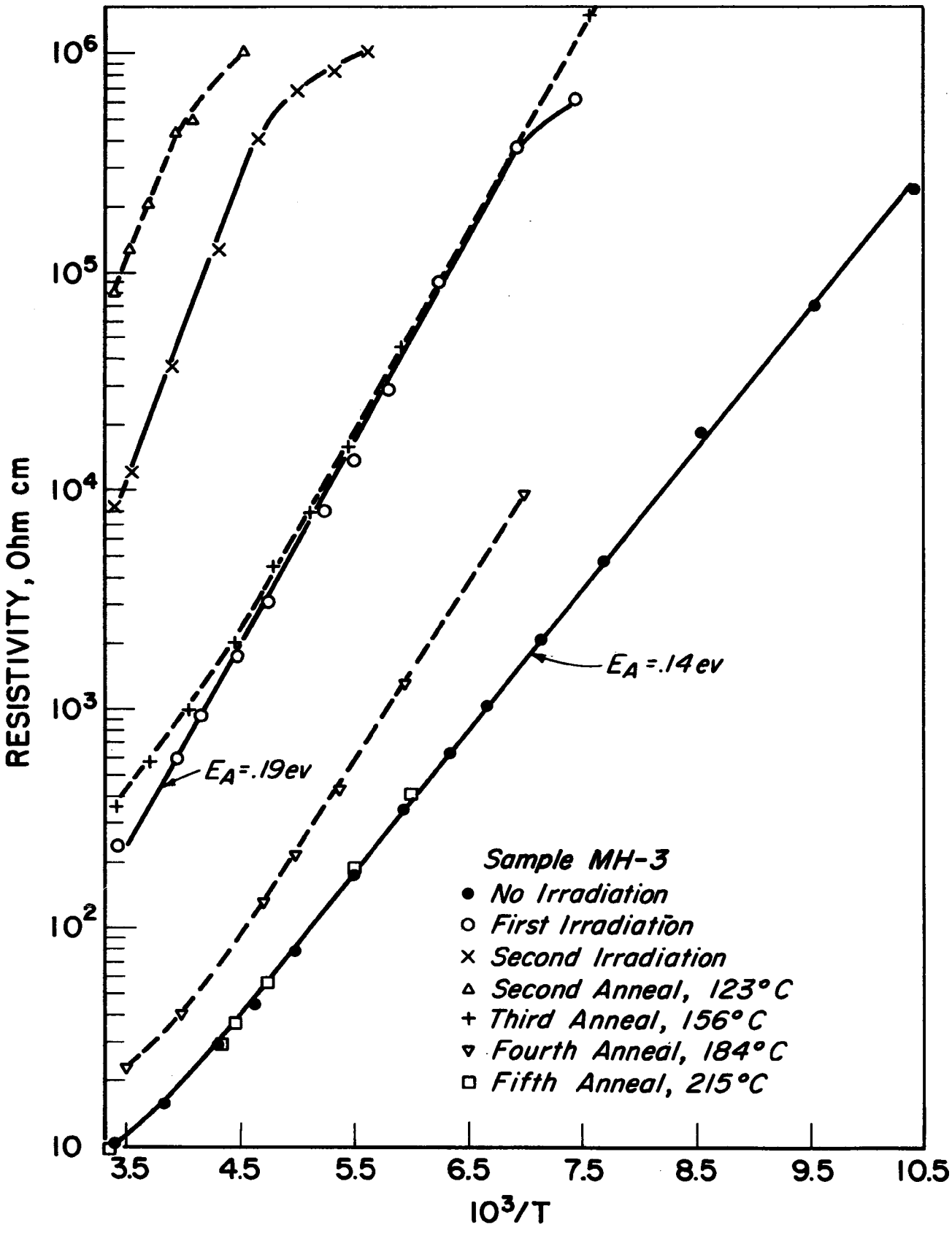


Fig. 20. Resistivity Versus 1/T for p-type CdTe Before and After Thermal Plus Fast Neutron Irradiation and also Isochronal Annealing. Annealing time: 10 min.

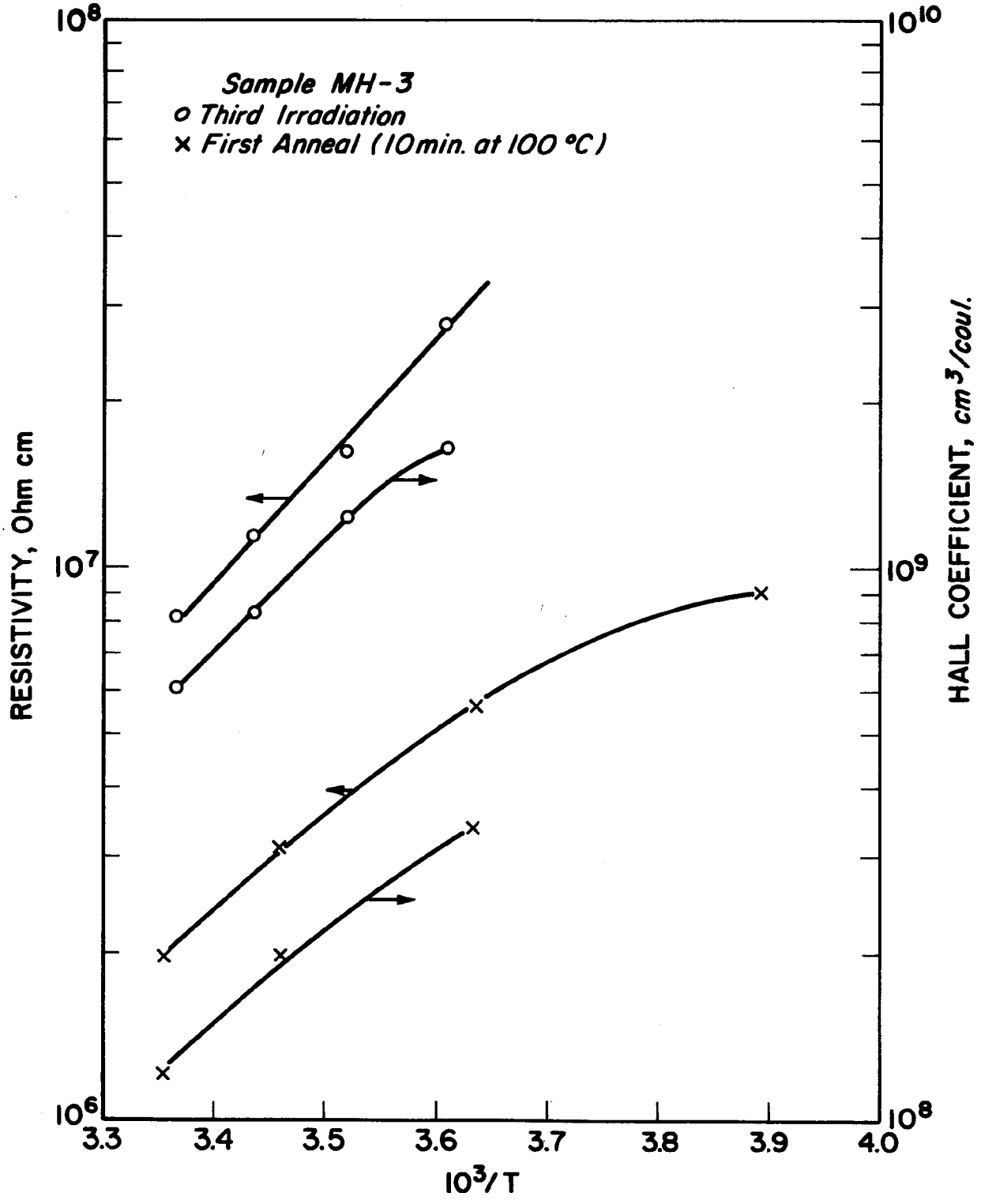


Fig. 21. Resistivity Versus 1/T for p-type CdTe After Thermal Plus Fast Neutron Irradiation and also Isochronal Annealing. Annealing time: 10 min.

and not to some extraneous effect such as oxidation or transmutation doping. If we assume that the mobility does not change during irradiation or annealing so that $p = c/\rho$, where c is a constant and ρ is the resistivity, and that the number of defects present is directly proportional to the number of holes removed, then for the nth anneal, we have

$$N_n^f = (p_o - p_n^f) = c\left(1/\rho_o - 1/\rho_n^f\right) \qquad (23)$$

where N_n^f is the number of defects present after the nth anneal, p_o is the hole concentration before irradiation, and p_n^f is the hole concentration after the nth anneal. The usual method of presenting annealing data, shown in Figure (22) is to plot the fraction of defects remaining after an anneal at temperature, T, versus T. By equation (23), the fraction of defects remaining is

$$f = \frac{1/\rho_o - 1/\rho_n^f}{1/\rho_o - 1/\rho_r}$$

where ρ_r is the resistivity after irradiation. Figure (22) shows that the defects anneal out between 160°C and 200°C.

It was also found that no annealing in CdTe takes place at room temperature. This was determined by measuring the resistivity of an irradiated sample over the period of a week. The resistivity did not change during this time.

The effect of fast neutrons on the MH material is illustrated in Figure (23) which gives the Hall coefficient versus reciprocal temperature for sample MH-2 which was irradiated along with sample MH-1. The energy level does not change and the increase in Hall coefficient over the total irradiation is much smaller than that for the samples exposed to thermal

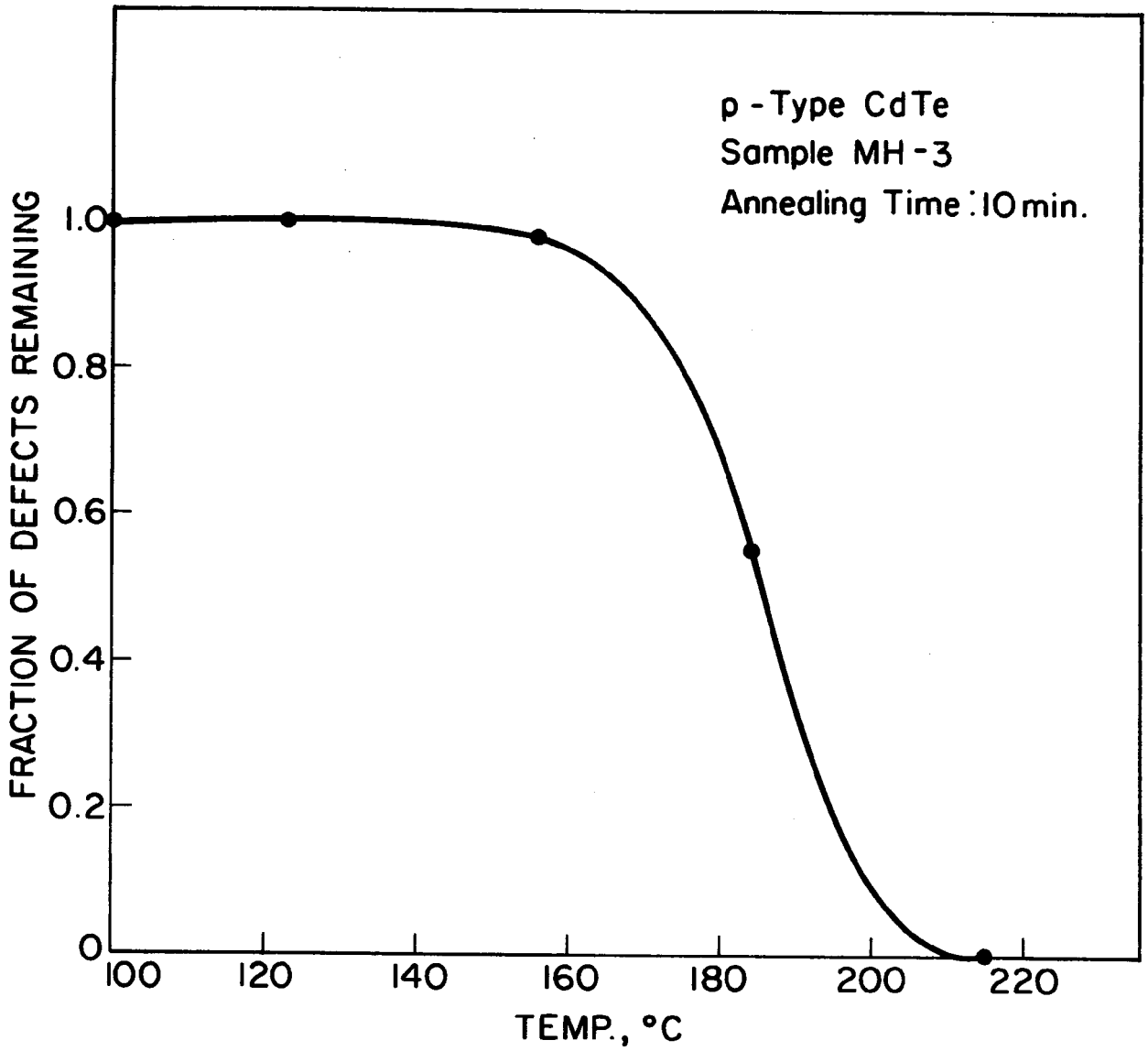


Fig. 22. Isochronal Annealing Curve for p-type CdTe After Thermal Neutron Irradiation

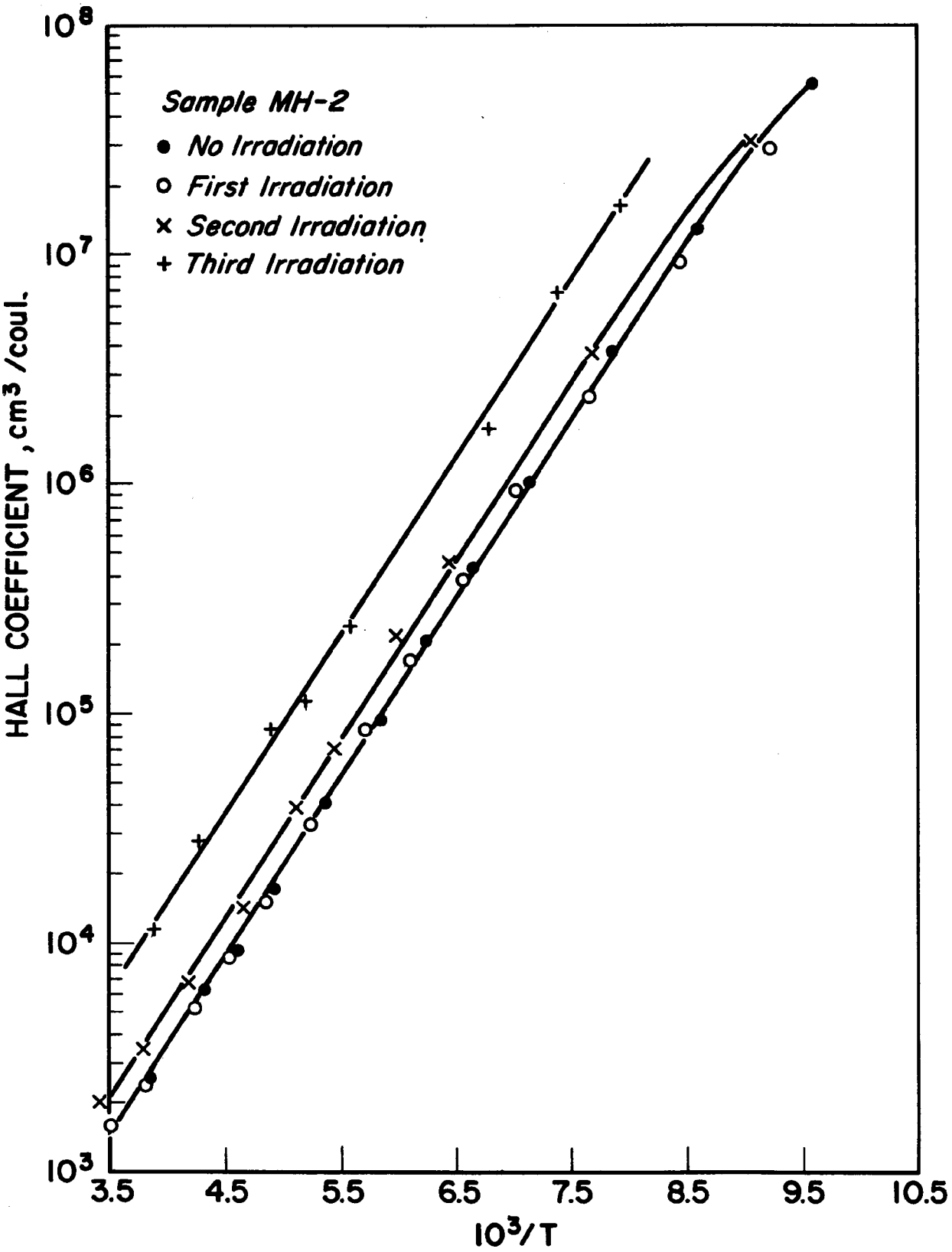


Fig. 23. Hall Coefficient Versus 1/T as a Function of Fast Neutron Irradiation of p-type CdTe

plus fast neutrons. Therefore, it is assumed that the hole removal shown in Figures (17) and (20) is essentially due to thermal neutrons only.

The effect of thermal neutron irradiation on the MH material can be summarized by presenting the hole concentration at $10^3/T = 3.5$ (286^oK) as a function of the number of absorption events/cm^3, $R = \Sigma_a \phi t$. Figure (24) is a linear plot of p versus R which is used to determine the initial hole removal rate. As indicated in the Figure, $dp/dR\Big|_{R=0} = -1.0$. This is the same order of magnitude as the initial electron removal rate for n-type CdTe. Hole removal over the entire irradiation range is shown on the semi-log plot in Figure (25). The hole removal varies exponentially with R until a limiting value of about 5×10^9 cm^{-3} is reached. This is similar to hole removal in silicon due to fast neutron bombardment (5).

C. Cadmium Sulfide

Electrical measurements similar to those carried out for CdTe were also made on a CdS sample. The variation of carrier concentration in this sample as a function of 1/T and thermal plus fast neutron irradiation is shown in Figure (26). The curves are similar to those for CdTe except for some important differences. The donor is deeper; $E_D = .017$ ev before irradiation and stabilizes at .029 ev after the sixth irradiation. In addition, the removal rate for CdS is much less than that for CdTe. This is demonstrated by constructing a graph similar to Figure (10). As for CdTe the n versus 1/T curves are analyzed using equations (21) and (22) (see page 45) except that $N_c = 4.52 \times 10^{14} T^{3/2}$ because of the difference in effective mass

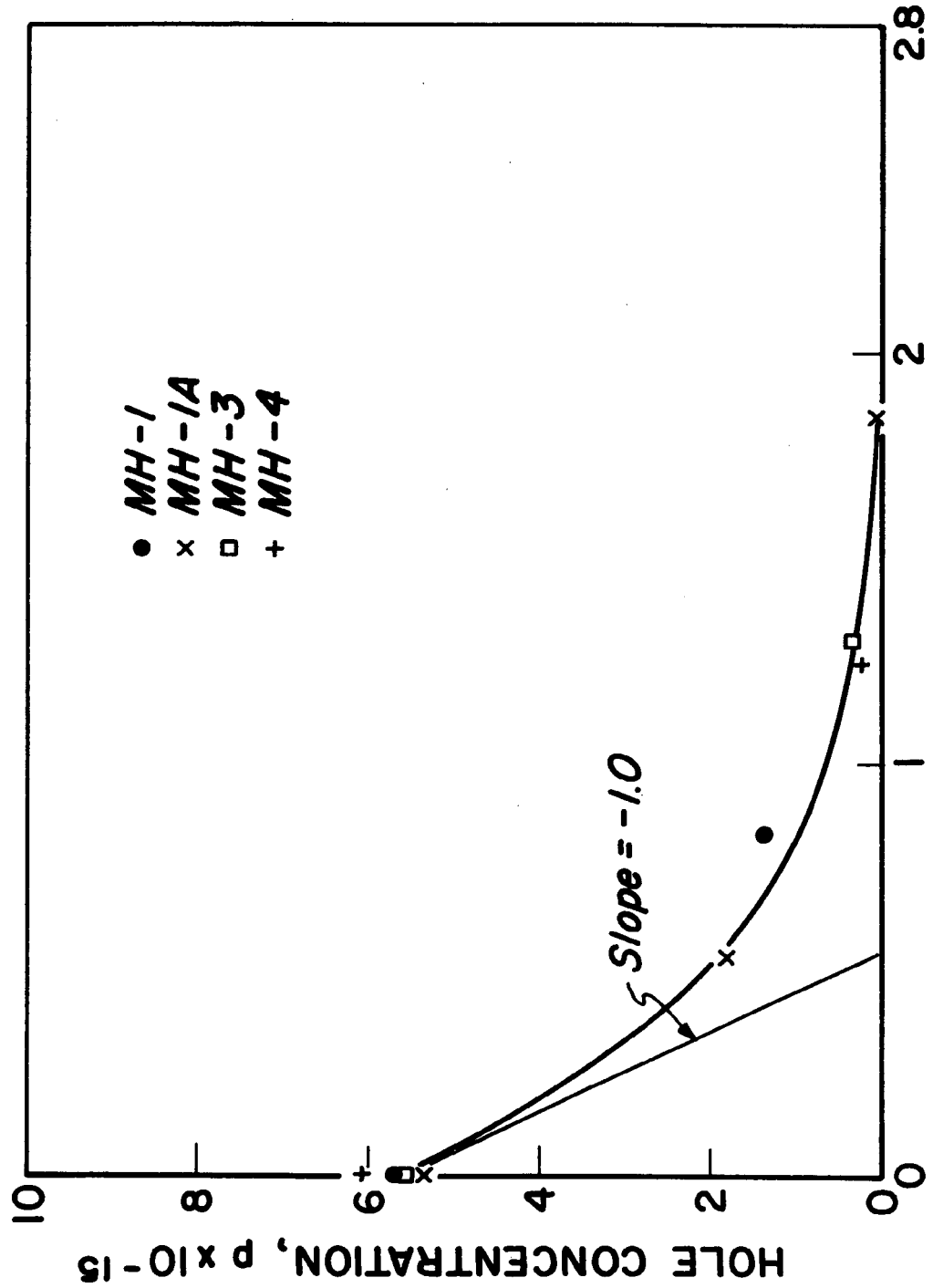


Fig. 24. Hole Concentration in p-type CdTe Versus Cumulative Number of Absorption Events for Short Irradiation Times

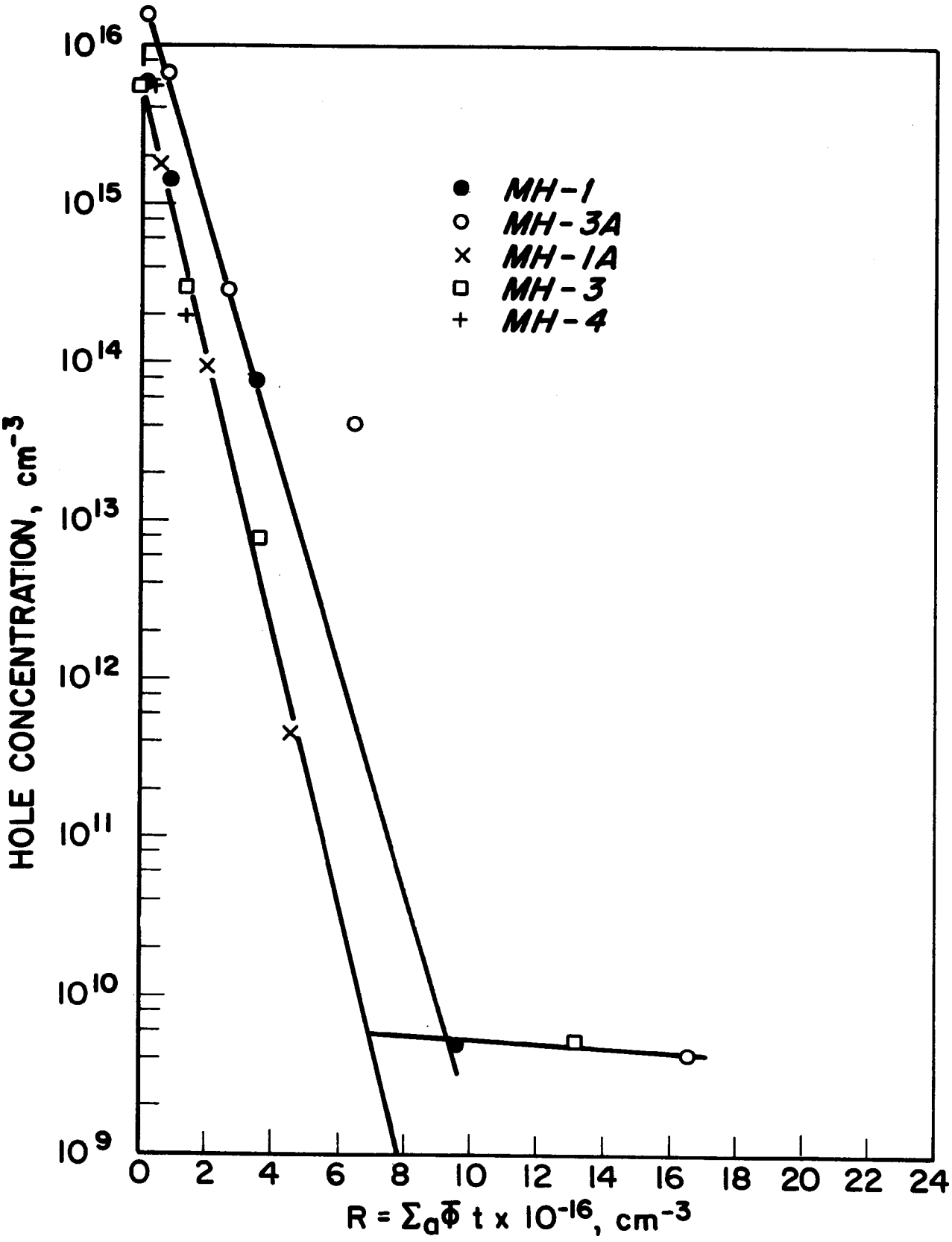


Fig. 25. Hole Concentration in p-type CdTe Versus Cumulative Number of Absorption Events Over the Entire Range of Irradiation

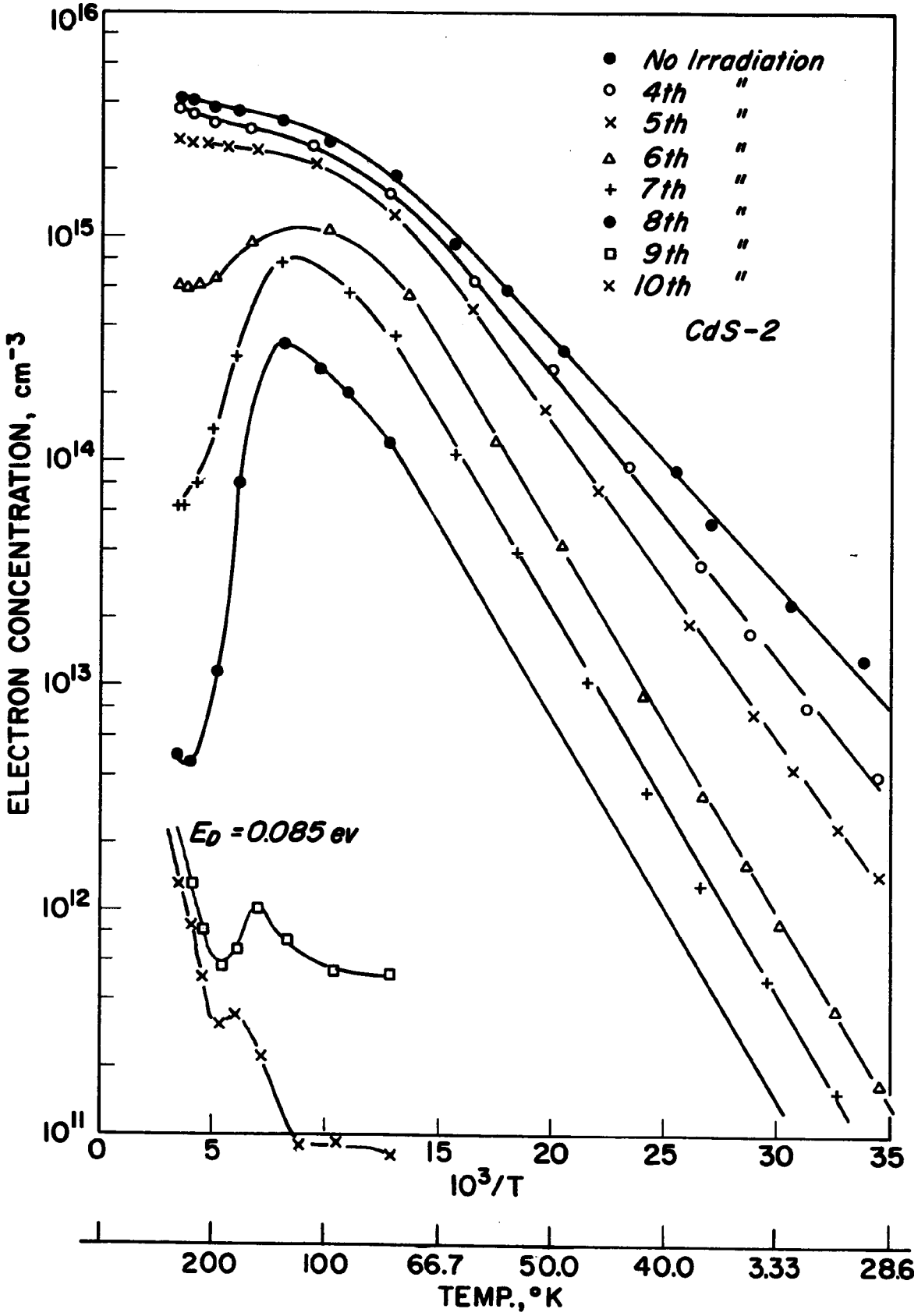


Fig. 26. Carrier Concentration in Bulk CdS as a Function of 1/T and Thermal Plus Fast Neutron Irradiation

($m_e^* = 0.205\ m_e$ for CdS (32)). The resulting plot of n_e versus R is shown in Figure (27). In this case the initial electron removal rate is about 0.1 electron per absorption, approximately one tenth that for n-type CdTe.

Returning, for the moment, to Figure (26), for short irradiation times the electron concentration, n, at high temperatures (greater than 100^oK) exhibits an exhaustion region. This is to be expected since the shallow donors are empty at higher temperatures. However, as irradiation proceeds n increases with decreasing temperature in this region as in the case of CdTe (see page 46). Further irradiation leads to a decrease in the anomalous behavior of n and to a return to normal behavior in the high temperature range. The shallow donor is exhausted at $10^3/T = 13$ and thermal excitation of electrons from a level at $E_c - .085$ ev begins as the sample is heated to higher temperatures.

The variation of resistivity with thermal neutron irradiation for the CdS sample is shown in Figure (28). As in the case of CdTe, the resistivity increases with irradiation, the curves maintaining approximately the same shape until the 9th irradiation corresponding to the appearance of the 0.85 ev level shown in Figure (26). After this irradiation, the resistivity increases as the sample is cooled. This reversal was also observed by Oswald (19).

7. Luminescence Measurements

A. General Comments

The luminescence observed in CdTe and CdS can be summarized

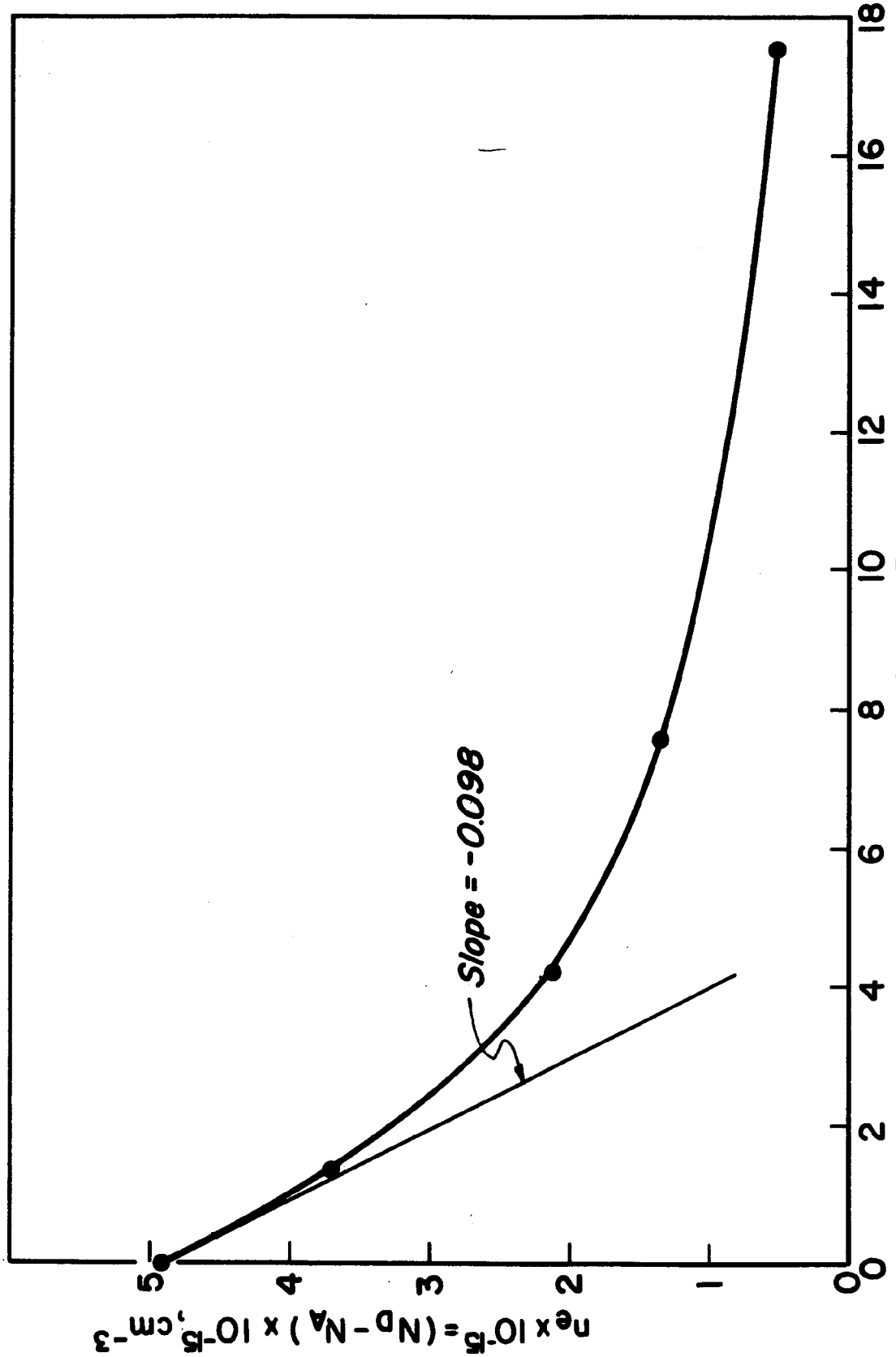


Fig. 27. Total Number of Electrons/cm^3 Available from Shallow Donors in CdS Versus Cumulative Number of Absorption Events

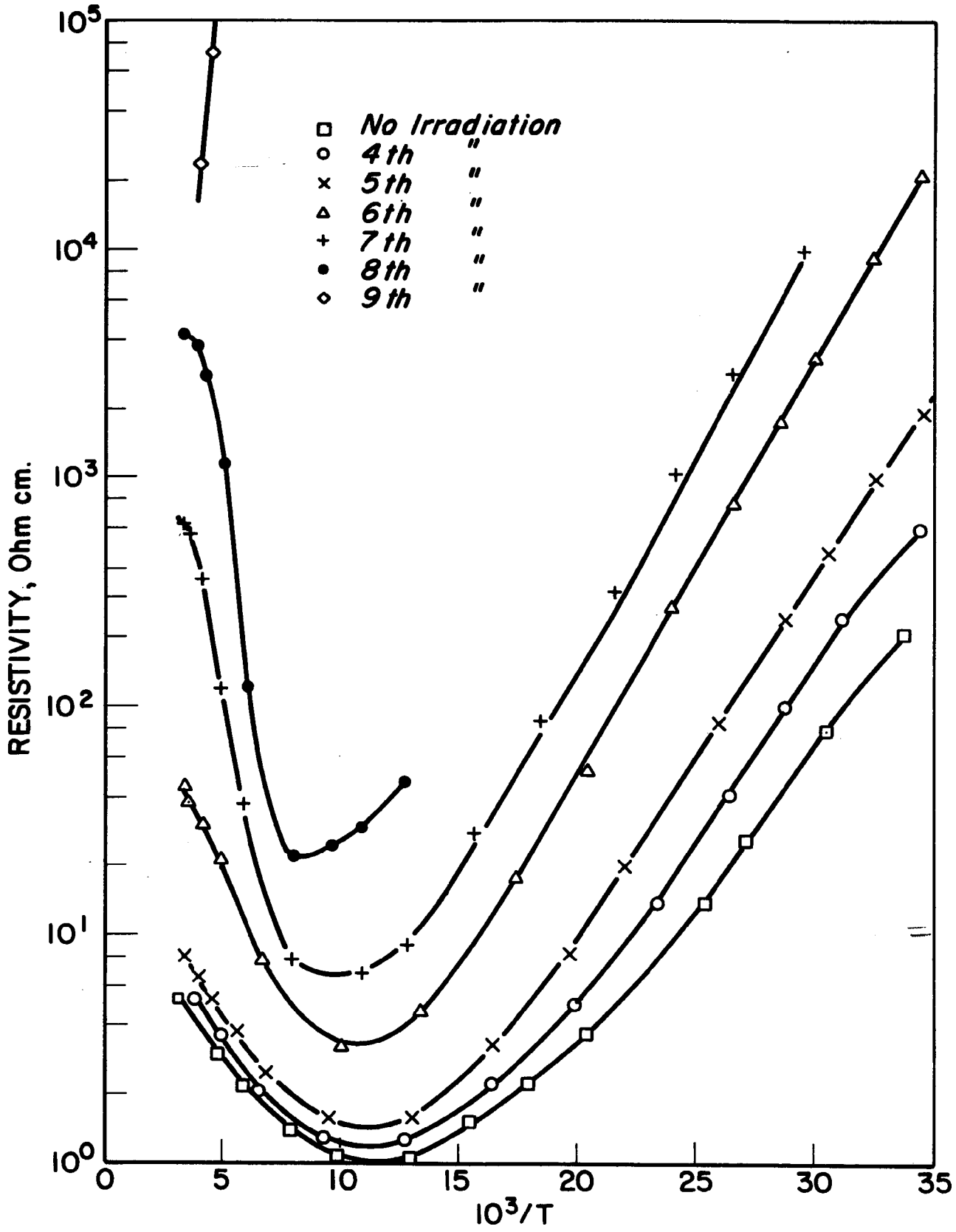


Fig. 28. Resistivity Versus 1/T as a Function of Thermal Plus Fast Neutron Irradiation for CdS

by dividing the spectrum up into three photon energy (or wavelength) regions as indicated in Figure (29). Before presenting the results in detail, some brief comments will be given on the types of emission bands found in each of the three regions.

1. Exciton Recombination Region. One of the assumptions inherent in the derivation of equation (21) for n (see page45) is that carriers do not interact with each other. If the attraction between holes and electrons is taken into account, one can then visualize the electron and hole moving through the crystal together as a pair due to their mutual attraction. By analogy with the hydrogen atom, one would expect this pair to possess a system of hydrogen-like energy levels. The electron-hole pair is then treated as a unit, called the exciton which can be compared to a hydrogen atom imbedded in a medium with dielectric constant, ϵ_s. Solving the Schrodinger equation for the hydrogen atom, one obtains the usual result for the energy levels,

$$E_H = \frac{-m_e e^4}{2\hbar^2 n^2} \equiv -\frac{W_H}{n^2}$$

Two assumptions are implicit in this result which are of importance here. First, the hydrogen atom is assumed to be in free space so that the potential energy is $-e^2/r$. However, for a hydrogen atom embedded in a medium with dielectric constant ϵ_s, the potential energy is $-e^2/\epsilon_s r$. Secondly, the effect of the nuclear mass on E_H has been ignored because $m_p \gg m_e$, where m_p is the proton mass. When the Schrodinger equation is solved and the nuclear mass is retained, one obtains

$$E_H^1 = -\frac{m_r' e^4}{2\hbar^2 n^2 \epsilon_s^2} = \frac{-m_r'}{m_e} \frac{W_H}{\epsilon_s^2 n^2}$$

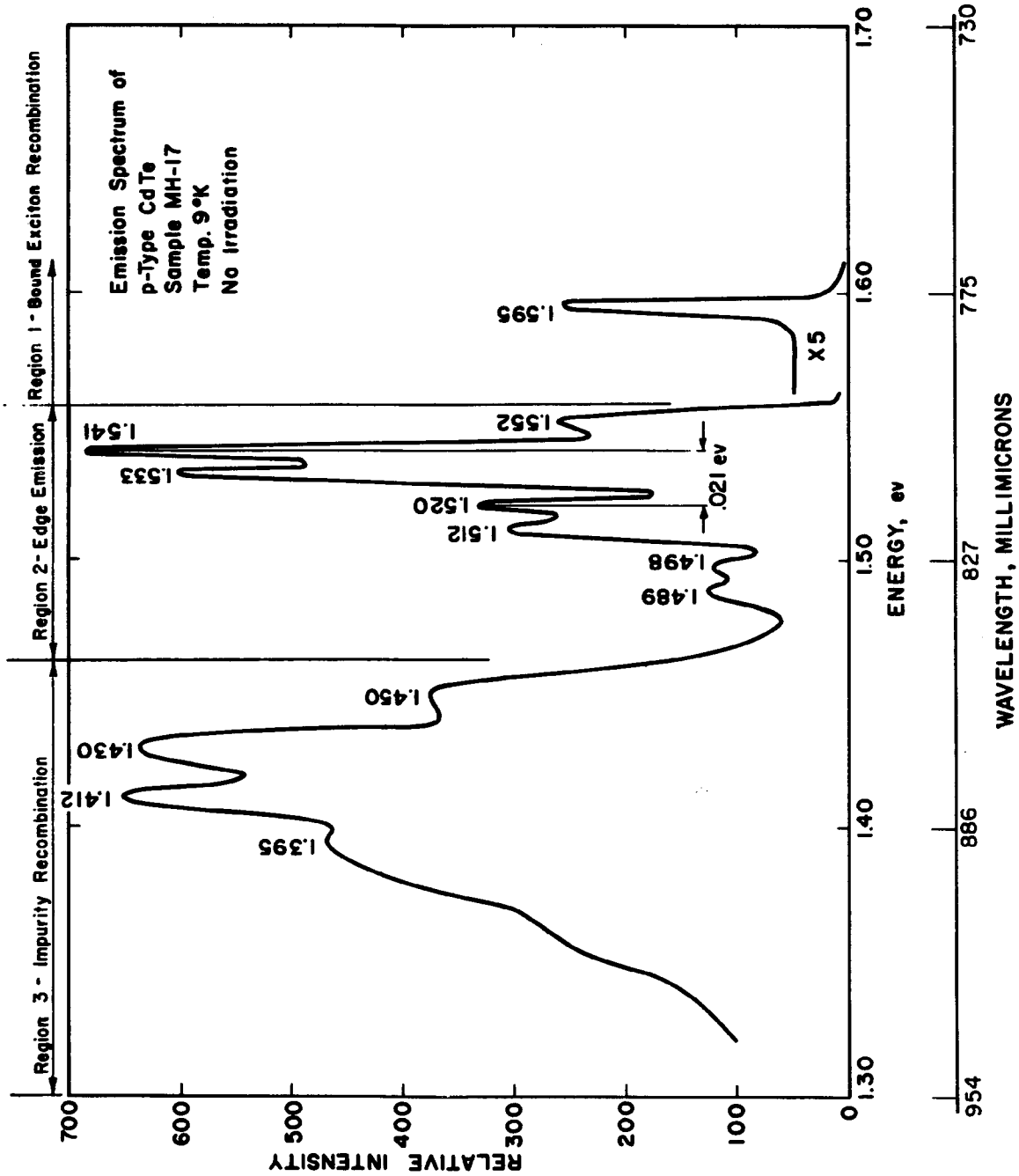


Fig. 29. A Typical Emission Spectrum for p-type CdTe

where the effect of ϵ_s has been included and $m_r^1 = \frac{m_e m_p}{(m_p + m_e)} \approx m_e$. This more general formula can be used directly for the hydrogen-like energy level system of the exciton. Ignoring the kinetic energy of the exciton, the exciton energy is

$$W_{ex}^n = -\frac{m_r}{m_e} \frac{W_H}{\epsilon_s^2 n^2}$$

where m_r is now the reduced mass of the electron-hole pair, $\frac{m_e^* m_h^*}{(m_e^* + m_h^*)}$. For CdTe, $m_e^* = 0.11\, m_e$ (37), $m_h^* = 0.63\, m_e$ (39), and $\epsilon_s = 10.6$ (37) so that the above equation gives

$$W_{ex}^1 = -0.0108 \text{ ev}$$

which is close to the measured value of 0.0095 ev (40) for CdTe. This is also the energy required to transform the exciton into a free electron in the conduction band and a free hole in the valence band. Therefore, the ground state of the exciton (n = 1), which corresponds to the first excited state of the crystal, lies at $E_c - .0108$ ev with the excited states lying closer to E_c.

As the exciton moves through the crystal, it will be influenced by small perturbations in the crystalline field, by dislocations, etc. This may result in recombination of the electron and hole; that is, annihilation of the exciton. The resultant energy will appear in the emission spectrum at $E_g - W_{ex}^1$ which corresponds to free exciton recombination. This emission band will be broadened by the inclusion of the kinetic energy of the exciton. Since $W_{ex}^1 = 0.0095$ ev in CdTe and the free exciton band is observed at 1.595 ev (40), the band gap (E_g) in CdTe at 4^o-10^oK is 1.605 ev.

Very narrow exciton bands are observed when the exciton is trapped by

an impurity resulting in the formation of an immobile complex. Upon recombination at the trap, the energy released will appear in the emission spectrum as a narrow band at an energy E_b below the free exciton energy where E_b is the binding energy of the exciton to the trapping center.

By purposely doping CdTe with several different impurities, Halsted (41) found an empirical relationship between the binding energy of an exciton to an impurity, E_b and the ionization energy of the impurity. For a particular doping agent, strong emission bands appeared in the 3rd, or impurity recombination region, and also in the exciton recombination region. The former band gave the ionization energy, while the latter gave E_b. The ratio of the binding energy to the ionization energy is 0.1 for neutral acceptors and 0.2 for neutral donors. These values hold for several II-VI compounds. Therefore, if an unknown bound exciton is observed, this ratio can be used to determine the ionization energy of the impurity.

2. Edge Emission Region. The edge emission, so-called because it occurs near the absorption edge, is found in most II-VI compounds as one or more sets of equally spaced bands (see Figure (29)). The lower energy bands in a particular set occur at regular energy intervals and correspond to the emission of a photon with simultaneous emission of 1, 2, 3, ... phonons. These phonon satellites are due to recombination of carriers which have given up part of their energy to the lattice.

In crystals such as CdTe and CdS which have different atoms at alternate lattice sites and are somewhat polar, optical vibrational modes of the

lattice are of importance. If the two oppositely charged atoms (i.e., Cd and Te) in the unit cell vibrate out of phase a strong dipole moment is created because the atoms are displaced in opposite directions. Consequently, these modes will couple strongly with any electromagnetic fields present and, hence, are called optical modes. Because of the strong coupling, the frequency of the optical modes often shows up in the absorption spectrum of a polar crystal as a strong absorption band in the infrared.

The fact that optical modes are of primary importance in CdTe has been demonstrated by Segall (37) who showed that the mobility of n-type CdTe in the lattice scattering range is due to scattering by longitudinal optical phonons. Using the Lyddane-Sachs-Teller relation, $\omega_l^2 = \omega_t^2 (\epsilon_s/\epsilon_\infty)$, where ω_l is the frequency of the longitudinal optical phonon and ω_t is the frequency of the transverse optical phonon, Halsted (42) showed that the separation between the no-phonon band and the phonon satellite (.021 ev) of the edge emission (see Figure (29)) is equal to the longitudinal optical phonon energy ($\hbar\omega_l$) in CdTe.

3. Impurity Recombination Region. The intensity and peak position of emission bands in this region depend crucially on the impurities or defects present in the material. Generally speaking, emission in this region is due to recombination of a free electron (or hole) with a hole (or electron) bound to the impurity or defect (42).

Before presenting the results of the luminescence measurements, the important emission bands are summarized in Tables (2) and (3). The suggested source of each band is also given. The interpretation of the bands depends, in part, on discussions given in Chapter 5.

	Region - Emission Band	Present in p-type CdTe?		Present in n-type CdTe?		Source of Emission Band
		Before Irradiation	After Long Irradiation	Before Irradiation	After Long Irradiation	
Exciton Recombination	1 - 1.593 ev	yes	no	yes, stronger than p-type	yes	Exciton bound to neutral chemical donor at E_c - .01 ev.
	1 - 1.589 ev	yes	yes	yes	yes	Exciton bound to neutral Te_i at E_v + .06 ev
	1 - 1.575 ev	yes	yes, strongest in region 1	yes,	yes, strongest in region 1	Exciton bound to neutral acceptor at E_v + .20 ev, possibly Cd_v
	1 - 1.565 ev	Sometimes	sometimes	sometimes	sometimes	Exciton bound to neutral impurity acceptor at E_v + .3 ev
Edge Emission	2 - 1.541 ev - X Series	yes	yes	yes	yes	Transition of free electron to Te_i at E_v + .06 ev
	2 - 1.533 ev - Y series	yes	yes, always weaker than X	yes	yes, always weaker than X	Recombination between electron bound to impurity donor at E_c - .01 ev and hole bound to Te_i at E_v + .06 ev.
Impurity Recombination	3 - 1.450 ev	yes	yes	yes, very weak	yes, very weak	Transition of free electron to acceptor at E_v +.15 ev, possibly Cd_v
	3 - 1.415 ev	no	no	no	yes	Possibly due to recombination at Cd_v at E_v + .20 ev.

TABLE (2) EMISSION BANDS IN CdTe

	Region - Emission Band	Present in CdS? Before Irradiation	Present in CdS? After Long Irradiation	Source of Emission Band
Edge Emission	2 - X series	yes	yes	Transition of free electron to S_i at E_v + .17 ev.
	2 - Y series	yes	yes, always weaker than X	Recombination between electron bound to impurity donor at E_c - .03 ev and hole bound to S_i at E_v + .17 ev.

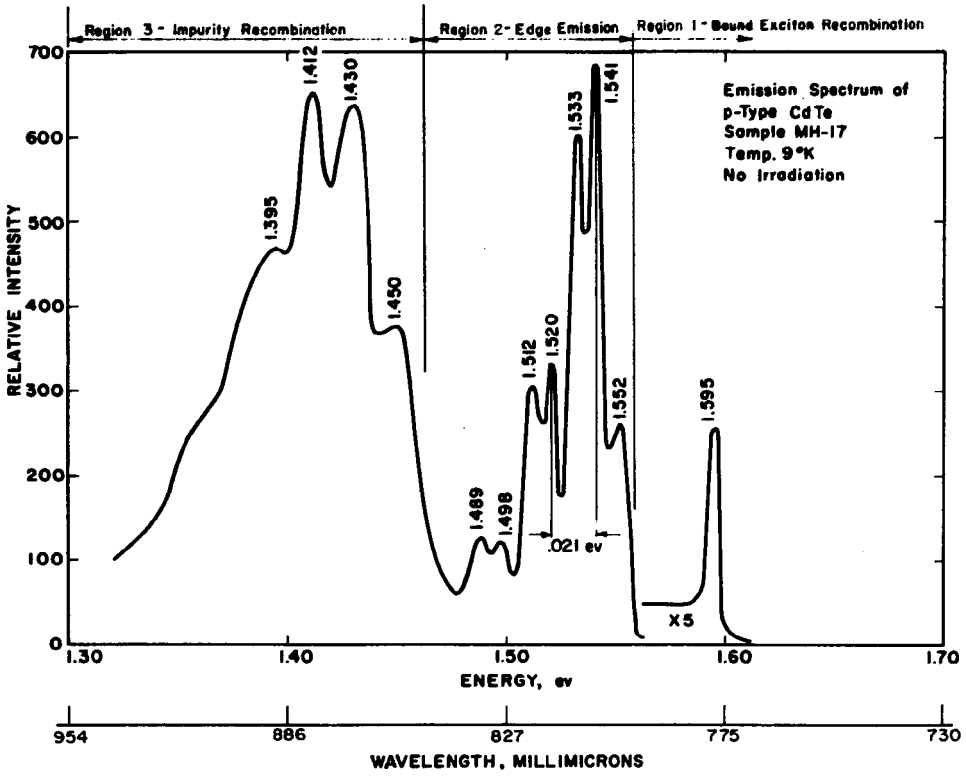
TABLE (3) Emission Bands in CdS

B. p-Type Cadmium Telluride

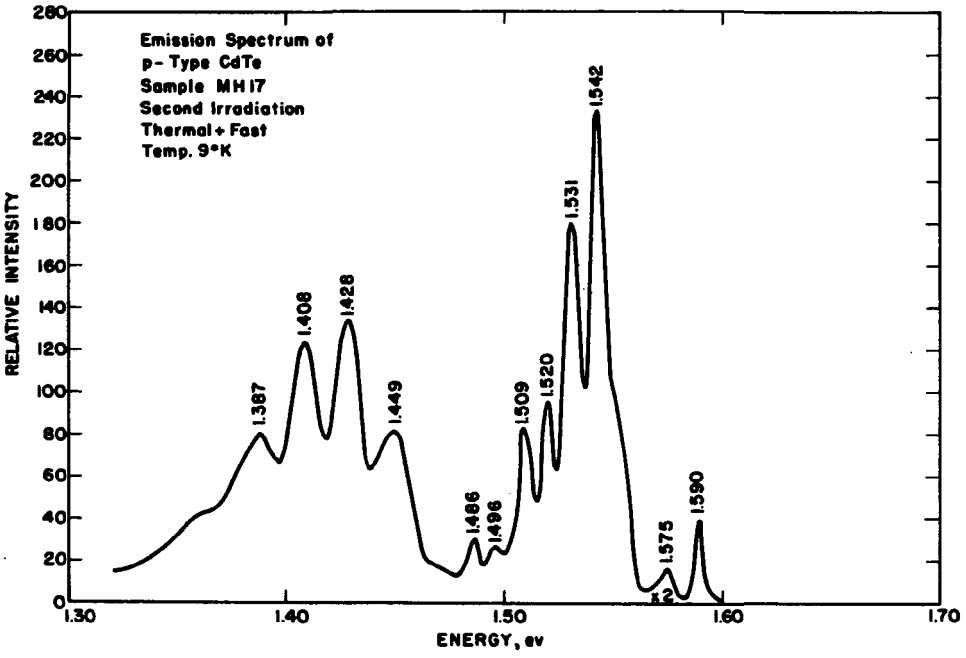
The emission spectra of approximately 15 p-type and n-type CdTe samples were measured. It was necessary to measure a relatively large number of samples because the emission occurs near the surface of the sample and, hence, is easily affected by extraneous factors such as oxidation and mechanical surface damage. A series of emission spectra for MH-17, a typical p-type sample, are shown in Figures (30) and (31). Although the emission spectra were measured out to 2.6 microns, no emission bands were observed above 1.0 micron for p-type CdTe. Therefore, this long wavelength region is not included in Figures (30) and (31).

The emission spectrum of p-type CdTe was also measured on the high resolution instrument at WPAFB. The spectrum obtained is the same as Figure (30a) except that two bands at 1.593 ev and 1.589 ev are observed in the bound exciton region while only one is shown at 1.595 ev in Figure (30a). Both the 1.593 ev band and the 1.589 ev band were less than kT in width indicating that the bands are due to bound excitons and not free excitons. This follows from the fact that the kinetic energy of the free exciton would broaden the emission band.

The variation in the intensity of the emission bands of interest with irradiation is shown in Figure (32) for p-type CdTe. Because the emission occurs near the surface, R was calculated using the surface flux, ϕ_s, and not the average flux within the sample. All the bands decrease in intensity with irradiation at about the same rate with the exception of the 1.575 ev band which remains roughly constant. Another general result is that no shift in peak position was observed, within experimental error, for any of the bands.

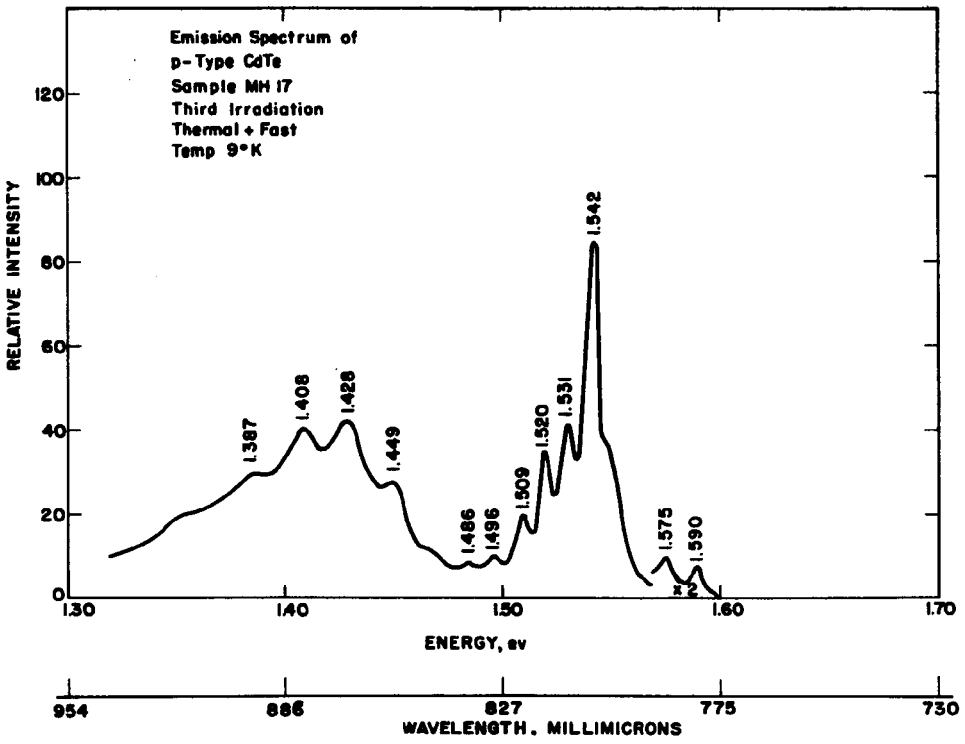


a) No Irradiation

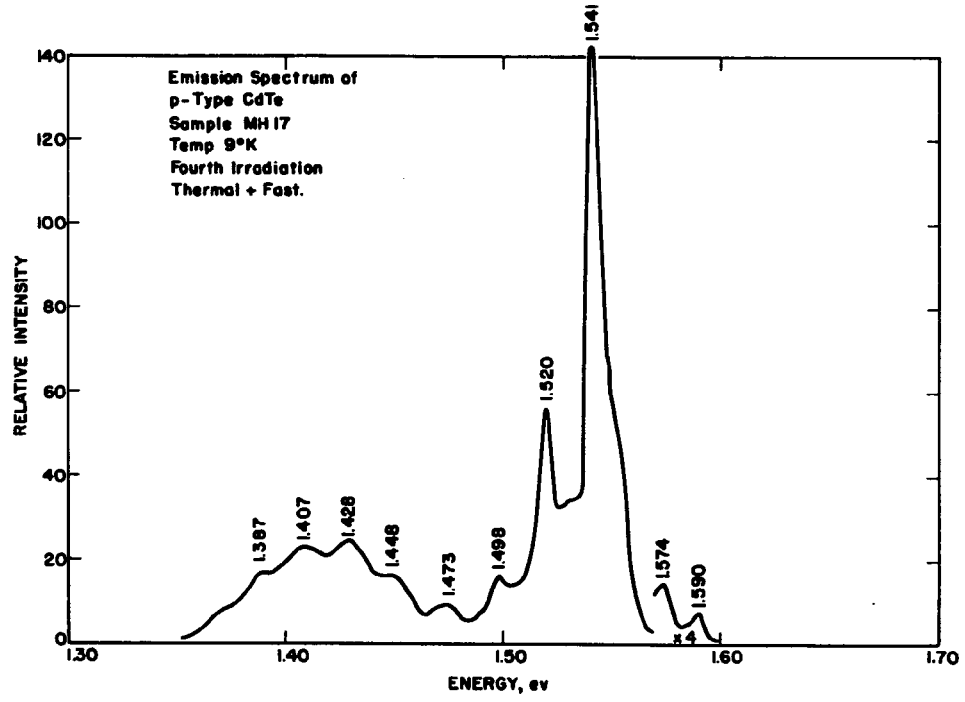


b) After Second Irradiation

Fig. 30. Emission Spectra of p-type CdTe as a Function of Thermal Plus Fast Neutron Irradiation.



a) After Third Irradiation



b) After Fourth Irradiation

Fig. 31. Emission Spectra for p-type CdTe as a Function of Thermal Plus Fast Neutron Irradiation

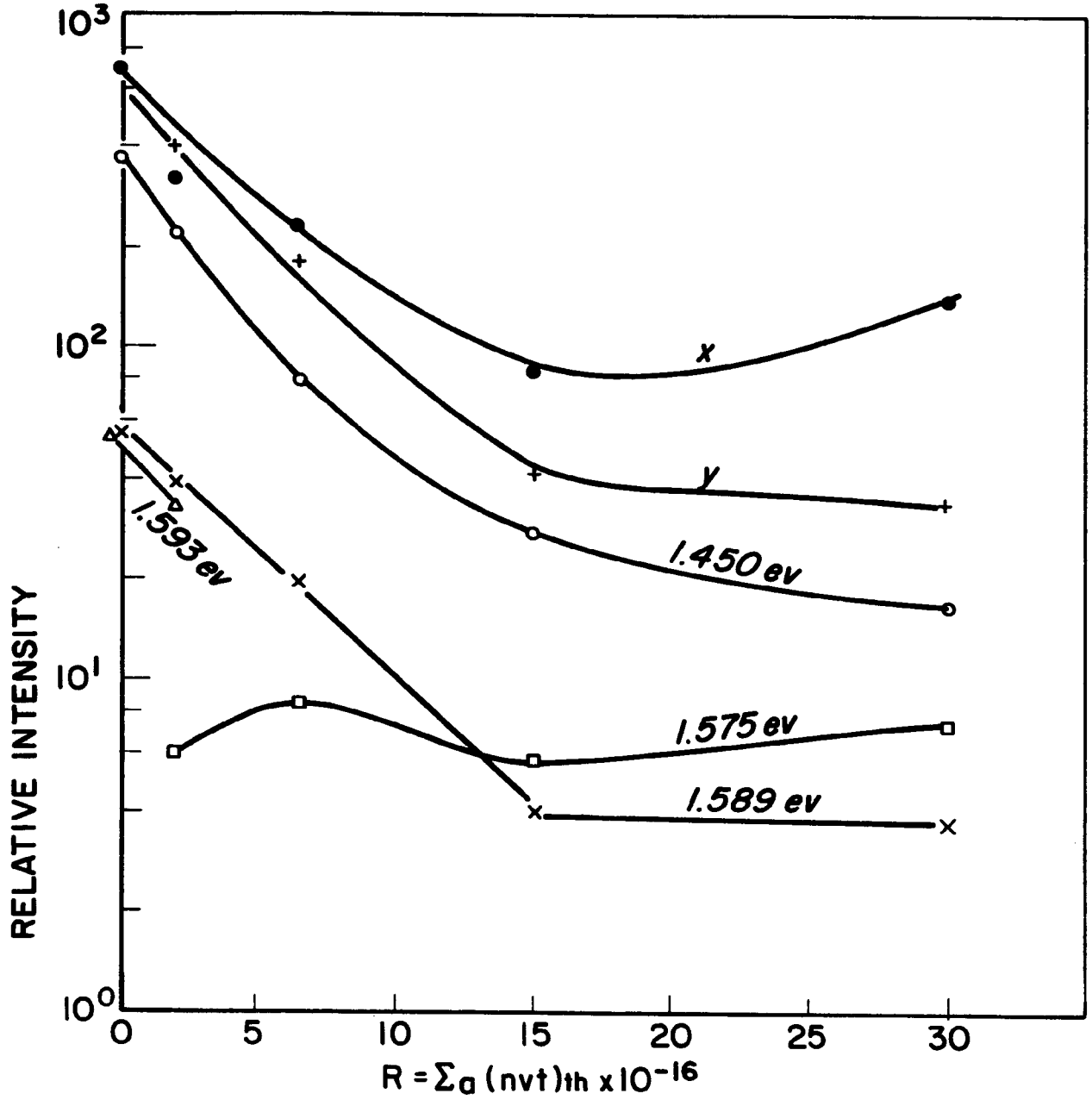


Fig. 32. Peak Intensity Versus Cumulative Number of Absorption Events for Emission Bands in p-type CdTe

The transmission was measured as a function of wavelength after several irradiations to find out if the decrease in emission intensity is due to increased self-absorption. The results, shown in Figure (33) for short wavelength, indicate that the absorption has changed very little over the entire wavelength range even though the third irradiation for this sample corresponded to a larger $(nvt)_{th}$ than the third irradiation of the emission samples. One concludes that any significant changes observed for emission bands near the edge are due primarily to variation in emission characteristics and not to increased self-absorption.

Measurement of the emission spectra of a few CdTe samples exposed to fast neutrons only showed that the decrease in emission intensity for fast neutron exposure was much smaller than that observed for thermal plus fast neutron irradiation. Having listed these general results, the changes observed in the emission bands of p-type CdTe due to irradiation will be discussed in more detail according to region (see Figure (29)).

1. Bound Exciton Region. In the majority of spectra an emission band is observed at 1.593 ev and not 1.595 ev as shown in Figure (30a). Also, the high resolution instrument at WPAFB revealed a value of 1.593 ev. Therefore, the true energy of the 1.595 ev band in Figure (30a) is believed to be 1.593 ev. Figures (30) and (31) indicate that this band disappears as irradiation proceeds. The emission band at 1.590 ev, shown in Figures (30) and (31), is at 1.589 ev as indicated by the high resolution instrument. This band, and one at 1.575 ev, are present before irradiation for many samples, but as indicated in Figure (30a) are unresolved for MH-17. To summarize, four

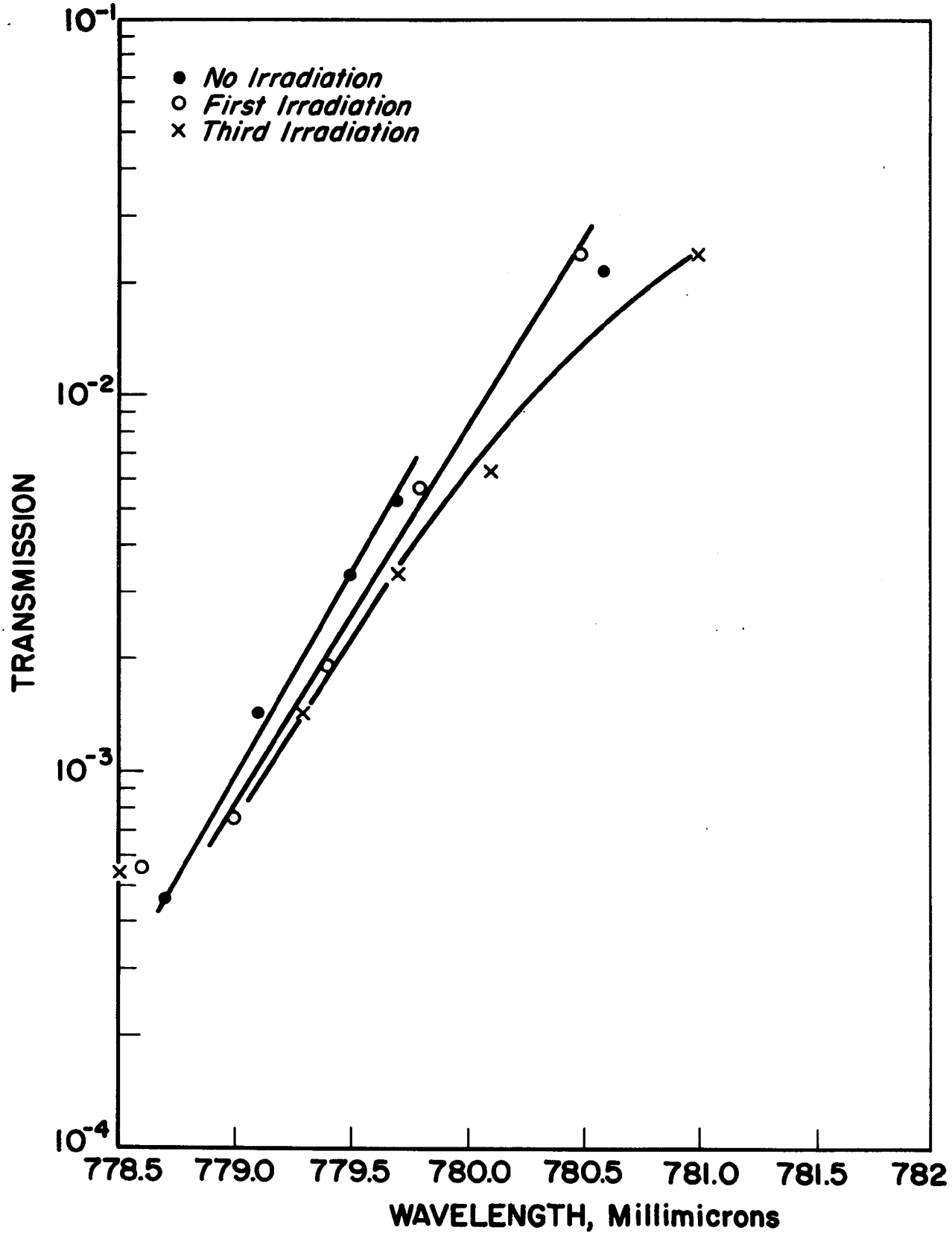


Fig. 33. Transmission Versus Wavelength for n-type CdTe as a Function of Thermal Plus Fast Neutron Irradiation. Temperature: 9°K

bound exciton bands are observed in p-type CdTe: 1.593 ev, 1.589 ev, 1.575 ev and 1.565 ev. All four are observed before irradiation although the 1.565 ev band is observed only in certain samples (not in MH-17). The 1.593 ev and 1.565 ev bands decrease rapidly in intensity as irradiation proceeds. The 1.589 and 1.575 ev bands remain with the 1.575 ev band dominating the bound exciton region after long irradiation. To discover the source of these four exciton bands, the ratios derived by Halsted (see page 76) are applied as indicated in Table (4).

Table 4

Bound exciton emission bands in CdTe

E_{ph} = Peak Position	Impurity-Exciton binding energy = $1.595 - E_{ph}$	Neutral donor Ionization energy = $(1.595 - E_{ph})/0.2$	Neutral acceptor ionization energy = $(1.595 - E_{ph})/0.1$
1.593 ev	0.002 ev	0.01 ev	0.02 ev
1.589	0.006	0.03	0.06
1.575	0.020	0.10	0.20
1.565	0.030	0.15	0.30

The 1.593 ev band is attributed to the donor observed in n-type Hall samples at E_c - .012 ev. Recombination at a neutral donor requires the existence of occupied donors in p-type material. However, at low temperatures one ordinarily expects all the donors to be empty in a p-type sample. Hall measurements on n-type material (see Figure (9)), show that thermal liberation of carriers from the shallow donors is insignificant at 9°K. The creation of electron-hole pairs by ultraviolet light is followed by trapping

of electrons at the empty shallow donors in p-type material. Because of insignificant thermal release, the electrons remain trapped and the requirement of the presence of neutral donors is satisfied.

The 1.589 ev band is attributed to an exciton bound to a Te_i at E_v + .06 ev. After firing undoped, n-type CdTe in Te vapor at 900°C, Lorenz (43) found that the material changed to p-type with a level at E_v + .05 to .06 ev. The hole concentration from this level increased with increasing Te firing time. Although Lorenz attributed this level to a Cd_v, the firing conditions also favor Te_i and we will adopt this assignment.

The discussion of the 1.575 ev band, which is deferred until the next Chapter, is based on the assignment of the 1.575 ev band to recombination of an exciton bound to a neutral acceptor at E_v + 0.20 ev. This level was observed in Hall samples of p-type CdTe after irradiation (see Figure (17)).

The 1.565 ev band is probably associated with impurities that possess levels at E_v + 0.3 ev (32) (39).

2. Edge Emission Region. The no-phonon peak of the high energy edge emission series, hereafter referred to as the X series, is at 1.541 ev for p-type CdTe in Figure (30a). The no-phonon peak of the low energy edge emission series (Y series) is at 1.533 ev. The relative intensity of these two peaks before irradiation varies from sample to sample. For some samples the X series is stronger while for other samples the Y series is stronger. For all the samples examined the X series is stronger

than the Y series after long irradiation times (see Figure (31b)). The explanation of the behavior of the edge emission in CdTe is reserved for the next Chapter since it depends, in part, on the interpretation of the electrical measurements.

3. Impurity Recombination Region. A no-phonon band at 1.450 ev with several phonon satellites is observed in p-type CdTe before irradiation (see Figure (30a)). The intensity of this series decreases with irradiation at about the same rate as the edge emission intensity. Subtracting from E_g, 1.605 - 1.450 = 0.15 ev., reveals that this emission band is associated with the level at E_V + 0.15 ev seen in all the p-type Hall samples before irradiation (see Figure (17)).

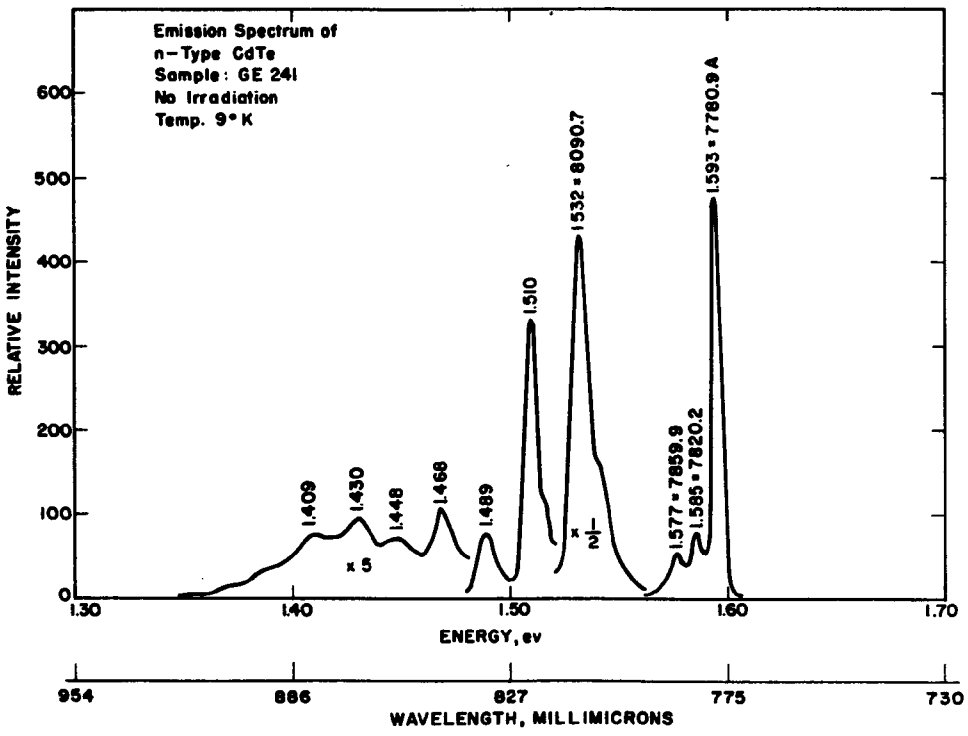
C. N-Type Cadmium Telluride

The variation in emission spectra with thermal neutron irradiation for a typical n-type sample is shown in Figures (34) and (35). The same general comments made for p-type CdTe apply to n-type CdTe:

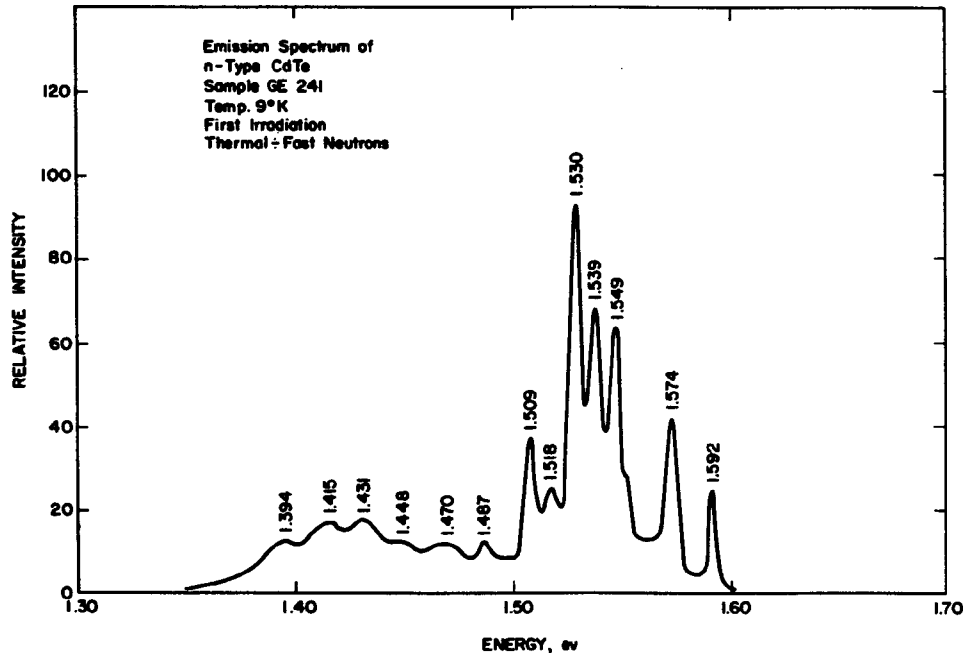
1. No emission bands were observed above 1.0 micron.
2. No shift in peak position with irradiation was observed for any of the bands.
3. Fast neutron effects are similar but much smaller.
4. With the exception of the 1.415 and 1.575 ev bands, the intensity of all the emission bands decreases rapidly with irradiation.

The last statement is illustrated in Figure (36) which gives the variation of peak intensity with irradiation for n-type CdTe.

As for p-type CdTe, the emission spectrum of un-irradiated n-type CdTe was also measured on the high resolution instrument at WPAFB.

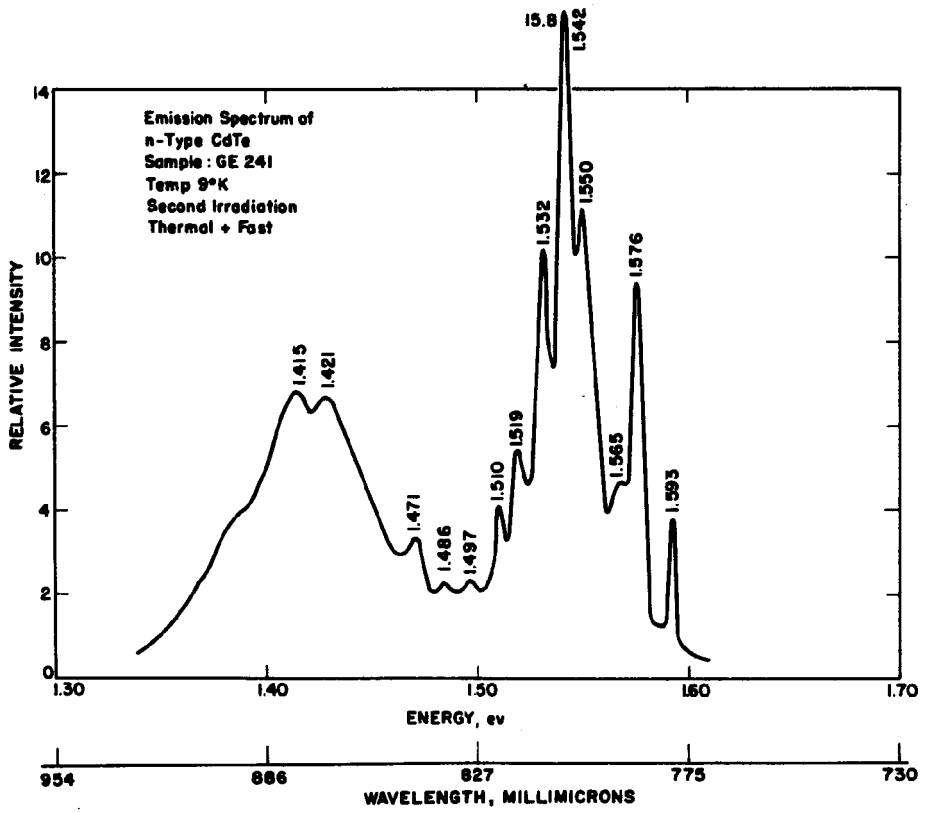


a) No Irradiation

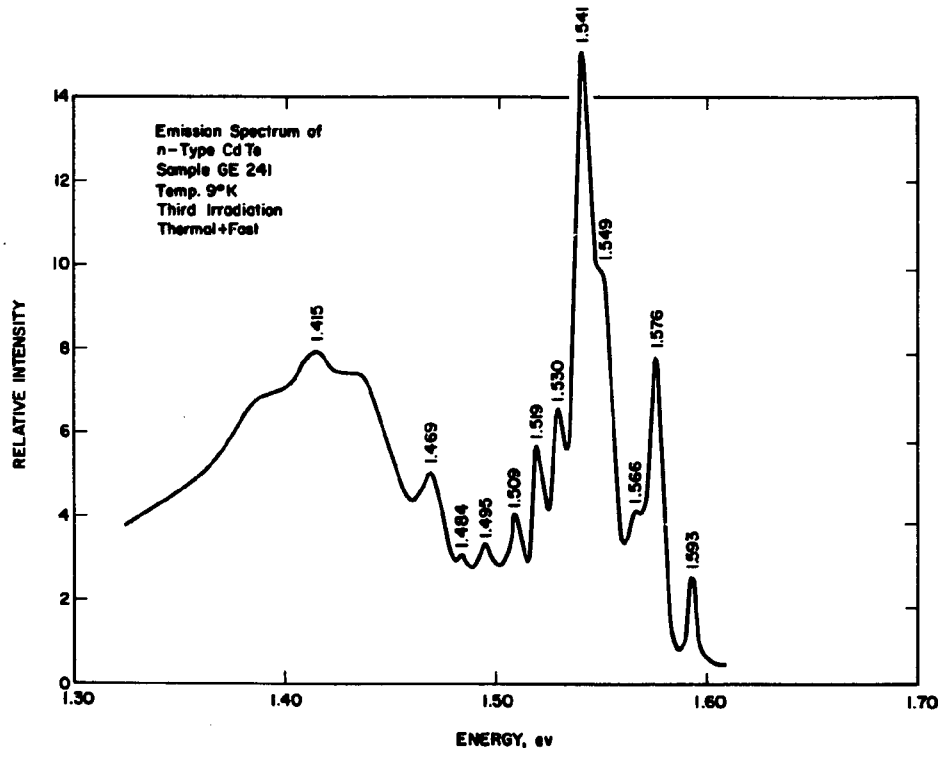


b) After First Irradiation

Fig. 34. Emission Spectra of n-type CdTe as a Function of Thermal Plus Fast Neutron Irradiation



a) After Second Irradiation



b) After Third Irradiation

Fig. 35. Emission Spectra of n-type CdTe as a Function of Thermal Plus Fast Neutron Irradiation

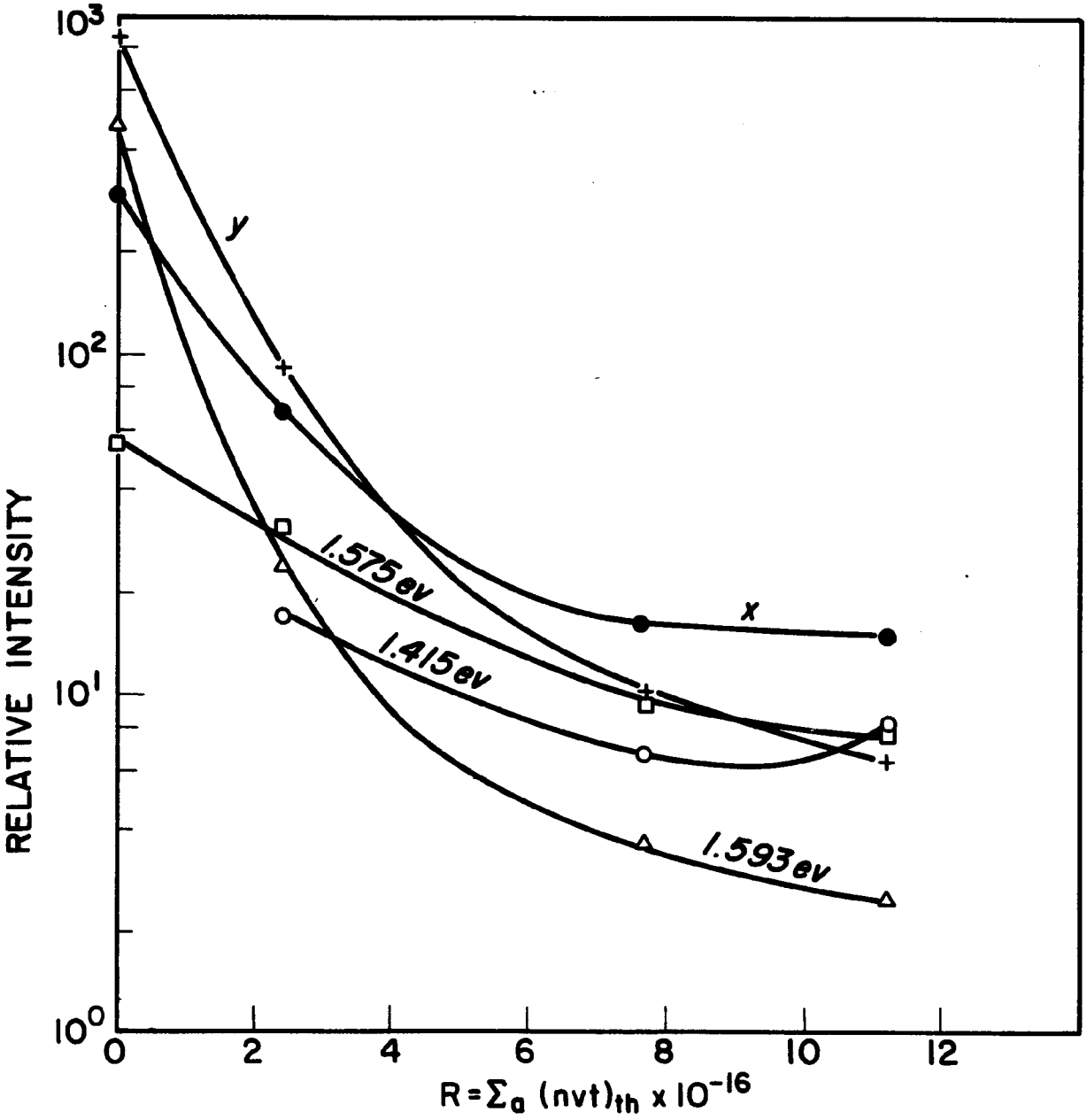


Fig. 36. Peak Intensity Versus Cumulative Number of Absorption Events for Emission Bands in n-type CdTe

The spectrum obtained is the same as Figure (34a) with the exception of the bound exciton region. Similar to p-type CdTe, the measurements at WPAFB reveal two exciton bands at 1.589 ev and 1.593 ev. The true energy of the 1.585 ev band shown in Figure (34a) is probably 1.589 ev.

The emission bands for n-type CdTe can be analyzed in more detail by region as was done for p-type material. The discussion will be brief because the effects observed in n-type CdTe are similar to those observed in p-type CdTe.

1. Bound Exciton Region. The same four bound exciton bands observed in p-type CdTe are observed in n-type CdTe: 1.593 ev, 1.589 ev, 1.575 ev, and 1.565 ev. The 1.593 ev band is stronger in n-type CdTe and does not decrease in intensity with irradiation as rapidly as in the case of p-type CdTe. Because of this, the lower intensity 1.589 ev band is masked throughout the irradiation by the 1.593 ev band. All four bands are present before irradiation although the 1.565 ev is too weak to be observed.

Since the same bands are observed, Table (4) and the subsequent identifications again apply. Therefore, one concludes that the impurities responsible for the 1.565 ev and 1.593 ev bands are present in both n and p-type CdTe as well as the Te_i and the E_v + .20 ev level.

2. Edge Emission Region. The same comments made concerning edge emission in p-type CdTe apply to n-type CdTe. For the particular sample shown in Figures (34) and (35) the Y series is much stronger before irradiation. However, other n-type samples were observed in which the X and Y series were of approximately equal intensities.

3. Impurity Recombination Region. Before irradiation, a series of bands with the no-phonon band at 1.45 ev is also observed in n-type CdTe. However, the intensity in n-type CdTe is smaller by almost 2 orders of magnitude than that in p-type CdTe. As irradiation proceeds, the bands in this region can no longer be resolved. The intensity of the main peak (1.415 ev) does not decrease nearly as fast with irradiation as the exciton and edge emission (see Figure (36)).

In general, the emission spectrum of n-type CdTe is similar to that of p-type CdTe after long irradiation times. This is illustrated by comparing Figure (31b) with Figure (37) which is for a second n-type sample after long irradiation time. In both cases, the exciton recombination region is dominated by the 1.575 ev band and the X series of the edge emission is much stronger than the Y series.

C. Cadmium Sulfide

The emission spectra of a few bulk CdS samples were also examined. The results for a typical sample are shown in Figure (38). In agreement with Oswald (4), both the edge emission and the bound exciton emission decrease with thermal neutron irradiation. As in the case of CdTe, the X series of the edge emission is dominant after long irradiation times.

The edge emission in CdS, and also CdTe, has rather unique temperature characteristics. The low energy edge emission series (Y series) is much stronger than the high energy edge emission series (X series) at 4.2°K. As the crystal is heated, the Y series diminishes and the X series becomes stronger. At 77°K the intensities have reversed and the X series is dominant.

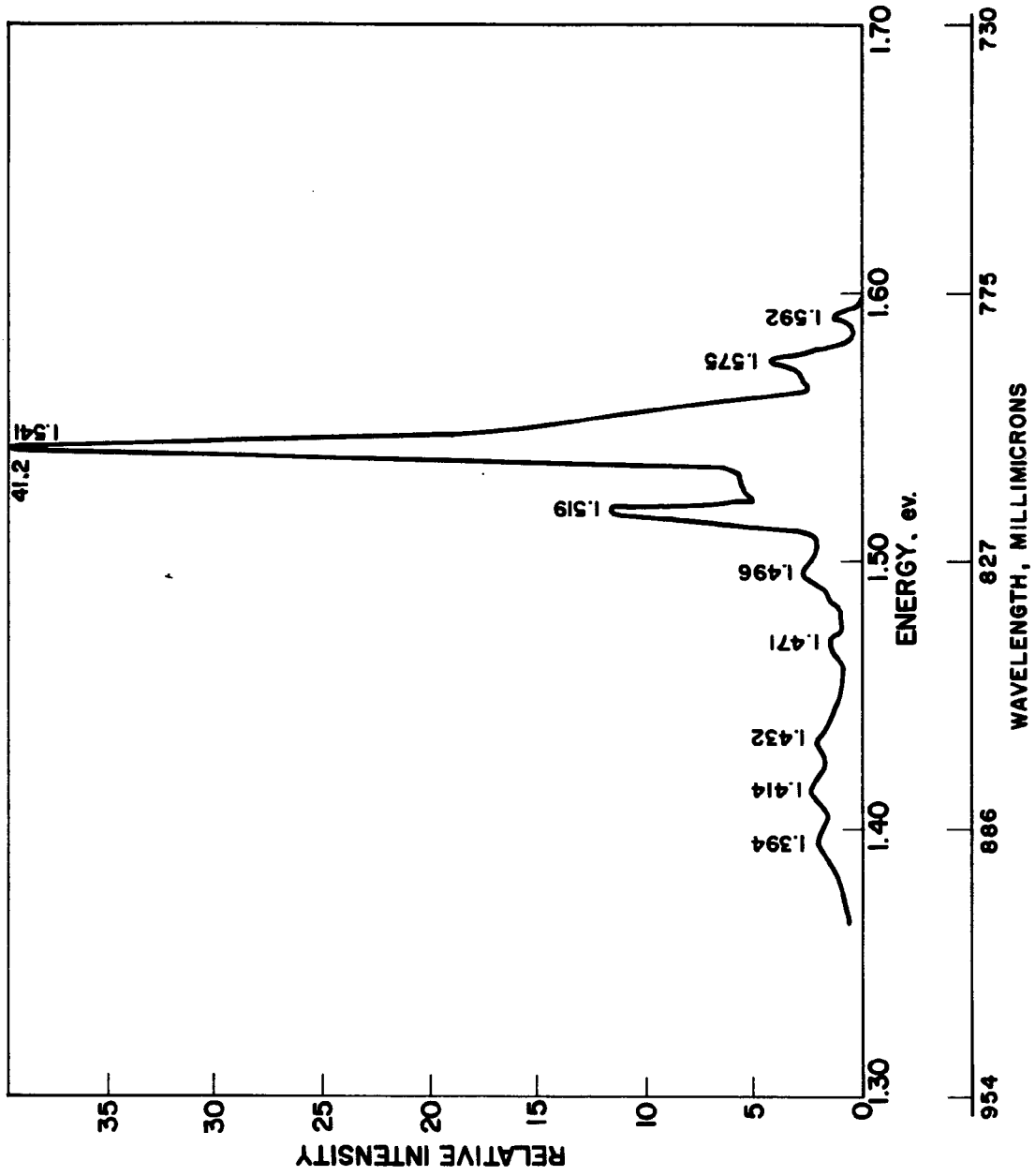


Fig. 37. Emission Spectrum of n-type CdTe After Long Thermal Neutron Irradiation Time

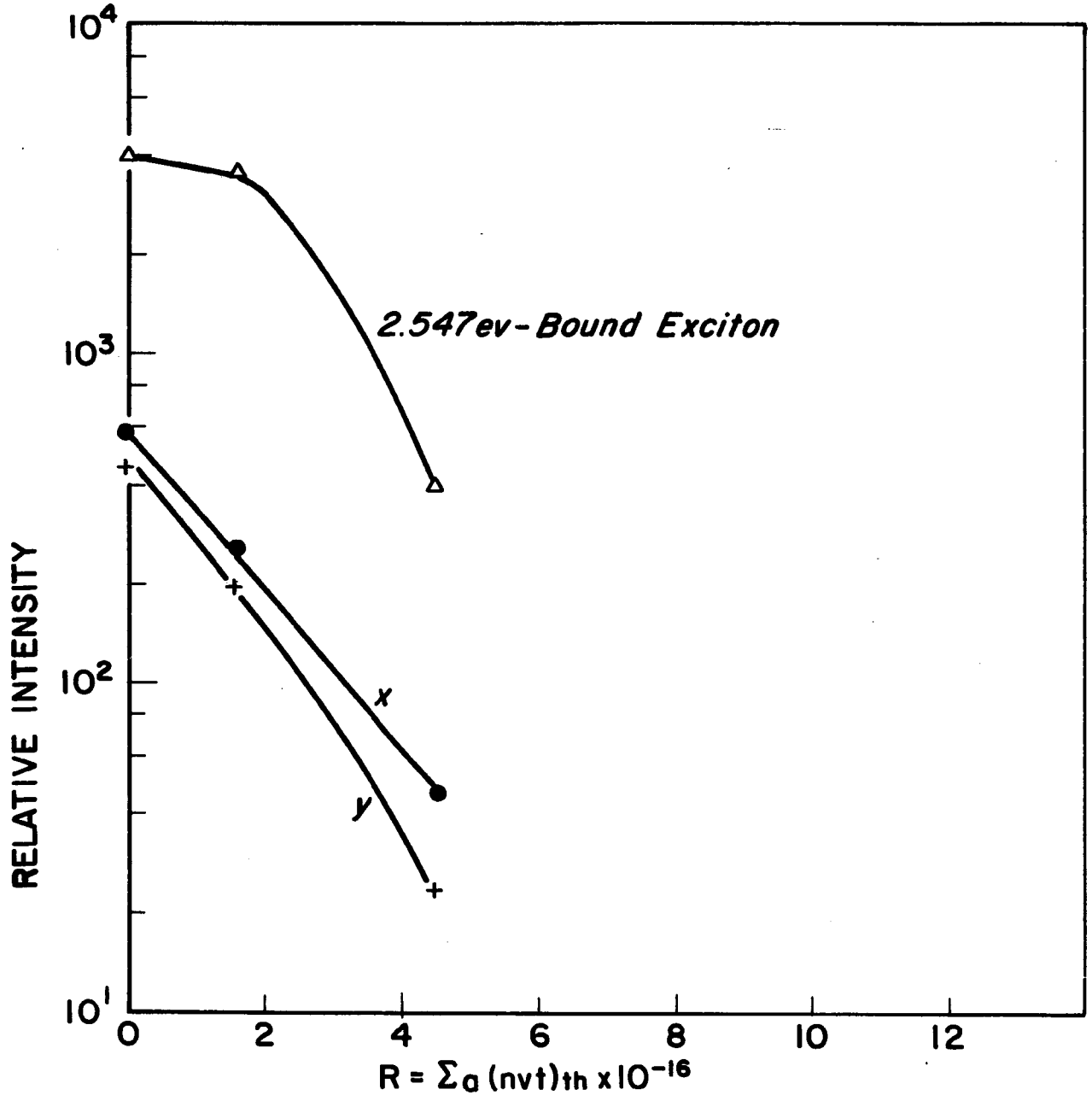
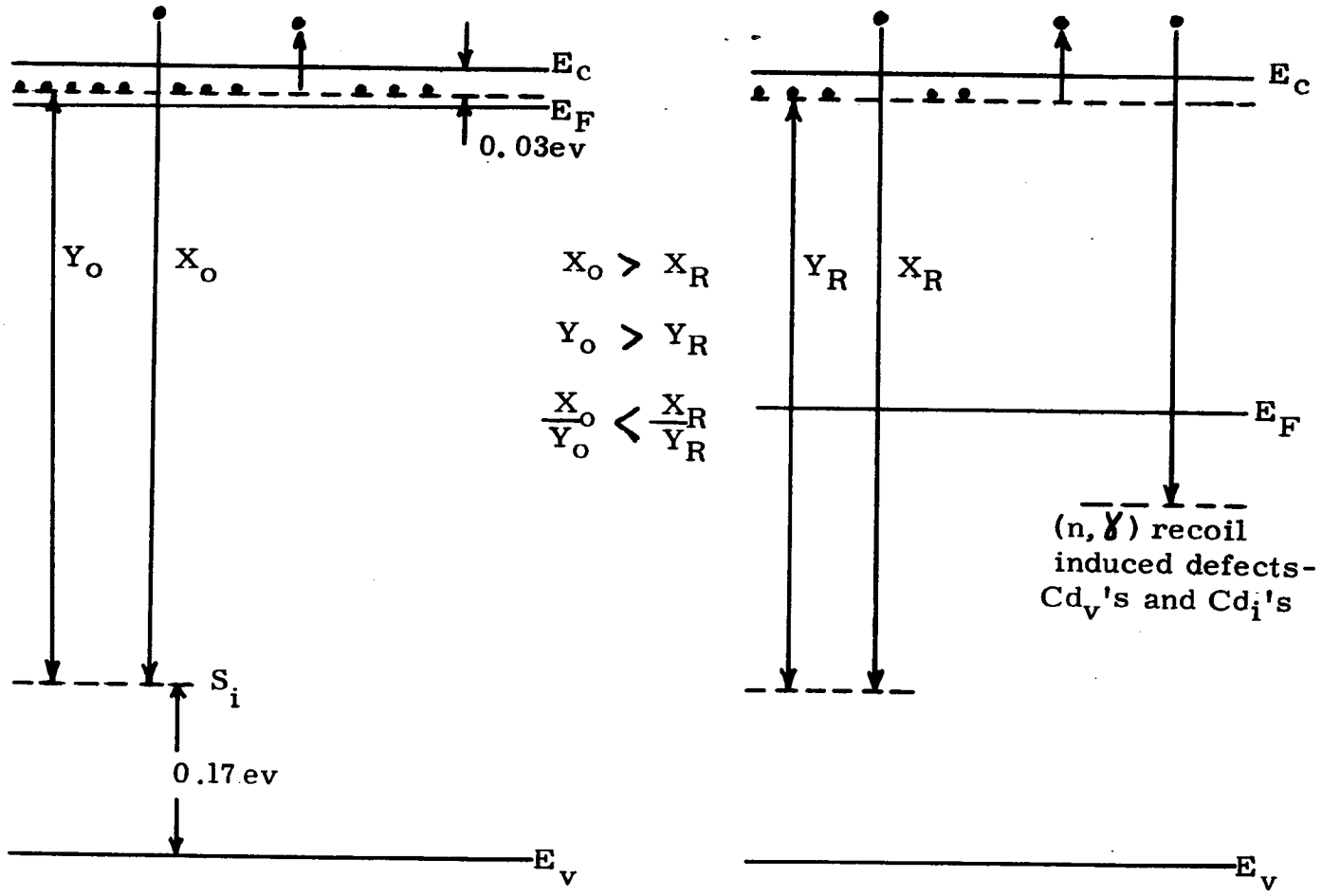


Fig. 38. Peak Intensity Versus Cumulative Number of Absorption Events for Emission Bands in CdS

Many explanations have been advanced for the edge emission in CdS. Lambe (44) suggested that the edge emission is due to recombination of bound electrons and free holes while Collins (45) proposed the opposite process. In an earlier paper, Kroger (46) suggested that there is one no-phonon band due to an exciton transition and that the rest of the bands, including the Y series, are due to phonon assisted recombination. To explain the temperature dependence of the two series, Grillot (47) proposed that both series are due to recombination of a free electron with a trapped hole. However, the hole trap is associated with a donor center. When the donor center is occupied at low temperature the energy level of the hole trap is perturbed. This leads to the second series at a different energy. Maeda (48) used the results of thermal luminescence to show that the X series is due to recombination between a bound electron and a bound hole. Pedrotti (49) proposed a model, which is illustrated in Figure (39a), that is based primarily on the temperature behavior of the edge emission. In this model the Y series is due to recombination between an electron bound to a shallow donor at E_c - .03 ev and a hole bound to an acceptor at E_v + .17 ev. If the donor is unoccupied recombination through the Y series cannot occur. Therefore, it follows that the Y series will be more intense at low temperatures where the majority of donors are occupied. As the sample is heated the number of occupied donors, and, hence, the Y series intensity, decreases while the X series, which is due to recombination of a free electron with a hole bound to the E_v + .17 ev acceptor, becomes stronger. Further heating results in complete

exhaustion of the donors and disappearance of the Y series. At this point, the edge emission spectrum is dominated by the X series.



a) Before Irradiation

b) After Irradiation

Figure (39). The effect of thermal neutron irradiation on the edge emission of CdS.

Colbow (50) used time dependent luminescence measurements to demonstrate the validity of the Pedrotti model. In this experiment, the sample was exposed to a short pulse of ultraviolet light and the peak positions of the two edge emission series were measured as a function

of time after the pulse. For recombination between an electron bound to a donor and a hole bound to an acceptor, the energy of the emitted photon is

$$E_{ph} = E_g - E_A - E_D + \frac{e^2}{\epsilon_s r} \qquad (24)$$

where E_g is the bandgap, ϵ_s is the static dielectric constant and r is the donor-acceptor pair separation. Following the light pulse the close pairs recombine first and the widely separated pairs recombine last. Therefore, a shift toward lower values of E_{ph} with time should be observed due to the changing value of r if the observed emission is a bound electron-bound hole transition. Colbow (50) observed this shift for the Y series but not for the X series which agrees with the Pedrotti model.

Vassell (51) produced edge emission in CdS by both of the following treatments: (1) bombardment with low energy electrons which could displace only S atoms and (2) heat treatment in a sulfur atmosphere. From these experimental facts, Vassell concluded that the S_i is the edge emission center. Kulp (52) bombarded CdS with low energy electrons and found a threshold energy for production of edge emission at 8.7 ev. Edge emission was also attributed to the S_i by Kulp. From the results of annealing CdS in a vacuum at 600°C, Handleman (53) attributed the edge emission to the Cd_v.

On the basis of the previous discussion, we assume that the edge emission mechanism in CdS is provided by the Pedrotti model and that the S_i is the edge emission center. This picture is summarized in

Figure (39a) where Y_o is the low energy series before irradiation and X_o is the high energy series before irradiation.

One can now examine the effects of thermal neutron irradiation on the edge emission to see if they can be explained within the context of the Pedrotti model. With the S_i as the edge emission center, the observed decrease in edge emission intensity as a result of thermal neutron irradiation tends to confirm our hypothesis that the production of sulfur defects by the recoil process is a minor effect (see page 22). A decrease in edge emission could occur for three reasons. First, the edge emission centers may be destroyed during irradiation. This is a rather remote possibility since these centers can be produced by heat treatments which take place at rather high temperatures. However, the presence of high energy internal gamma rays could possibly provide a unique annealing mechanism for destruction of these centers. Second, and more probable, is the indirect effect of the introduction of deep levels, that is, cadmium vacancies and interstitials. During illumination by the ultraviolet light quasi-Fermi levels are established in the upper and lower halves of the band gap which govern the distribution of electrons and holes, respectively. As in the case of the dark Fermi level, the electron quasi-Fermi level is also affected by the introduction of deep levels. An increase in the concentration of deep levels will pull the quasi-Fermi level towards the center of the gap as indicated in Figure (39b). This, in turn, will reduce the fraction of occupied shallow donors and, hence, result in a decrease in intensity of the Y series. The X series will not be affected appreciably, because it is due to the recombination of free electrons.

This corresponds to the observation that the X series dominates after irradiation. With regard to the ratio, X/Y, thermal neutron irradiation is similar to raising the temperature - both produce a deeper Fermi level and, hence, a larger X/Y.

Third, and most important, is the direct effect of the introduction of deep levels which can act as recombination centers because their hole capture and electron capture cross-sections are similar. Oswald (4) has demonstrated that the levels introduced by thermal neutron irradiation act as radiative recombination centers (see page 25). Since these recombination centers represent another sink for electrons and holes, the edge emission decreases, for the same electron-hole generation rate, because of the competing recombination at deep levels as shown in Figure (39b). This corresponds to the observed behavior in CdS.

V. DISCUSSION OF RESULTS AND CONCLUSIONS

In the discussion of electrical measurements on n and p-type CdTe, it will be shown that approximately one Cd_v and one Cd_i are produced per absorption while Te defects are produced at a much slower rate. The variation of $(N_D - N_A)$ with $R = \Sigma_a \Phi t$ is accounted for by postulating defect annealing during irradiation but not after irradiation. The defects anneal out between 160°C and 200°C.

Electron removal in CdS as a function of the number of absorptions is also explained by the presence of isolated vacancies. However, one must assume that a large excess of Cd defects were present before irradiation. This agrees with the well-known fact that CdS is difficult to produce in exactly stoichiometric proportions.

In Section 12 the luminescence spectra will be discussed. We have already shown that the effect of thermal neutrons on the edge emission in CdS can be explained by assuming the Pedrotti model for the edge emission mechanism and the S_i as the edge emission center. For CdTe, we will make a comparison with CdS and postulate that the Te_i is responsible for the edge emission along with the Pedrotti model. It will be shown that this model can account for the variation of edge emission in CdTe with thermal neutron irradiation. Changes occurring in other regions of the spectrum due to thermal neutron irradiation are also analyzed.

8. Hall and Resistivity Results

A. n-Type Cadmium Telluride

The decrease in n_e with irradiation shown in Figure (10) is attributed

to the introduction of acceptors. In Chapter 2 it was shown that an excess of Cd defects are produced by thermal neutron induced recoil. Later in this Section we will provide experimental evidence that Te defects are not produced in significant quantities by the recoil process. Several authors have shown that the Cd_V plays a major role in determining the properties of CdTe and CdS. Kroger (35) and deNobel (54) altered the stoichiometry of CdTe by annealing p-type CdTe in Cd vapor. The observed change from p-type to n-type following annealing was attributed to the introduction and annihilation of various native defects including the Cd_V. Yamada (39) also annealed CdTe in Cd vapor and found a level at E_V + .20 ev which he attributed to the Cd_V. Lorenz (55) annealed pure, n-type CdTe in a vacuum at high temperature which vaporizes Cd from the sample leaving a deficiency of Cd (Cd_V's). After the anneal the CdTe was p-type. Woodbury (56) suggested that the large increase in resistivity observed in CdS after annealing in sulfur vapor is due to compensation of the donors by Cd_V's. On the basis of these comments, we suggest that the electron removal in n-type CdTe with irradiation is due to the introduction of cadmium vacancies which act as acceptors.

As indicated in Chapter 2 (see page25), annealing during irradiation strongly affects the removal rate due to thermal neutron induced recoil in several materials. Consequently, it is assumed that recombination of defects during irradiation is responsible for the non-linearity of n_e versus $R = \Sigma_a \phi t$ shown in Figure (10). This is reasonable since the sample temperature is higher than room temperature (30-50°C) and a

large amount of ionizing gamma radiation from the decaying Cd^{114} nuclei is present. Therefore, when the sample is placed in the reactor, cadmium vacancies and cadmium interstitials are generated at a constant rate depending on the flux. This is accompanied by the recombination of cadmium vacancies and cadmium interstitials which depends on the cadmium vacancy concentration, $[Cd_v]$, and the cadmium interstitial concentration, $[Cd_i]$. Upon removal from the reactor, generation and recombination cease and the Cd_v's present at that time are frozen into position. This follows from the fact that no annealing, with respect to the electrical properties, was observed after irradiation. On the basis of this simple model, one can write the following equation for $[Cd_v]$ at any time, t, during irradiation:

$$\frac{d[Cd_v]}{dt} = a^2 - K[Cd_v][Cd_i] \approx a^2 - K[Cd_v]^2 \qquad (25)$$

where a^2 is the generation rate of vacancies and interstitials, given by $\Sigma_a \phi \bar{\nu}$ and K is a rate constant of the form (57),

$$K = zV K_o \exp\left[-E_m/kT\right] \qquad (26)$$

where z is the number of interstitial sites immediately surrounding a lattice site (estimated as approximately 10), V is the volume per lattice site (the reciprocal of the number of atoms per cm^3), K_o is a constant, E_m is the migration energy of the defects and T is the temperature. The derivation of equation (26) for K can be visualized in the following manner. Suppose that annealing of defects in a crystal is due to the motion of interstitials which occasionally encounter immobile vancanies. If the number

of jumps per sec an interstitial makes at temperature T is defined by $K_o \exp\left[-E_m/kT\right]$, then the total number of jumps occurring in one sec per cm^3 is

$$\left[Cd_i\right] K_o \exp\left[-E_m/kT\right]$$

Assuming that an interstitial jumping to an interstitial site next to a vacancy will recombine with the vacancy, the number of recombinations taking place per sec per cm^3 is the number of jumps times the probability that the lattice site next to the interstitial is a vacancy. This probability, which is the fraction of vacant sites in the crystal, is given by

$$\left[Cd_v\right] \Big/ \left(\frac{N_o \rho}{M.W.}\right) = V \left[Cd_v\right]$$

where N_o is Avogadro's number, ρ is the density, and M.W. is the molecular weight. Since there are several interstitial sites surrounding each vacancy this probability must be increased by multiplying by z. Therefore, the number of recombinations taking place per sec per cm^3 is

$$\left(z \left[Cd_v\right] V\right)\left(\left[Cd_i\right] K_o \exp\left[-E_m/kT\right]\right) = K \left[Cd_v\right]\left[Cd_i\right]$$

In setting $\left[Cd_v\right] \approx \left[Cd_i\right]$, in equation (25), we have assumed the production of Frenkel defects. It is also assumed that the material is of nearly stoichiometric proportions so that $\left[Cd_v\right]$ and $\left[Cd_i\right]$ are approximately zero before irradiation. This last assumption leads to the initial condition $\left[Cd_v\right] \approx 0$ at R = 0. Integrating equation (25), one obtains

$$\left[Cd_v\right] = \frac{a}{\sqrt{K}} \tanh\left(a\sqrt{K}\, t\right)$$

or, in terms of $R = \Sigma_a \Phi t$

$$\left[Cd_v\right] = \left[Cd_v\right]_\infty \tanh\left(\gamma R\right) \qquad (27)$$

where $\gamma = \frac{a\sqrt{K}}{\Sigma_a \Phi}$ and $\left[Cd_v\right]_\infty = a/\sqrt{K}$. For γR greater than 2.0, $\tanh(\gamma R)$

approaches one and $[Cd_v]$ approaches its steady state value of $[Cd_v]_\infty$. Suppose that a vacancy traps an electron in a time which is short compared to the lifetime of the vacancy. This is reasonable since the trapping process is enhanced by the intense gamma ray field which results from the decay of the excited Cd^{114} nuclei following thermal neutron absorption by Cd^{113}. In this case, $[Cd_v]$ is equal to n_e^r, the number of electrons removed from the shallow donors, and one can write

$$n_e^o - n_e \equiv n_e^r = [Cd_v]_\infty \tanh(\gamma R) \qquad (28)$$

where n_e^o is the value of n_e before irradiation. Using two experimental points for each sample from Figure (10), $[Cd_v]_\infty$ is eliminated from equation (28) and the following values are obtained for γ,

$$\gamma = 3.7 \times 10^{-6} \quad \text{for GE-231}$$

$$\gamma = 3.4 \times 10^{-6} \quad \text{for GE-232}$$

γ should be a constant for the same material. The difference between γ_{231} and γ_{232} can be accounted for by examining the experimental parameters in more detail. The generation rate, a^2, is just $\Sigma_a \bar{\phi} \bar{\nu}$ where $\bar{\nu}$ is the average number of displacements produced for absorption. Previously, it was indicated that for most of the recoil events the only displacement produced is the recoiling Cd nucleus. Consequently, postponing further discussion of $\bar{\nu}$ for the moment, it is assumed that $\bar{\nu} = 1$ and, therefore,

$$\gamma = \sqrt{\frac{K}{\Sigma_a \phi}}$$

For GE-231 the average flux at the surface of the sample, ϕ_s, was 6.5×10^{10} neutrons/cm^2 .sec and the sample thickness, d, was .0595 cm. The corresponding values for GE-232 were $\phi_s = 8.3 \times 10^{10}$ cm^{-2} sec^{-1} and d = 0.0586 cm.

Using these values, $\Sigma_a \Phi$ is calculated from equation (14) (see page 22):

$$\Sigma_a \Phi \approx \frac{\phi_s}{d} \quad \text{cm}^{-3} \text{ sec}^{-1}$$

The ratio of the two γ's can now be calculated as

$$\frac{\gamma_{231}}{\gamma_{232}} = \sqrt{\frac{(\Sigma_a \Phi)\ 232}{(\Sigma_a \Phi)\ 231}} = 1.10$$

Recalling that $\gamma_{232} = 3.4 \times 10^{-16}$, the above ratio gives $\gamma_{231} = 3.4 \times 10^{-16} \times 1.10 = 3.7 \times 10^{-16}$

which agrees with the experimental value of γ_{231}.

It is also interesting to compare the calculated γ with the experimental values. For both GE-231 and GE-232, $\Sigma_a \Phi$ is about 10^{12} cm^{-3} sec^{-1} so that $\gamma \approx \sqrt{K} \times 10^{-6}$. Recall that K is

$$K = z\ V\ K_o \exp\left[-E_m/kT\right]$$

Typical values for K_o and E_m are 10^{13} sec^{-1} and 0.8 ev, respectively (58). Assuming that T = 120°C is the equivalent temperature during irradiation, $\sqrt{K} \approx 6 \times 10^{-10}$ and $\gamma \approx 6 \times 10^{-16}$ in agreement with the experimental values.

Comparing with the literature, Brown, et al (59) examined high temperature annealing of p-type germanium and found that it obeyed second-order kinetics. At T = 120°C, their data gives N K = 1/1700 where N is the number of defects introduced. Assuming that N is approximately equal to the initial hole concentration (1.5×10^{15} cm^{-3}), K is 4×10^{-19} and $\gamma \approx 6 \times 10^{-16}$. Although the annealing process we observed is quite different from that studied by Brown, et al, this calculation of γ does give an order-of-magnitude comparison.

In order to test the validity of equation (28), n_e^r is plotted versus tanh (γR) for both samples. As shown in Figure (40), a straight line is obtained for both

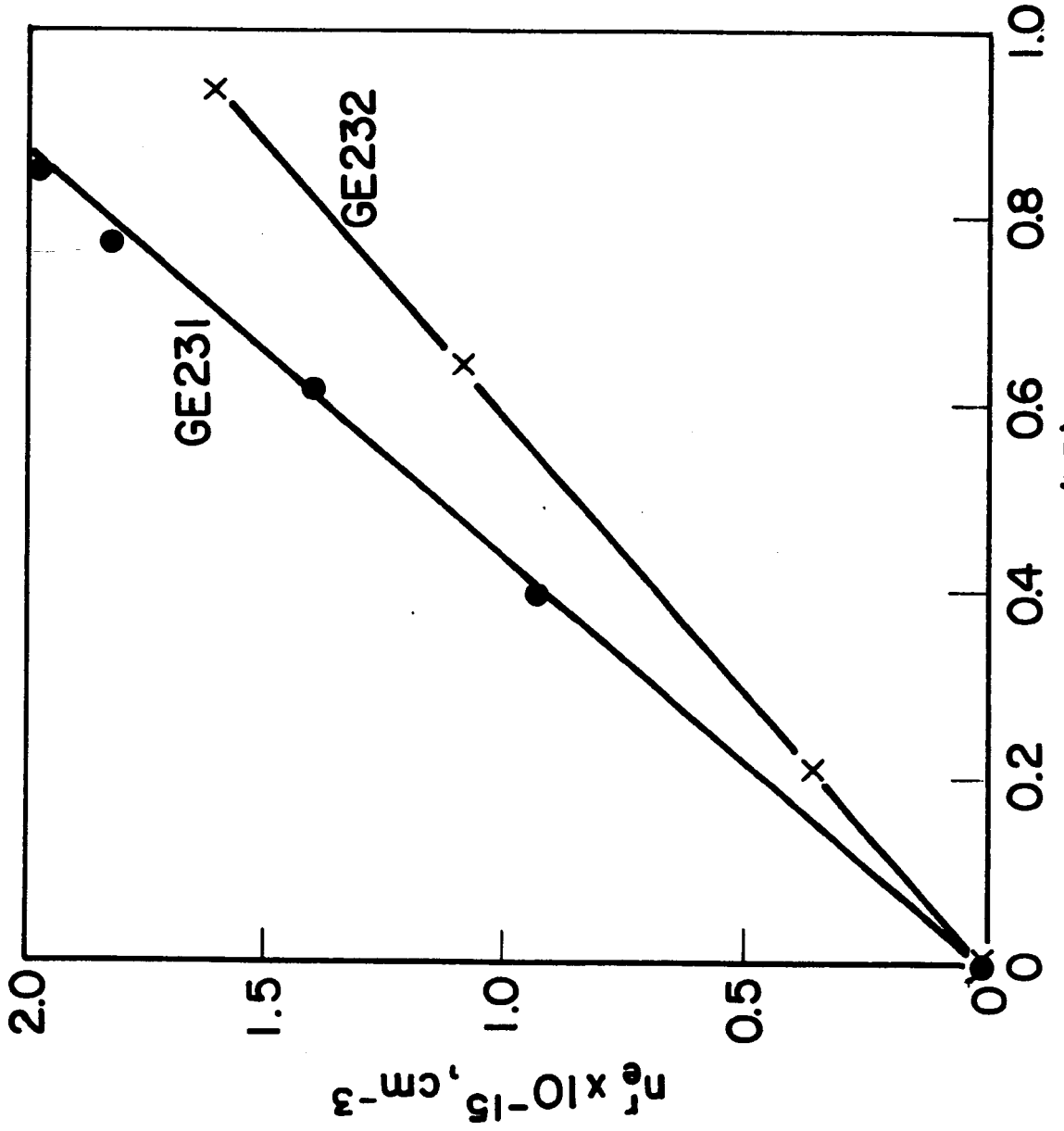


Fig. 40. Number of Electrons Removed per cm^3 in CdTe Versus Tanh (δR) Where R = $\Sigma_a \bar{\phi}$ t

samples indicating that equation (28) for n_e^r satisfactorily predicts the electron removal in CdTe due to the thermal-neutron-induced-recoil process.

These lines possess another interesting characteristic. As indicated in the following table, the slope of each line, $[Cd_v]_\infty$ is approximately equal to the experimental value of the total number of electrons originally available from the shallow donors, n_e^o.

Sample	Slope of n_e^r vs. tanh (γR)	n_e^o
GE 231	2.32×10^{15} cm^{-3}	2.33×10^{15} cm^{-3}
GE 232	1.70×10^{15}	1.72×10^{15}

Therefore, from the experimental results we infer that the equation for n_e^r is

$$n_e^r = n_e^o \tanh (\gamma R) \tag{29}$$

Having determined experimentally that $[Cd_v]_\infty \approx n_e^o$, one can verify this equality by imposing the condition $dn_e^r/dR = 0$ when $n_e^r = n_e^o$ since, at this point, there are no more electrons available from the shallow donors. To apply this boundary condition, one differentiates equation (28),

$$\frac{dn_e^r}{dR} = \gamma [Cd_v]_\infty \operatorname{sech}^2 (\gamma R)$$

or, in terms of n_e^r,

$$\frac{dn_e^r}{dR} = \gamma [Cd_v]_\infty \left(1 - \frac{n_e^{r2}}{[Cd_v]_\infty^2} \right)$$

Setting $n_e^r = n_e^o$ and $dn_e^r/dR = 0$,

$$[Cd_v]_\infty = n_e^o$$

which agrees with the experimental determination of $[Cd_v]_\infty$.

Further agreement with experiment is found by comparing the experimental value of $\left.\frac{dn_e}{dR}\right|_{R=0}$ with that obtained from equation (29),

$$\left.\frac{dn_e}{dR}\right|_{R=0} = -n_e^o \gamma$$

For the two samples studied,

Sample	$-n^o\gamma$	Experimental $\left.\frac{dn_e}{dR}\right\|_{R=0}$
GE 231	-.59	-.60
GE 232	-.85	-1.0

The preceding interpretation of electron removal in CdTe also agrees with Cleland, et al's (30) observation that the removal rate increases with decreasing irradiation temperature (see Table (1), page 25). Differentiating equation (27) and retaining $a/\sqrt{K}$ as the constant,

$$\frac{d\,[Cd_v]}{dR} = \frac{a^2}{\Sigma_a \phi}\ \text{sech}^2\left(\frac{a\sqrt{K}}{\Sigma_a \phi}\ R\right) \qquad (30)$$

The temperature dependence of the annealing rate is contained in K which is proportional to $\exp[-E_m/kT]$. As the temperature decreases, the exponential factor decreases and, hence, K also decreases. Since the sech^2 is inversely proportional to its argument, $d[Cd_v]/dR$ will increase with decreasing temperature for the same value of R. Since it has been assumed that all the Cd_v's are occupied by electrons, the preceding statement is equivalent to saying the removal rate increases with decreasing irradiation temperature as observed by Cleland, et al (30).

Recalling that $a^2 = \Sigma_a \phi\, \bar{\nu}$, equation (30) gives

$$dn_e^r/dR\,\big|_{R=0} = d[Cd_v]/dR\,\big|_{R=0} = \bar{\nu}$$

Since $dn_e^r/dR\,\big|_{R=0}$ is equal to $n_e^o\,\gamma$, whose average value is 0.75, $\bar{\nu}$ is also equal to 0.75. Before comparing this value of $\bar{\nu}$ with that calculated in Chapter 2, it should be emphasized that any Te displacements produced are not included in the $\bar{\nu}$ derived from analysis of the results. Since more

Cd than Te displacements are expected, a small number is added to $\bar{\nu} = 0.75$ so that a reasonable value of $\bar{\nu}$ for both Cd and Te displacements is one. Recall that the average recoil energy, $\bar{E}_r$ calculated by Oswald (4) was 143 ev. Using $E_d = 8$ ev for CdS, $\bar{\nu}$ is

$$\bar{\nu} = \frac{\bar{E}_r}{2E_d} = \frac{143}{16} \approx 9 \text{ displacements/absorption}$$

which does not agree with the experimental value of one. However, based on our arguments concerning gamma ray correlations (see page 20) $\bar{\nu}$ was calculated to be approximately one for $E_d = 15$ ev in CdTe. The fact that this agrees with the experimental value lends credibility to our picture of the recoil process in which only the first one or two gamma rays impart a significant recoil momentum to the Cd^{114} nucleus.

The anomalous behavior of n at high temperatures (see Figure (11) and page 46) after irradiation has not been reported by others for CdTe or CdS. However, Klontz (60) found a similar effect in germanium which had been irradiated with electrons at $0^{\circ}C$. Klontz attributed the anomalous behavior to a complex defect whose energy level shifted when the charge state of the complex changed. The shift resulted in pulling a new level out of the valence band into the energy gap which, in turn, lead to a decrease in carrier concentration with increasing temperature. Although a similar explanation might apply to CdTe, further evidence is required before this behavior can be assigned to a particular complex defect in CdTe.

Another explanation for the anomalous behavior is that the single band model does not adequately describe the Hall coefficient at higher temperatures. In other words, conduction at higher temperatures may be due, in

part, to a second type of carrier which has a much lower mobility. If this were the case, the high temperature region of the graphs of n vs 1/T would be incorrect because R would no longer equal -1/ne. One possibility is that free holes are present in addition to electrons since the hole mobility is much lower than the electron mobility. However, this possibility is rather remote because the generation of electron-hole pairs is extremely small in the temperature range where the anomalous behavior occurs. A second explanation is that a higher sub-band exists in the conduction band in which low mobility electrons reside. As the temperature rises, this sub-band would become more populated and, for a constant n, the Hall coefficient would increase according to the equation relating the Hall coefficient to the densities of the high and low mobility electrons (61). An increase in Hall coefficient with temperature would be equivalent to the anomalous behavior observed in our results. Conduction by both low and high mobility electrons accompanied by a reversal in the Hall coefficient has been observed in GaSb and GaAs (61). When applied to our case, however, this explanation meets with difficulty because the anomalous behavior is not observed before irradiation. However, the ratio of the population of the higher sub-band to that of the lower band depends only on temperature. Therefore, we must postulate that thermal neutron irradiation affects the structure of the conduction band so that the population ratio is also irradiation dependent. Clearly, the anomalous behavior of n is a rather complicated phenomenon and requires further experimental and theoretical analysis.

Another effect which is observed at high temperatures after long irradiation times is the energy level at E_c - .06 ev. When n-type CdTe, which exhibits initially only a shallow donor, is heat-treated in Cd vapor at 900°C, the level at E_c - .06ev is revealed by Hall measurements (55). The same result is obtained if the material is bombarded with 1.5 Mev electrons (55). In addition, the defect responsible for this level can be removed by annealing indicating that it is a native defect. On the basis of the kinetics of electron capture at the E_c - .06 ev level, Lorenz (55) concluded that a double acceptor center was responsible for this level. Because the CdTe must be fired in Cd vapor to produce the double acceptor center, Woodbury (56) concluded that the native defect responsible for the E_c - .06 ev level is the tellurium vacancy. He also found that the double acceptor center is produced in much greater number when the material contains halogen impurities. Woodbury concluded further that the double acceptor is a tellurium vacancy bound to a halogen donor. He adopted the term, "VX center" for this complex defect.

Unlike electron irradiation, the production of the VX center by thermal neutron induced recoil is a rather weak effect which also tends to confirm our hypothesis that more Cd than Te displacements are produced.

We have attributed the decrease in n_e to Cd_v production. However, one would also expect the VX center, which is an acceptor, to cause a decrease in electron concentration. Indeed, VX center formation

by electron irradiation or heat treatment in Cd vapor results in a general decrease in n (55). However, in these two cases, the VX center dominates conduction after a much smaller decrease in n.

Recall that, in addition to the Te_V (VX center), the Te_i is also capable of acceptor action in CdTe. This follows from our assignment of the Te_i to the level at $E_V + .06$ ev observed by Lorenz (43) after heat treating CdTe in Te vapor (see page 87). However, the production of this center by thermal neutron irradiation is insignificant as will be confirmed by measurements on p-type CdTe and also luminescence measurements.

In general, then, it appears that Cd_V's, Te_V's and Te_i's are all capable of producing acceptor centers in CdTe. However, in the case of thermal neutron induced recoil the Cd_V is the dominant defect with respect to electron removal.

It is interesting to compare equations (18) and (19) (see page 23) with the results of fast neutron irradiation of n-type CdTe. Recall that for GE-200 and GE-231, the cadmium ratio was calculated as 7.1. Then, for GE-231, equation (18) gives $Nth/N_F = 28.7$ while equation (19) gives $Nth/N_F = 9.0$. Before irradiation n_e is 2.3×10^{15} cm^{-3} while n_e is 0.4×10^{15} after the fifth irradiation of GE-231. Therefore, $n^r_{e_{th}} = 1.9 \times 10^{15}$ electrons/cm^3 are removed in the first five irradiations which correspond to a total irradiation time of 45 min. For equal irradiation times, assume that $n^r_{e_{th}}/n^r_{e_F}$ equals Nth/N_F. Noting that the irradiation time for GE-200 was 3.8 hours, the number of electrons one would expect

to remove with this amount of fast neutron irradiation, based on equation (18), is

$$n_{e_F}^r = \frac{(1.9 \times 10^{15})\ (3.8)}{(28.7)\ (0.75)} = 3.5 \times 10^{14}\ cm^{-3}$$

$n_{e_F}^r$ as calculated from equation (19) would, of course, be about 3 times this value or $1 \times 10^{15}\ cm^{-3}$. Inspection of Figure (16) indicates that n_e does not change as much as 3.5×10^{14}. If Nth/N_F was greater than 30.5, the predicted value of $n_{e_F}^r$ would be smaller and more in agreement with experiment. In fact, N_{th}/N_F must be larger than 30 for this case because N_F was calculated using data (Harris, et al (15)) which are valid near the core. However C-3, the irradiation position for GE-200 and GE-231, is approximately 12 in. or 30 cm from the core face. At this distance, Harris, et al's data show that the flux from 1 to 3 Mev is depressed and does not follow the exponential variation with energy. Recalling that the most important contribution to N_F was due to 1 to 3 Mev neutrons, one can see that the true N_F is much lower than the calculated value. As indicated in Chapter 2, N_F was calculated for the p-type samples which were irradiated quite close to the core face. Although the calculation does not agree with experiment, it shows the correct trend. Also, it is in better agreement with experiment than N_{th}/N_F calculated from simple damage theory.

B. p-Type Cadimum Telluride

In general, the effect of thermal neutron irradiation on p-type CdTe is similar to that in n-type CdTe. The hole concentration

decreases with increasing irradiation time over the entire temperature range. The results for n-type CdTe were explained by postulating the introduction of deep acceptors, primarily Cd vacancies, but also Te vacancies (VX centers). However, for p-type material, the introduction of deep acceptors several kT above the Fermi level, E_F, will have a negligible effect on p, the hole concentration, while introduction of acceptors below E_F will result in an increase in p. Consequently, one must conclude that occupied states, that is, donors are also introduced. Since it has already been established that no shallow donors are introduced, the thermal neutron induced donors must be deep donors, possibly below the center of the band gap. These occupied levels will act as hole traps thereby reducing the hole concentration. The introduction of donors is a reasonable extension of the model used to explain the electron removal in n-type CdTe. If isolated Cd vacancies are present, one can assume that Cd interstitials, which will act as donors, are also present, either as isolated defects or bound to impurities or dislocations. It is possible that, upon the production of a Frenkel defect, the Cd_i could rapidly diffuse to the crystal surface. This is not probable, however, because of the high recombination rate during irradiation which requires the presence of Cd interstitials. Also, the fact that the Cd_V's anneal out above 100°C (see Figure (22)) indicates that Cd_i's are present.

Earlier, it was stated that the Cd_V, Te_i and Te_V are capable of acceptor action in CdTe. Therefore, one might expect to see levels due to these native defects after irradiation of p-type material. The Te_i possesses a level at $E_V + .05 \pm .01$ ev (see page 87). The fact that this level is not observed after irradiation of p-type CdTe tends to confirm our picture of the recoil process in which Te defects are produced in small quantities.

Several authors (35) (39) (54) have shown that the level of the Cd_V is at $E_V + .15$ ev or $E_V + .20$ ev. Recall that the p-type CdTe samples are dominated by a level in this vicinity before irradiation (see Figure (17)). Therefore, if the Cd_V is at $E_V + .15$ or .20 ev and the Cd_V's are introduced at a greater rate than Cd_i's then one would not expect p to decrease with irradiation. Or, if one assumes that the introduction rate of Cd_V's equals the introduction rate of Cd_i's, then each new acceptor (Cd_V) would be compensated by each new donor (Cd_i) and p would not change very much with irradiation. Suppose, however, that the Cd_i is capable of trapping two holes (giving up two electrons). If this were true, there would be one hole trapped for each Cd_i introduced; that is, one hole from the acceptor states which were present before irradiation. The first hole trapped by the Cd_i came from the Cd_V introduced with the Cd_i. In this case one would expect the hole removal rate to be approximately equal to the electron removal rate for n-type

CdTe. One can see that this is true by recalling that

$$\left.\frac{dn_r^e}{dR}\right|_{R=0} = 0.8 \text{ electrons/absorption}$$

while

$$\left.\frac{dp_r}{dR}\right|_{R=0} = 1.0 \pm 0.2 \text{ holes/absorption}$$

To recapitulate, it is postulated that the Cd_v possesses an energy level at E_v + .15 to .20 ev and that Cd_i's are introduced at the same rate as Cd_v's. The Cd_i's are deep donors which are capable of trapping two holes.

The introduction of deep donors is confirmed further by the mobility curves for the MH material (Figure(19)). Before irradiation the mobility is inversely proportional to temperature which is indicative of lattice scattering. After the first irradiation, however, the temperature dependence is reversed. This indicates the presence of a large number of ionized scattering centers. Thermal neutron induced Cd_i's which have trapped holes and become positively charged can account for this change in mobility.

Recall that the comparison of the experimental N_{th}/N_F with the calculated N_{th}/N_F for n-type CdTe did not show agreement because of the irradiation position. However, for p-type CdTe the irradiation position corresponds more closely with the fast neutron spectrum used to calculate equation (18) for N_{th}/N_F.

The Hall coefficient of sample MH-2, which was exposed to fast neutrons only, does not change after the first irradiation (see Figure 23)). If the comparison between MH-1 and MH-2 is made after the second irradiation, one is already in the region where annealing during irradiation is significant. That is, dp/dR is less than dp/dR at R = 0 (see Figure(24)). However, annealing during irradiation was not taken into account in the derivation of equations (18) and (19) (see page 23) for N_{th}/N_F. These equations were concerned only with the generation of defects. Therefore, in order to make a proper comparison, one must use dp/dR at R = 0; that is, the straight line in Figure (24) is taken is the variation of p with R. The equation of the line is

$$p = 5.5 \times 10^{15} - R$$

or

$$\Delta p = p_o - p = R$$

The average flux for the first two irradiations of MH-1 was 9.7×10^{11} neutrons/cm^2 . sec. The saturated activity is then

$$A_{th} - A_{cd} = \frac{9.7 \times 10^{11}}{3.73} = 2.6 \times 10^{11} \text{ gm}^{-1} \text{ sec}^{-1}$$

For the first two irradiations of MH-2, the average saturated activity of the Cd covered gold foils is $A_{cd} = 2.4 \times 10^{10}$ gm^{-1} sec^{-1}. Therefore, the cadmium ratio is given by

$$R_{cd} - 1 = \frac{2.6 \times 10^{11}}{2.4 \times 10^{10}} = 10.6$$

Using this value and the thickness of MH-2 (.0492 cm) one obtains, from equation (18),

$$\frac{N_{th}}{N_F} = \frac{(31.9)\ (10.6)}{(.0492)\ (107)} = 64$$

To compare this value with experiment, one assumes that

$$\frac{\Delta p_{th}}{\Delta p_F} = \frac{N_{th}}{N_F}$$

After the second irradiation, $\Delta p_{th} = R = 3.5 \times 10^{16}$ cm^{-3} for MH-1 and $\Delta p_F = 0.6 \times 10^{15}$ cm^{-3} for MH-2. Therefore

$$\frac{\Delta p_{th}}{\Delta p_F} = \frac{3.5 \times 10^{16}}{0.6 \times 10^{15}} = 59$$

which agrees rather well with N_{th}/N_F. However, N_{th}/N_F calculated from simple damage theory (equation (19)) is only

$$\frac{N_{th}}{N_F} = 1.27\ R_{cd} = (1.27)\ (11.6) = 14.7$$

The agreement between N_{th}/N_F and $\Delta p_{th}/\Delta p_F$ can not be taken too seriously. This follows from the fact that the connection between these two quantities is not a simple one. For example, the following factors have not been taken into account:

1. The presence of ionizing radiation during thermal neutron irradiation but not during fast neutron irradiation. However, this has been partially accounted for by ignoring annealing.

2. The imbalance between the production of Cd and Te defects during thermal neutron irradiation.
3. The effect of large clusters of defects which result from fast neutron irradiation.

C. Cadmium Sulfide

Comparison of Figures (9) and (26) shows that the variation of n in CdS with thermal neutron irradiation is similar to that in CdTe. Again, the anomalous behavior of n is observed at high temperatures along with the formation after long irradiation of a level at E_c - .085 ev. Woodbury (56) pointed out that this level is equivalent to the E_c - .06 ev level in CdTe (see page112) and is due to a S_i bound to a halogen donor. Hence, the level at E_c - .085 ev is the VX center in CdS.

As in the case of CdTe, a non-linear variation of n_e with $R = \Sigma_a \bar{\phi} t$ is also observed (see Figure (27)). An important difference between CdTe and CdS is that the initial removal rate in n-type CdTe is nearly an order of magnitude greater than that in CdS indicating that a different mechanism may be responsible for electron removal in CdS. This possibility is confirmed by the inability to fit n_e vs. R for CdS with the function tanh (γR), used for CdTe.

As for CdTe, one also expects an excess of Cd defects to be produced in CdS by the recoil process. Extending the analogy further, the electron removal in CdS is also attributed to acceptor

action by cadmium vacancies. In deriving the equation for $[Cd_v]$ it was assumed that $[Cd_v] \approx [Cd_i] \approx 0$ at R = 0. However, it is well-known that CdS is difficult to grow in exactly stoichiometric proportions. Therefore, it is assumed that the CdS samples used in this study contain a large excess of cadmium so that $[Cd_i]$ is approximately constant during the early stages of irradiation when removal from the shallow donors is important. The equation for $[Cd_v]$ then becomes

$$\frac{d\,[Cdv]}{dt} = \alpha - \beta[Cdv]$$

where α is the generation rate ($\alpha = \Sigma_a \bar{\phi} \bar{\nu}$) and β is a constant which is related to K (see page 103) by,

$$\beta = K\ [Cd_i] \qquad (32)$$

Integrating equation (31) and equating $[Cd_v]$ to n_e^r,

$$n_e^r = \frac{\alpha}{\beta}\left(1 - \exp\left[-\frac{\beta}{\Sigma_a \bar{\phi}} R\right]\right) \qquad (33)$$

where the independent variable is now $R = \Sigma_a \bar{\phi}\, t$. Using two experimental points from Figure (27), β is eliminated from equation (33) and $\frac{\alpha}{\beta}$ is found to be 4.5×10^{15}. By taking the derivative of equation (33) and applying the condition $\frac{dn_e^r}{dR} = 0$ at $n_e^r = n_e^o$, one can show that $\alpha/\beta = n_e^o$, similar to the case for CdTe (see page 108). Since $n_e^o = 4.9 \times 10^{15}$, there is some disagreement between n_e^o and the experimental value of α/β. The difference

can be accounted for by competing processes, experimental error, and variation in $[Cd_i]$.

To test the validity of equation (33), $\log (4.5 \times 10^{15} - n_e^r)$ is plotted versus R. The results, shown in Figure (41), indicate that this equation adequately describes electron removal in CdS over the range of irradiation shown on the Figure. This tends to confirm our hypothesis that electron removal in CdS is due to isolated cadmium vacancies in the presence of a large excess of cadmium interstitials.

The slope of the line in Figure (41) gives $\frac{\beta}{\Sigma_a \phi} = 2.2 \times 10^{-17}$

so that the equation for n_e^r is

$$n_e^r = 4.5 \times 10^{15} \left(1 - e^{-2.2 \times 10^{-17} R}\right) \qquad (34)$$

From the experimental data, $\Sigma_a \phi$ is 6.9×10^{12} cm^{-3} sec^{-1} and, therefore, β is 1.4×10^{-4}. Assuming that K is the same order of magnitude for both CdS and CdTe equation (32) gives

$$[Cd_i] \approx \frac{\beta}{K}$$

$$[Cd_i] \approx \frac{1.4 \times 10^{-4}}{10^{-20}} = 1.4 \times 10^{16} \quad \text{cm}^{-3}$$

where $K \approx 10^{-20}$ is taken from page (106). This value of $[Cd_i]$ is characteristic of typical impurity concentrations.

Since $\alpha/\beta = 4.5 \times 10^{15}$ and $\alpha = \Sigma_a \phi D$,

$$D = 4.5 \times 10^{15} \left(\frac{\beta}{\Sigma_a \phi}\right) = 4.5 \times 10^{15} \times 2.2 \times 10^{-17} = 0.099$$

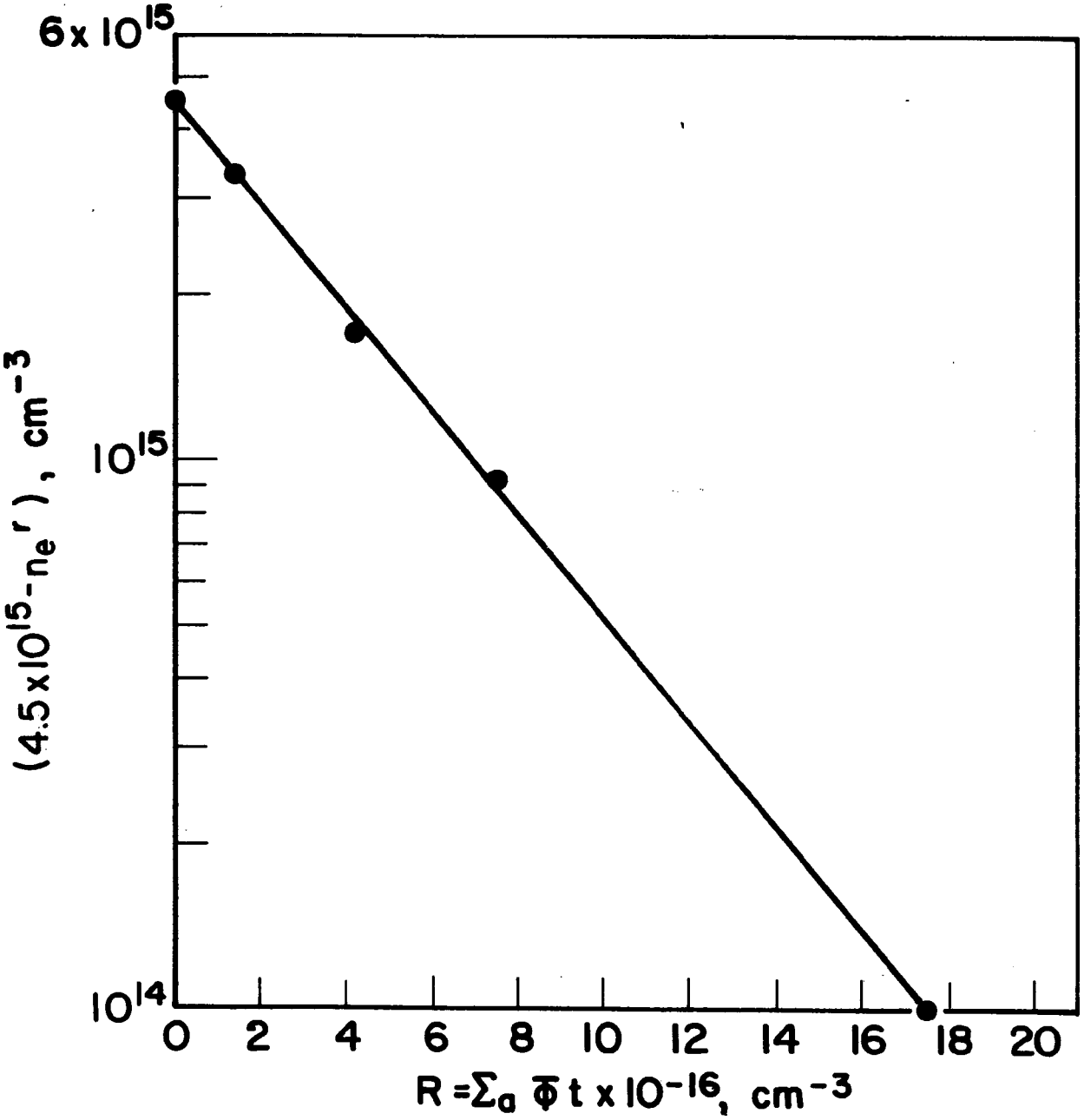


Fig. 41. Electron Removal in CdS Based on Constant Cadmium Interstitial Concentration

This value of $\bar{\nu}$ agrees with the experimental value of the slope at R = 0 in Figure (27) and also with Cleland's (31) observation that the removal rate in CdS is 0.1 (see page 25).

Similar to CdTe, the VX center (see page 112) is observed in CdS at E_c - .089 ev (see Figure (26)) after long irradiation times. The VX center (sulfur vacancy) is also formed in CdS which has been bombarded with electrons. However, for electron irradiation, the VX center dominates conduction after a decrease in n which is much smaller than that observed for the recoil process. This is in accordance with our hypothesis that more Cd than S defects are created by the recoil process.

9. Luminescence Spectra in Cadmium Telluride

Because the edge emission in CdTe is very similar to that in CdS, both in character and in its response to thermal neutron irradiation, we will adopt the model used for CdS to explain the edge emission in CdTe. The CdS model adapted to the edge emission in CdTe is illustrated in Figure (42). Specifically we assume that the Pedrotti model is the edge emission mechanism in CdTe and the Te_i is the edge emission center. It follows that the Y series is due to recombination of a hole bound to a tellurium interstitial with an electron bound to a shallow donor. The X series results from a free electron recombining with a hole trapped at the Te_i. Recall that Lorenz (43) found a level at E_v + .05 to .06 ev in CdTe which had been fired in Te vapor. Attributing this level to a Te_i and assuming that the shallow donor is the same one observed in the electrical measurements (E_c - .012 ev), the Y series emission band should be at

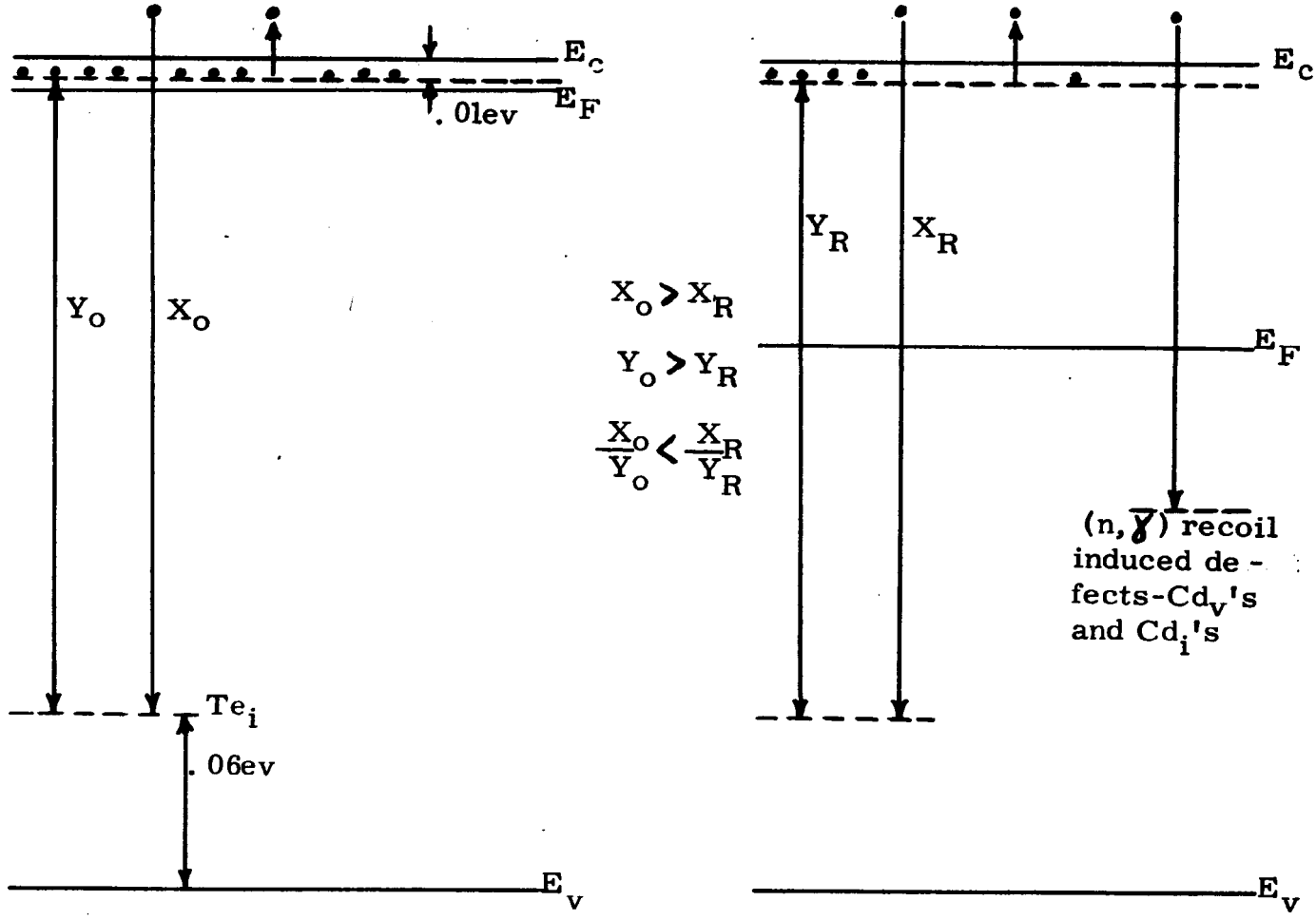
$$E_y \approx E_g - E_A - E_D = 1.605 - 0.06 - 0.012$$

$$\approx 1.533 \text{ ev}$$

While the X series should be at $E_y + .012 = 1.545$ ev. Both of these values agree to within .004 ev of the observed X and Y peak positions (see Figure (30a)) which tends to confirm the model of the edge emission illustrated in Figure (42a).

In Chapter 2, we developed the hypothesis that Cd defects are produced at a much faster rate than Te defects. The discussion of the electrical measurements given in this Chapter tends to confirm this hypothesis. Consequently, if the Te_i is the edge emission center and the Cd_v's and Cd_i's introduced by irradiation are effective recombination centers, one would expect to observe a decrease in edge emission with irradiation. This agrees with the observed behavior and lends credibility to our model of the edge emission.

In the discussion of edge emission in CdS, three possible reasons were given for the observed decrease in edge emission. These reasons also apply to CdTe. The competing recombination at deep levels attributed to Cd_v's and Cd_i's introduced by irradiation has already been mentioned in the previous paragraph. Since no emission band was detected which grew with irradiation, we assume that the deep levels associated with the Cd_v's and Cd_i's are non-radiative recombination centers. This competing process is illustrated in Figure (42b).



a) Before Irradiation

b) After Irradiation

Figure (42). The effect of thermal neutron irradiation on the edge emission in CdTe.

The fact that the X series is stronger than the Y series after long irradiation times in both n and p-type CdTe is also explained in the same manner as for CdS. That is, the introduction of deep levels pulls the Fermi level towards the center of the gap as shown in Figure (42b). This, in turn, reduces the fraction of occupied donors which leads to a decrease in intensity of the Y series.

For CdS, it was also suggested that the edge emission centers may be destroyed during irradiation. This possibility also exists for CdTe.

To summarize, the observed behavior of the edge emission in CdTe which is exposed to thermal neutrons can be explained by adopting the Pedrotti model as the edge emission mechanism and the Te_i as the edge emission center.

There is some indication that the intensity of the X series of the edge emission begins to increase after long irradiation times. This was observed for MH-17 (see Figure (32)) and for two n-type samples. It was indicated earlier that Te defects are produced at a slow rate. After long irradiation times when the behavior has stabilized and the Te_i (proposed edge emission center) concentration has had a chance to build up these defects may begin to play a more important role.

The emission bands observed in the exciton recombination region were discussed in detail in the last Chapter. However, the 1.575 ev band merits further discussion because it dominates the exciton recombination region after long irradiation times. It is one of the few bands which does not decrease significantly in intensity with irradiation. In addition, it is seen in both n and p-type CdTe. For these reasons it is tempting to assign this band to a native defect. Recall that from electrical measurements and the work of others (35) (39) there is evidence that the cadmium vacancy is at E_v + .20 ev in agreement with the 1.575 ev band (see page87). If one makes this assignment, it must be assumed that the initial Cd_v

concentration present in n-type material before irradiation is small enough so that equation (27) for $[Cd_V]$ still applies to the electrical measurements, but large enough to give the 1.575 ev band. This is necessary because equation (27) (see page 104) was derived on the basis that $[Cd_V] \approx 0$ at R = 0.

One might look for further evidence of the Cd_V at $E_V + .20$ ev in the low energy emission region. As $[Cd_V]$ becomes larger, it is reasonable to expect free electron recombination with a hole trapped at the Cd_V. This would occur at 1.605 ev - 0.20 ev = 1.405 ev. Because of the presence of strong emission bands in this energy region in p-type CdTe the expected emission band at 1.405 ev would probably show up only in n-type CdTe. Although the peaks in this region cannot be resolved for n-type CdTe (see Figure (35)) after moderate irradiation, there is some indication of the appearance of an emission band in this region as irradiation proceeds. Figure (32) shows that the 1.450 ev band decreases at the same rate as the Y series of the edge emission for p-type CdTe. In contrast to this, the decrease in the 1.415 ev band in n-type CdTe is negligible compared to the decrease in intensity of the Y series (see Figure (36)). This may be due to the appearance of a weak emission band, possibly at 1.405 ev, in this region of the spectrum of n-type CdTe.

An alternate interpretation of the Cd_V is possible, based on the emission band at 1.450 ev which is seen in both n and p-type CdTe. In accordance with Halsted's (42) observation that the 1.450 ev band occurs in Cd deficient CdTe, this emission band can be attributed to recombination of a

free electron with a hole bound to a Cd_V at E_V + 0.15 ev. Since this level is observed in p-type Hall samples before irradiation and the 1.450 ev band is much stronger in p-type CdTe, one can postulate that the main difference between the p and n-type CdTe is the presence of a large Cd_V concentration in p-type CdTe before irradiation. However, the fact that the E_V + .15 ev level is found in all samples may merely suggest that it is due to an impurity which usually occurs in Cd or Te metal.

Other interpretations of the edge emission are also possible. Interpretation of the edge emission based on the peak positions of the bands is complicated by the fact that the Te_i (E_V + .06 ev) is the same distance above E_V as the VX center is below E_C (E_C - .06 ev) Consequently, the peak position of the X series could also be due to recombination of a free hole with an electron at the VX center. This interpretation was given by Halsted (62). Because the Te_i is assumed to be paired with a donor and the VX center also has a donor as one member, an interpretation similar to Grillot's (47) might also apply (see page 96). In any case, Te defects are involved and one still reaches the conclusion that thermal neutron irradiation should not result in an increase in edge emission intensity.

Because the emission spectrum is sensitive to surface effects one needs to consider the possibility that oxidation may be responsible for some of the changes observed. Indeed, samples that were irradiated in polyethylene capsules during preliminary investigations were covered with heavy, oily films after long irradiation. This film was soluble in

HCl as the oxides of Te are. The oily character of the film makes it easy to recognize even a small amount on a cleaved surface. Therefore, visual inspection was valuable in determining the presence of oxide film. If such a film was seen, the sample was discarded. Halsted (63) has studied the effect of oxides on the edge emission of CdTe. After treatment in an oxidizing environment, the peak positions of the edge emission shifted. However, a shift was not observed after thermal neutron irradiation. Therefore, it is concluded that the influence of oxidation on the emission spectra was minor.

At this point, a comment on the introduction of I^{127} might also be made. Recall that an $(nvt)_{th}$ of 10^{16} cm^{-2} would result in approximately 3×10^{13} I^{127} nuclei/cm^3. However, Hall measurements show that practically all the electrons (2×10^{15} cm^{-3}) are removed in an n-type sample after an $(nvt)_{th}$ of only 10^{15} neutrons/cm^2. Consequently, this effect is assumed to be an insignificant one.

10. Suggestions for Further Experiments

Additional experimental work is required to produce further clarification of the effect of thermal neutron induced recoil on the properties of CdS and CdTe. Clearly what is needed is a coordinated effort in which the effects of thermal neutrons are compared with the effects produced by other types of irradiation and variations in stoichiometry. In particular, it would be interesting to study the effects of electrons and heat treatments on the emission spectrum of CdTe. Also, much valuable information could

be obtained by doing low temperature irradiations and eliminating the effects of annealing. Because of the short mean free path of thermal neutrons, measurements which can be done as a function of depth into the material, emission spectra, for example, should also provide a great deal of information. However, this would require exceedingly uniform and homogeneous material. Valuable results would also be obtained by repeating the experiments described herein on very pure or intrinsic CdTe.

Another interesting experiment, originally suggested by Oswald (64), would be to perform Colbow's (50) measurement (see page 97) on the red center in CdS and the edge emission in CdTe. In the case of CdS, this experiment could be performed as a function of irradiation time. One could then study the pair separation, r, at a certain time after the excitation flash as a function of irradiation. These experiments would reveal whether or not the emission band studied is due to a bound-to-bound transition. If it is, the variation in r would give information about the concentration of defects introduced as a function of $(nvt)_{th}$.

VI. REFERENCES

1. L. Szilard and T. A. Chalmers, Nature, 134, 462 (1934)

2. H. C. Schweinler, J. Appl. Phys., 30 no. 8, 1125 (1959)

3. R. M. Walker, J. Nuc. Materials, 2, no. 2, 147 (1960)

4. R. Oswald and C. Kikuchi, Nuclear Science and Eng., 23, 354-360 (1965).

5. D. S. Billington and J. H. Crawford, Jr., Radiation Damage in Solids, Princeton University Press, Princeton, New Jersey (1961).

6. F. Seitz, Disc. Faraday Soc., 5, 271 (1949).

7. B. A. Kulp in Radiation Damage in Semiconductors, 7th International Conference on the Physics of Semiconductors, Vol. 3, Academic Press, 173 (1965).

8. D. J. Hughes and R. B. Schwartz, BNL-325, (1958)

9. B. R. S. Buckingham, K. Parker and E. D. Pendlebury, AWRE-0-28/60.

10. R. V. Meghreblian and D. K. Holmes, Reactor Analysis, McGraw-Hill, New York, (1960).

11. H. C. Schweinler in Chemical Effects of Nuclear Transformations, International Atmoic Energy Agency, Vienna, 1, 64, (1963).

12. A. M. Weinberg and E. P. Wigner, The Physical Theory of Neutron Chain Reactors, Univ. of Chicago Press, Chicago (1958).

13. Elwyn, Lane, Langsdorf and Monahan, Phys. Rev., 133B p. 84 (1964)

14. W. A. Harrison and F. Seitz, Phys. Rev. 98, 1530 (1955).

15. L. Harris, G. F. Knoll and J. S. King, Trans. Am. Nucl. Soc., 8, 73 (1965).

16. Directory of Nuclear Reactors, 2 and 3, International Atomic Energy Agency, Vienna (1960).

17. J. B. Trice, Nucleonics, 16, no. 7, 81 (1958).

18. W. J. Price, Nuclear Radiation Detection, McGraw-Hill, New York (1958).

19. R.B. Oswald, Doctoral Thesis, Nuclear Eng. Dept., Univ. of Mich. (1964).

20. L.V. Groshev, A.M. Demidov, V.N. Lutsenko and V.I. Pelekhov, Atlas of Gamma Ray Spectra from Radiative Capture of Thermal Neutrons, Pergamon Press (1959).

21. R.R. Coltman, C.E. Klabunde, D.L. McDonald and J.K. Redman, J. Appl. Phys., 33, 3509 (1962).

22. Nuclear Data Sheets, National Research Council, Committee on Nuclear Science, 1958-1965.

23. R.M. Walker, J. Nuc. Materials, 2, no. 2, 147 (1960).

24. G.A. Bartholomew and L.A. Higgs, Compilation of Thermal Neutron Capture Gamma Rays, AECL-669.

25. J.N. Brazos and R.M. Steffen, Phys. Rev., 102, 753 (1956).

26. J.S. Martinez, Doctoral Thesis, Univ. of Calif., UCRL-6526.

27. R.R. Coltman, J.K. Redman, C.E. Klabunde, G.F. Fielder, ORNL-3676, Gl (1964).

28. M.V. Chukichev and V.S. Vavilov, Soviet Physics-Solid State 3, no 5, 1103 (1961).

29. J.W. Cleland, in Proceedings of the Inter. School of Physics "Enrico Fermi", Course 18, Radiation Damage in Solids, 384 (1962).

30. J.W. Cleland, R.F. Bass and J.H. Crawford in Radiation Damage in Semiconductors, 7th Inter. Conf. on the Physics of Semiconductors, 3, Academic Press, 401 (1965).

31. J.W. Cleland and R.F. Bass, ORNL-3480, 188 (1963).

32. R.O. Chester, ORNL-3767 (1965).

33. R. Oswald and C. Kikuchi IEEE Space and Nuclear Radiation Effects Conf., University of Mich., Ann Arbor (1965).

34. N.B. Urli, J. Phys. Soc. Japan, 21, Supplement, 259 (1955)

35. F.A. Kroger and DeNobel, J. Electronics, 1, 190 (1955)

36. T. Ichimiya, T. Niimi, K. Mizuma, O. Mikami, Y. Kamiya, and K Ono, in Solid State Physics in Electronics and Telecommunications (Proceedings of the International Conference held in Brussels, June 2-7, 1958), edited by M. Desirant and J.L. Michielo, Academic Press, Inc., New York, 1960 2, p. 845.

37. B. Segall, M.R. Lorenz, and R.E. Halsted, Phys. Rev., 129, no. 6, 2471-2481 (1963).

38. H.M. Hersh, Phys. Rev., 105, 1158 (1957)

39. S. Yamada, J. Phys. Soc. Japan, 15, No. 11, 1940 (1960).

40. D.T.F. Marple, Appendix O, Report No. AFARL-TR-64-145, General Electric Research Lab., October, 1964.

41. R.E. Halsted and M. Aven, Report No. 65-RL-3863G, Jan., 1965.

42. R.E. Halsted, M.R. Lorenz and B. Segall, J. Phys. Chem. Solids, Vol. 22, 109 (1961).

43. M.R. Lorenz and B. Segall, Physics Letters, 7, No. 1, 18 (1963).

44. J.J. Lambe, C.G. Klick and D.L. Dexter, Phys. Rev., 103, 1715 (1956).

45. R.J. Collins, J. Appl. Phys. 30, 1135 (1959).

46. F.A. Kroger and H.G.C. Meyer, Physica, 20, 1149 (1954).

47. Grillot, Acta Physica Polonica, 26, no. 3-4, 547 (1964).

48. Maeda, J. Phys. Chem. Solids, 26, 1419 (1965).

49. L.S. Pedrotti and D.C. Reynolds, Phys. Rev., 120, 1665 (1960).

50. K. Colbow, Phys. Rev., 141, no. 2, 742 (1966).

51. W.C. Vassell and D.K. Donald, Ford Scientific Laboratory Technical Report No. SL-64-14, March, 1964.

52. B.A. Kulp and R.H. Kelley, J. Appl. Phys., 31, No. 6, 1057 (1960).

53. E.T. Handelman and D.G. Thomas, J. Phys. Chem. Solids, 26, 1261 (1965).

54. D. deNobel, Philips Res. Rept. 14, 361 (1959)

55. M.R. Lorenz, B. Segall and H.H. Woodbury, Phys. Rev., 134, no. 3A, A751 (1964).

56. H.H. Woodbury and M. Aven in Radiation Damage in Semiconductors, 7th International Conference on the Physics of Semiconductors, Vol. 3, Academic Press, 179 (1965).

57. G.J. Dienes and G.H. Vineyard, Radiation Effects in Solids, Interscience (1957).

58. J.W. Corbett, Electron Radiation Damage in Semi conductors and Metals, Supplement 7, Solid State Physics, edited by F. Seitz and D. Turnbull, Academic Press, New York, (1966).

59. Brown, Augustyniak, and Waite, J. Appl. Phys., 30, 1258 (1959).

60. E.E. Klontz and S.W. Mackay in Radiation Damage in Semiconductors, 7th Inter. Conf. on the Physics of Semiconductors, 3, Academic Press, 41 (1965).

61. O. Madelung, Physics of III-V Compounds, John Wiley and Sons, New York, p. 131 (1964).

62. R.E. Halsted and B. Segall, Phys. Rev. Letters, 10, No. 9, 392 (1963).

63. R.E. Halsted, 79, ASD Tech. Rep. 61-242.

64. R. Oswald, Private Communication.